The role of aluminium from supplementary cementitious materials in controlling alkali-silica reaction

THÈSE N^{O} 5429 (2012)

PRÉSENTÉE LE 19 JUILLET 2012

À LA FACULTÉ DES SCIENCES ET TECHNIQUES DE L'INGÉNIEUR
LABORATOIRE DES MATÉRIAUX DE CONSTRUCTION
PROGRAMME DOCTORAL EN SCIENCE ET GÉNIE DES MATÉRIAUX

ÉCOLE POLYTECHNIQUE FÉDÉRALE DE LAUSANNE

POUR L'OBTENTION DU GRADE DE DOCTEUR ÈS SCIENCES

PAR

Théodore CHAPPEX

acceptée sur proposition du jury:

Prof. P. Stadelmann, président du jury
Prof. K. Scrivener, directrice de thèse
Dr P. Bowen, rapporteur
Dr M. Broekmans, rapporteur
Dr E. Gallucci, rapporteur

ÉCOLE POLYTECHNIQUE
FÉDÉRALE DE LAUSANNE

Suisse
2012

ABSTRACT

Alkali silica reaction (ASR) is a long-term reaction between certain aggregates containing amorphous silicate phases and the alkalis from the cement paste. These silicates react with the alkalis present in the pore solution of the cement paste and form an expansive gel in the presence of water, resulting in the macroscopic expansion and cracking of concrete. Supplementary cementitious materials (SCM), replacing a part of the Portland cement (PC) in blended pastes, are known to reduce or even stop expansion due to ASR. Studies indicate that the main reason for this is the decrease in alkalinity of the pore solution of the cement paste, which in turn is attributed to the change in composition of the C-S-H, the main cement hydrate. However, knowledge on the effect of SCMs on ASR control is incomplete, especially the role of aluminium.

The first part of this work focuses on the effect of aluminium and silicon incorporation in C-S-H, provided by SCMs, on the composition of the pore solution of blended pastes. It was found that, contrary to the common idea, the incorporation of aluminium in C-S-H does not increase its alkali fixation capacity, suggesting that the greater effectiveness of SCMs containing alumina is due to other reasons.

In a second part, it is proposed that the additional aluminium acts directly on the reactive phases of the aggregates. Marine chemistry and geology theories about the dissolution mechanisms of amorphous silicates were applied to cementitious systems. Aluminium species, provided by certain SCMs and present in the pore solution, are incorporated in the silica surface and limit the dissolution of amorphous silica of the aggregates, limiting ASR. The effect of aluminium was shown through a study of reactive aggregates in simulated pore solutions. The mechanism was explained through a more fundamental study with pure amorphous silica plates put in simulated pore solutions.

Finally, the impact of various alkali cations on ASR was studied to better understand the reactions inducing gel formation.

Keywords: Concrete, Alkali, silica, C-S-H, aluminium, aggregates

RESUME

La réaction alcali granulat (RAG) est une réaction de dégradation de certains bétons sur le long terme. Elle touche les bétons dont les granulats contiennent certaines phases siliceuses amorphes ou mal cristallisées. Cette silice réagit avec les alcalins présents dans la solution de pore du ciment et forme un gel alcali-silice expansif au contact de l'eau, menant à la fissuration et à l'expansion des structures en béton. L'ajout d'addition minérale, remplaçant une partie du ciment portland dans un béton, est connue pour contrôler cette réaction. Certaines études indiquent que la raison principale pour laquelle ces additions contrôlent la RAG est la réduction de l'alcalinité de la solution de pore, qui elle même est attribuée à un changement de composition du C-S-H, l'hydrate principal du ciment. Les mécanismes contrôlant la RAG restent cependant méconnus, et plus particulièrement le rôle de l'aluminium.

La première partie de ce travail étudie l'effet de l'incorporation d'aluminium et du silicium dans le C-S-H, fournis par les additions minérales, sur la composition de la solution de pore de pâtes mixtes. Il a été démontré que, contrairement aux idées reçues, l'incorporation d'aluminium dans le C-S-H n'augmente pas la capacité de cette phase à fixer les alcalins de la solution de pore. Il est donc proposé que l'effet bénéfique de l'addition d'oxyde d'aluminium dans les bétons réactifs soit dû à un autre mécanisme.

Dans une seconde partie, il est démontré que l'aluminium supplémentaire agit directement sur la phase réactive des granulats, la silice amorphe. Les mécanismes de dissolution de la silice amorphe étudiés en chimie marine et en géologie ont été adaptés aux systèmes cimentaires. L'aluminium, fourni par les additions minérales et présent dans la solution de pore, est incorporé sur la surface de la silice, limitant sa dissolution, et de ce fait, limitant la formation de gel de RAG dans les granulats. L'effet de l'aluminium a été démontré par l'étude de granulats réactifs mis dans une solution de pore simulée, ainsi que par l'étude plus fondamentale de silice amorphe en solution.

Finalement, l'impact de différents alcalins sur la RAG a été étudié, afin de mieux comprendre les mécanismes opérant lors de la formation de gel.

Mots clés : béton, alcalins, silice, C-S-H, aluminium, granulats

CHAPTER 1 INTRODUCTION

1.1. Background

A majority of dams in Switzerland and a lot of large structures were built decades ago implementing the technologies available at the time. Today, some of these structures exhibit durability problems, including symptoms of alkali silicate reaction (ASR). ASR is one of the most important reasons for concrete degradation after corrosion of reinforcing steel. ASR occurs through a combination of the alkaline pore solution of the concrete, amorphous silicates found in certain type of aggregates and water. Reactive silicates are found with different mineralogies, such as chalcedony, feldspars, biotite and muscovite e.g. [1]. ASR causes aggregates expansion and deterioration of concrete.

ASR was first identified in California in 1940. The reaction mechanism was described by Dent Glasser [2] as penetration of hydroxide ions into the disordered silica structure, breaking siloxane bridges and attacking terminal silanol groups

$$SiO_2 + OH^- \rightarrow SiOH + SiO^-$$

$$SiO_2 + 2\ OH^- \rightarrow 2SiO^- + H_2O$$

$$SiOH + OH^- \rightarrow SiO^- + H_2O$$

Meanwhile, sodium and potassium ions, present as impurities in the cement and sometimes released by the aggregates themselves into the pore solution of cement e.g. [3], migrate into the silica framework and neutralize the negative anion charges, forming an alkali silica gel:

$$SiO^- + Na^+ \rightarrow SiONa.$$

Alkali silica gel can adsorb water, resulting in a volume increase. The internal stresses in the aggregates caused by the growth of the gel cause the cracking and damage of concrete as in Figure 1.1.

Figure 1.1. Highly ASR affected wall in the Swiss Alps (personal collection)

There is to date no possibility stopping ASR expansion in existing structures. The waterproofing of dams was tried in the past, but there is always sufficient water to provoke expansion, and it would take hundreds of years to dry out. It is however possible to reduce the stresses induced by concrete expansion on dams. The method consists in vertical cutting at regular intervals with a diamond wire. It is called “slot cutting”. This creates 1 to 2 cm wide slots. These slots release the stresses induced by concrete expansion. The concrete continues expanding until the contact of the sides creates stresses in the structure again. With this technique, the dam can be exploited some more years before the rebuild. Figure 1.2 shows an example of a newly cut Swiss dam. Light is visible through the 2 cm wide slice.

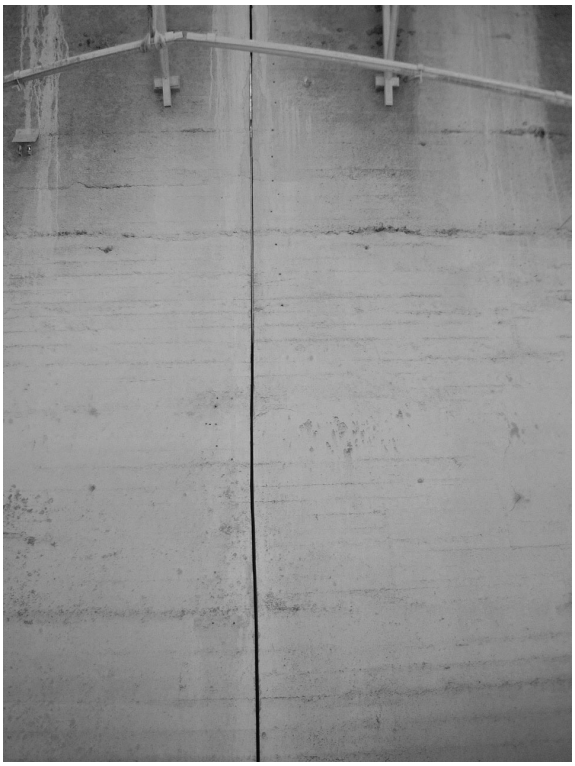

Figure 1.2. Slot cutting of a Swiss reactive dam. (personal collection)

It is possible to avoid ASR expansion in newly build structures. One solution is to use non-reactive aggregates, but this is often not feasible because of unavailability of non-reactive aggregates or the constraint of using local aggregates for environmental and financial reasons. It is evident that structures like dams or tunnels have to use the aggregates from excavation or those present on the construction site. Moreover, in Switzerland, the majority of aggregates are observed showing some signs of alkali reactivity.

The use of low alkali cement was often suggest as being a solution to avoid ASR. It was however observed, through the testing of large concrete blocks, that deleterious expansion can occur even when low alkali cements are used [4]. The alkalis present in the cement are sufficient to create reaction products over the long term in certain conditions. The alkalis released from certain mineral phases present in the aggregates may also have an influence on the ASR [5]. Moreover, Ca^{2+} proceed to an ion exchange with alkalis in the alkali silica gel, transforming it to C-S-H [6]. Slowed by diffusion due to their greater diameter and double charge, calcium ions bind in the gel structure later than alkali ions. This mechanism releases

alkalis, available again to attack more poorly crystallized silica. The reaction can progress until the exhaustion of reactive starting material.

It has been widely shown that the best way to avoid ASR is through the use of supplementary cementitious materials (SCM) (slags and pozzolans) in blended cements. Thomas has recently reviewed the effect of SCMs on ASR [7].

SCMs are cementitious compounds, chemically close to Portland Cement (PC). Most of SCMs are richer in silica and alumina than PC. Examples of such SCMs are:

- fly ash, a by-product from the production of electricity from coal,
- ground granulated blast furnace slag, a by-product of iron production,
- silica fume, a by-product of production of silicon metal,
- metakaolin, produced by calcination of kaolinitic clays,

The ternary diagram in Figure 1.3 shows the relative compositions of SCMs and PC. These alternative compounds have many advantages, mainly with respect to durability and environmental issues.

Numerous laboratory studies and decades of field experience have shown SCMs to be effective to avoid deleterious ASR in concrete made with reactive aggregates. Nevertheless the exact mechanism by which this is brought about is unclear. Furthermore not all SCMs are equally effective.

The problem is that the amount of SCM necessary is specific to each aggregate type and needs to be determined by tedious testing, whose applicability to field conditions is questionable. Indeed the most efficient tests of reactivity take a year to yield reliable results, which is often far too long to pre-test a concrete formulation.

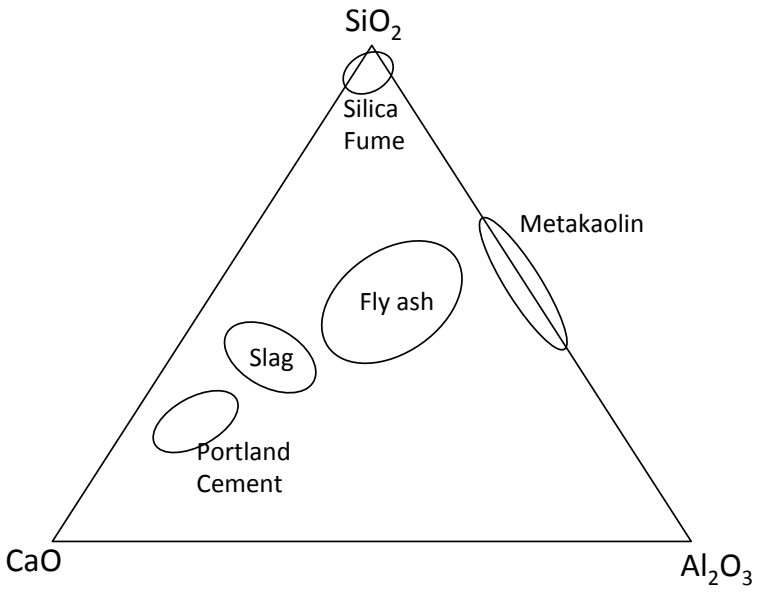

Figure 1.3. Ternary diagram of cementitious materials

1.2. Objective of the study

The overall objective of this work is to better understand the fundamental mechanisms by which SCMs prevent deleterious ASR and so permit faster and more reliable methods to identify durable combinations for concrete. Focus is given to the role of alumina addition, of which the exact contribution regarding ASR is not clear.

It has been observed that SCMs containing alumina seem to be more effective in reducing ASR than those containing only silica [8-10]. It is known that the addition of SCMs in PC pastes can lower the pH of the pore solution [1-3] and this is considered to be related to the change in composition of the main binding phase, calcium silicate hydrate, C-S-H [11, 12]. SCMs tend to increase the amount of silicon and/or aluminium present in the C-S-H. The increase of the amount of silanol sites in the C-S-H was proposed to fix alkalis, resulting in the reduction of the pH of the pore solution [11, 13]. The increase of aluminium sites in the C-S-H structure was also proposed to fix alkali and so further reduce alkalinity [12]. This is however not completely proven and remains an assumption that has to be confirmed.

1.3. Experimental approach

The experiments are built up on a multi scale basis as seen in Figure 1.4. Fast reacting SCMs, silica fume (containing only silica) and metakaolin (containing both silica and alumina) were used. In order to get results in the timescale of a PhD study, mortars with reactive aggregates were cast and put in accelerated conditions (alkaline solution, 38°C), to observe expansion. To better understand the mechanisms, the pastes and the aggregates were also studied separately.

The pastes were analysed principally by scanning electron microscopy (SEM), by thermo gravimetric analysis (TGA) and pore solution were extracted (PSE) and analysed by inductive coupled plasma (ICP). The impact of SCMs on the composition of the C-S-H in pastes and on the composition of the pore solution was observed.

The reactive aggregates were immersed in simulated pore solution and analysed by SEM image analysis, to get information about their degradation state.

A more fundamental study was done with pure amorphous silica plates, corresponding to the reactive phase of the aggregates, immersed in simulated pore solutions, and analysed by SEM, X-ray photoelectron spectroscopy (XPS) and atomic force microscopy (AFM), to learn about the mechanisms at the atomistic level.

Finally, mortars and pastes with various concentrations of alkalis were cast and studied, to get information about the effect of alkalis on the ASR.

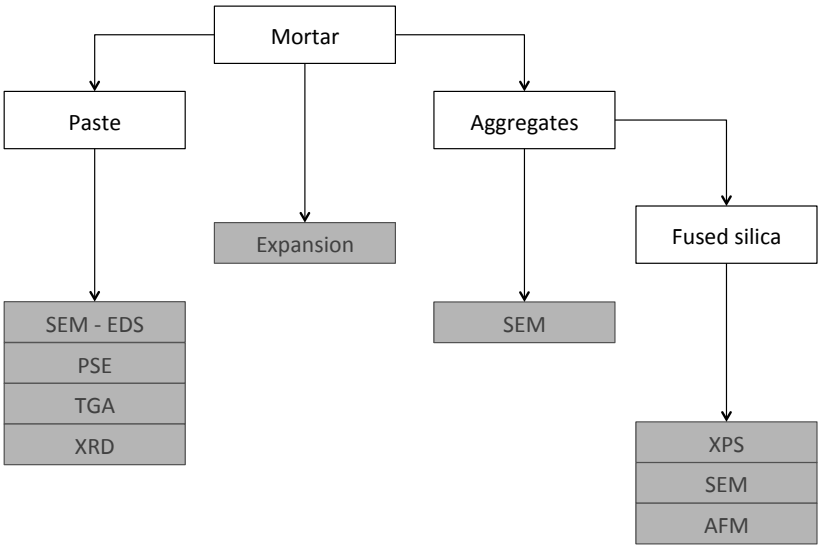

Figure 1.4. Shematic representation of the experimental planning

1.4. Structure of the work

This thesis aims to study the mechanisms controlling ASR with the use of SCMs, mainly to understand the effect of aluminium addition on the control of ASR. The effect of the amount and type of certain alkali cations was also studied to better understand reaction and optimize laboratory tests.

This document is structured as follows:

- **Chapter 2** shows the effect of aluminium and silicon incorporation in C-S-H on the composition of the pore solution in cement pastes. Special attention is given to the effect of aluminium addition.

- In **Chapter 3**, a new mechanism is proposed to explain the beneficial effect of aluminium addition on ASR. This mechanism is adapted to concrete from geochemistry and marine chemistry. Aluminium in the pore solution reduces the dissolution of silica in reactive aggregates. The study tries to understand the incorporation mechanism of aluminium on the silica surface and the way in which these species reduce the dissolution rate of silica in concrete. The study is done on a

multi scale basis, studying separately the blended pastes, the aggregates and the reactive phase of the aggregates, the amorphous silica.

- **Chapter 4** is separated in two main parts, the effect of sodium and potassium on ASR, and the second part about the effect of lithium on ASR. As all alkalis seems to behave differently in ASR, this study tries to investigate the influence of pore solution and microstructural evolution of the cement paste subject to different sources of alkalis.

- **Chapter 5** gives the general conclusions and perspectives of this thesis.

1.5. References

[1] A. Leemann, L. Holzer, Alkali-aggregate reaction,Identifying reactive silicates in complex aggregates by ESEM observation of dissolution features, Cement and Concrete Composites, 27 (2005) 796-801.

[2] L.S. Dent Glasser, N. Kataoka, The chemistry of 'alkali-aggregate' reaction, Cement and Concrete Research, 11 (1981) 1-9.

[3] M.A.T.M. Broekmans, Structural properties of quartz and their potential role for ASR, Materials Characterization, 53 (2004) 129-140.

[4] M. Thomas, B. Fournier, K. Folliard, J. Ideker, M. Shehata, Test methods for evaluating preventive measures for controlling expansion due to alkali-silica reaction in concrete, Cement and Concrete Research, 36 (2006) 1842-1856.

[5] J. Lindgård, Ö. Andiç-Çakır, I. Fernandes, T.F. Rønning, M.D.A. Thomas, Alkali-silica reactions (ASR): Literature review on parameters influencing laboratory performance testing, Cement and Concrete Research, 42 (2012) 223-243.

[6] L.S. Dent Glasser, N. Kataoka, On the role of calcium in the alkali-aggregate reaction, Cement and Concrete Research, 12 (1982) 321-331.

[7] M. Thomas, The effect of supplementary cementing materials on alkali-silica reaction: A review, Cement and Concrete Research, 41 (2010) 209-216.

[8] W. Aquino, D.A. Lange, J. Olek, The influence of metakaolin and silica fume on the chemistry of alkali-silica reaction products, Cement and Concrete Composites, 23 (2001) 485-493.

[9] J. Duchesne, M.-A. Bérubé, Long-term effectiveness of supplementary cementing materials against alkali-silica reaction, Cement and Concrete Research, 31 (2001) 1057-1063.

[10] T. Ramlochan, M.D.A. Thomas, R.D. Hooton, The effect of pozzolans and slag on the expansion of mortars cured at elevated temperature: Part II: Microstructural and microchemical investigations, Cement and Concrete Research, 34 (2004) 1341-1356.

[11] S.-Y. Hong, F.P. Glasser, Alkali binding in cement pastes: Part I. The C-S-H phase, Cement and Concrete Research, 29 (1999) 1893-1903.

[12] S.-Y. Hong, F.P. Glasser, Alkali sorption by C-S-H and C-A-S-H gels: Part II. Role of alumina, Cement and Concrete Research, 32 (2002) 1101-1111.

[13] A.M. Boddy, R.D. Hooton, M.D.A. Thomas, The effect of the silica content of silica fume on its ability to control alkali-silica reaction, Cement and Concrete Research, 33 (2003) 1263-1268.

CHAPTER 2* ALKALI FIXATION OF C-S-H IN BLENDED CEMENT PASTES AND ITS RELATION TO ASR

The aim of this chapter is to understand how the C-S-H composition of cement pastes containing SCMs affects the pore solution. It is commonly thought that silicon and aluminium from SCMs are responsible for the decrease in alkalinity of the pore solutions of blended pastes. The role of aluminium, however, remains uncertain and has to be investigated. Different blended pastes of silica fume and metakaolin were cast, to obtain the same Si/Ca ratio of the C-S-H but with different aluminium contents on a reasonably short timescale. This method gives the opportunity to compare separately the impact of silicon and aluminium incorporation in C-S-H on the pore solution composition. Focus is given to the role of aluminium. EDS micro analysis technique was performed to determine the C-S-H compositions. In parallel, pore solutions were extracted and analysed.

* Basis of publication: T. Chappex, K. Scrivener, Alkali fixation of C–S–H in blended cement pastes and its relation to Alkali-SilicaReaction, Cem. Concr. Res. (2012), doi:10.1016/j.cemconres.2012.03.010

2.1. State of the art

2.1.1. Dissolution of silica phases in alkaline solutions

The dissolution rate of a solid mineral is a surface controlled process, controlled by the surface species detachment by reactants like H_2O, H^+ and OH^- [1]. In the case of basic solutions, which characterize pore solutions of the cement paste, minerals are dissolved mainly by OH^- species. The reaction occurs in two main steps:

1. The reactant, here OH^-, creates surface species with the mineral surface sites
2. The hydrated surface species are detached and form aqueous species in solution.

It is known that the concentration of alkalis in solution has an impact on the dissolution of siliceous minerals. Dove et al. [2, 3] studied the impact of alkalis and alkaline earth cations on the dissolution rate of quartz. Small concentration of electrolytes strongly increased the dissolution rate, and the influence was seen to be the greatest for NaCl and KCl solutions, followed by LiCl, $MgCl_2$ and H_2O. The surface coordinates as SiOH are modified to surface complexes such as SiO^- and SiO^--Na^+ in alkaline bulk solutions [4]. Dove and Elston [4] plotted the dissolution rate of quartz from several studies as a function of the fraction of >SiO^--Na^+ sites on the surface of silica, as shown in Figure 2.1. It appears that an increasing number of SiO^--Na^+ sites increases the dissolution rate. They also investigated the dissolution rate of quartz as a function of the pH of bulk solution, as shown in Figure 2.2. The dissolution rate of quartz increases with increase in the pH.

It is possible to understand the increase of dissolution rate in alkaline solutions, by considering molecular orbital calculations. For example, Strandh et al. [5] showed that the attachment of alkali cations on the surface of silica tends to increase the Si-O-Me angle and change the bond length, weakening Si-O bonds which are then easier to break (Figure 2.3). Thus, an in crease of alkali hydroxide concentration in the bulk solution results in an increase of the fraction of weakened bonds, and an increase of the reactant, OH^-, both of which increase the dissolution rate of silica. These alkali ions have an important impact on the dissolution rate of quartz, more than on other minerals [6]. This highlights the importance of

reducing the alkalinity in cement paste pore solution of concretes containing alkali reactive aggregates, ASR being controlled by the dissolution rate of the amorphous phases.

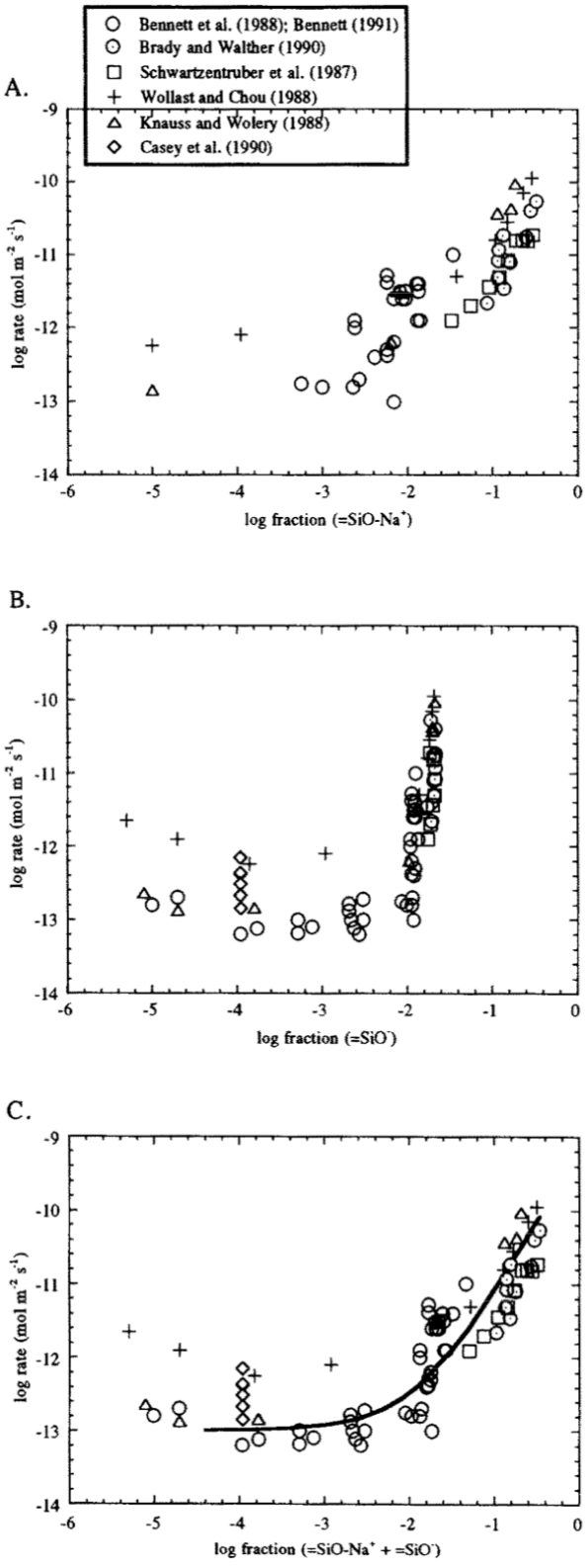

Figure 2.1. The dissolution rate of quartz vs. the fraction of each surface species calculated using the solution composition (pH, sodium concentration, and ionic strength) specific to each individual experiment from seven studies. (a) dissolution rate vs. the logarithmof $SiO^{-}\text{—}Na^{+}$ sites;(b) dissolution rates vs. the logarithm SiO^{-}; (c) dissolution rate vs. the logarithm $SiO^{-} + SiO^{-}\text{—}Na^{+}$ from [4]

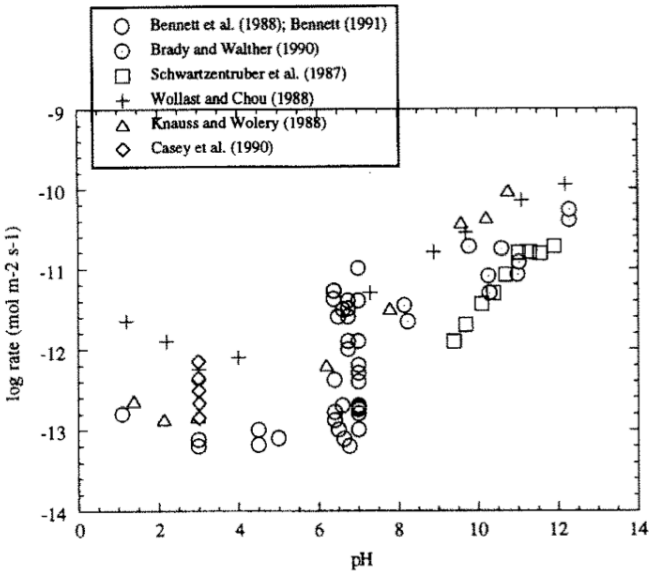

Figure 2.2. Reported dissolution rates (mol.m^{2}s^{-1}) of quartz at 25° C as a function of pH from seven studies from [4]

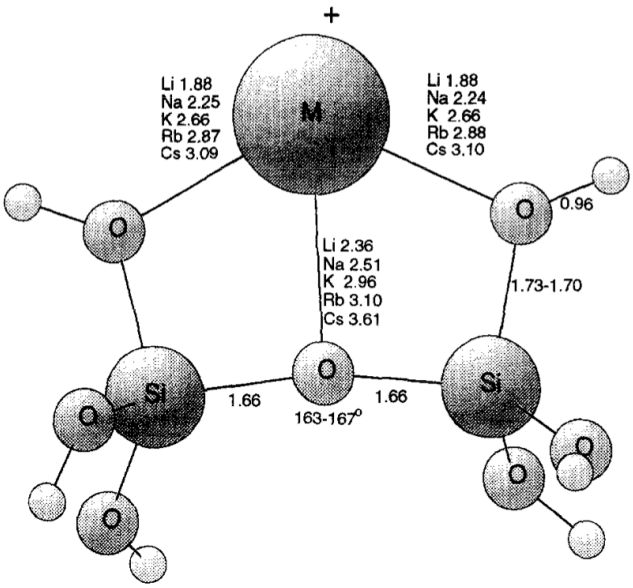

Figure 2.3. Optimized structures of alkali cation interaction with siloxane bridge of hydroxylated surface. Distances in Å and angles in degrees [5]

2.1.2. The addition of SCM and its influence on the alkalinity

It has been shown that the presence of SCMs decreases the pH of the pore solution of cement paste over and above that expected by simple dilution [7-10].

Gruber et al. [9] observed the evolution of pH in metakaolin (MK) blended pastes. The substitution of 20 % of PC by MK reduced the [OH^-] concentration of the pore solution from 0.75 M to 0.15 M at 2 years. Some researchers have shown that mineral additions have an impact on the concentration of alkalis in the pore solution of the cement paste [7, 11, 12]. Boddy et al. [13], for example, observed by pore solution extraction, that the decrease of [OH^-] was proportional to the decrease in alkali concentration in the pore solution in a ratio 1:1.

Boddy et al. analysed the concentration of the pore solutions of different blended pastes containing various amounts of silica fume [11, 13]. The expansion of mortars with reactive aggregates for the same systems was followed by the ASTM C 1260-94 test procedure (80°C in a 1 M NaOH solution). Increasing levels of silica fume led to a decrease in the alkali concentration of the pore solutions, and delayed expansion of the mortars. The delay in expansion probably corresponds to the time at which the capacity of the systems to reduce alkalinity is overwhelmed by the incoming alkali from the soak solution.

There are several indications that alumina rich SCMs, such as fly ash, slag or metakaolin are more efficient against ASR than pure silica additions such as silica fume, which are sometimes claimed to only have a delaying effect [14-16]. The exact role of alumina in suppressing deleterious ASR is however unclear. Some studies show that alumina rich SCMs have an effect on the pore solution composition of blended pastes over time. Duchesne [14] analysed the pore solution concentration in [OH^-] of blended pastes over 9 years. The blends were silica fume, fly ashes and slags substitutions at different levels. An increase of the level of substitution resulted in a decrease of the alkalinity of the system, in the same way as pure silica addition. However, there is no direct comparison of the effect of silica versus alumina. Without such comparison, the role of alumina remains uncertain.

SCMs like fly ash, silica fume or metakaolin, are known to undergo a pozzolanic reaction during cement hydration. This reaction transforms portlandite (CH) to C-S-H, richer in Si

and/or Al than C-S-H from plain PC hydration. It is commonly accepted that this change in the C-S-H composition is responsible for the decrease in alkalinity of the pore solution.

2.1.3. The alkali fixation in the C-S-H phase

The C-S-H structure is made of calcium oxide layers with chains of silicate tetrahedra attached, similar to the natural calcium silicate hydrate tobermorite [17]. The main way in which C-S-H differs from tobermorite is that the calcium to silica ratio is much higher. The difference can be accounted for mainly by the missing "bridging" tetrahedra in the silicate chains and perhaps by calcium in the interlayer. A schematic representation of a C-S-H structure is shown in Figure 2.4.

It is well established that aluminium can substitute for silicon in the bridging tetrahedra. [18, 19]. Love et al. [20] quantified aluminium incorporation by TEM analysis on blended pastes. For classical blends enriched in aluminium, like blast furnace slags or metakaolin, it was measured that the Al/Ca ratio tends to increase linearly with the increase of the Si/Ca ratio, as presented in Figure 2.5, here for 20% of OPC substitution by metakaolin.

Hong and Glasser [21, 22] studied the absorption of sodium and potassium by C-S-Hs synthesized from reagents in the laboratory. They observed that by increasing the Si/Ca or the Al/Ca of the C-S-H, the fixation of potassium and sodium increased. The hypothesis proposed to explain the effect of additional alkali fixation with more silanol groups, is that the strong bases NaOH and KOH neutralize the acidic sites Si-OH of the C-S-H layers. Moreover, the acidity of silanol groups should increase rapidly as the Ca/Si ratio decreases.

The effect of aluminium on the alkali fixation is explained by another mechanism. The incorporated aluminium in the silanol layer leads to a free negative valence, resulting in the compensation of this charge by the positive alkali ions Na^+ and K^+.

The Si/Ca ratio of the synthesized products were 0.66, 0.85 and 1.2. The corresponding Al/Ca ratios for these three pastes were 0.08, 0.055 and 0.044. By comparing these values with the measured blends from Love et al. it appears that the synthesized C-S-H phases are very different from the 20% metakaolin blends. The principal difficulty of this type of study is to

fully control the chemistry of the synthesized phases, which is not always possible. Hong and Glasser mentioned in their study that they had difficulties knowing the coordination of aluminium and the homogeneity of the synthesised C-S-H. Another study by Stade done in 1989 [23] tends to confirm these difficulties. He observed that the synthesized C-S-H containing aluminium were less able to incorporate potassium than aluminium free systems, which is in contradiction with the study of Hong and Glasser.

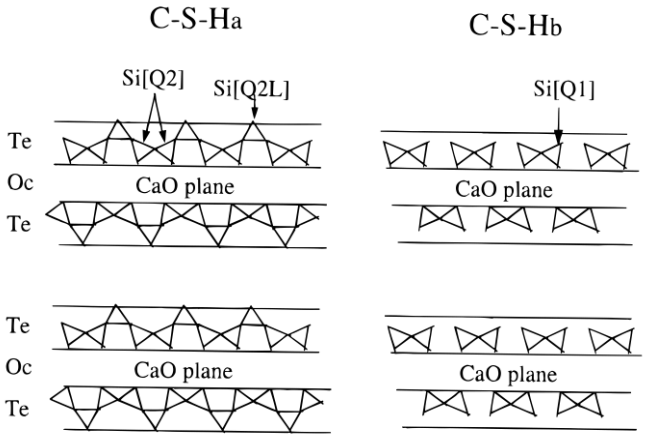

Figure 2.4. Silica chains in the C-S-H structure. For nonsubstituted structures, the Ca/Si molar ratio is 0.66 for C-S-Ha when no calcium is in the interlayer space. This ratio is superior at 1.5 for the C-S-Hb structure. In C-S-Ha, Ca in the octahedral plane is 7-fold coordinated [24].

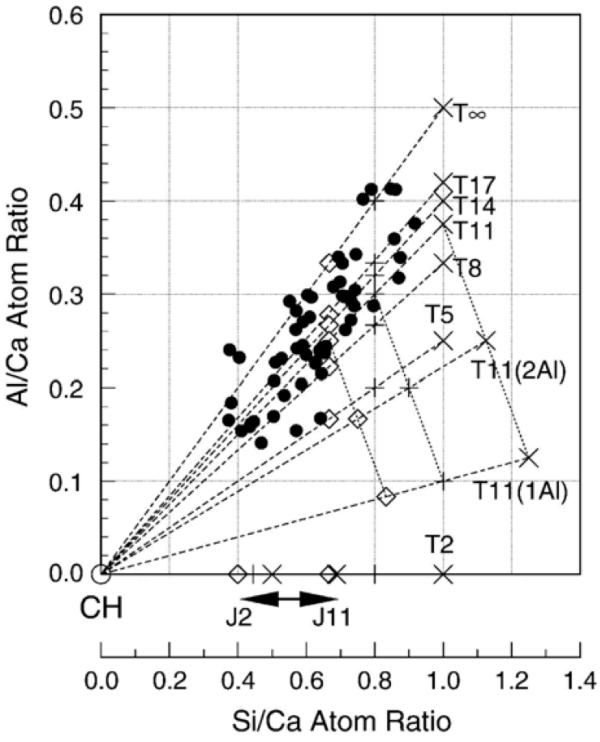

Figure 2.5. TEM-EDX data for outer product C-S-H of a KOH activated 20% metakaolin blended paste**.** Symbols represent the compositions of tobermorite- (T) or jennite-based (J) structural units with different levels of protonation of the silicate chains [20].

2.2. Materials and methods

2.2.1. Materials

The aim of the experimental program was to produce blended pastes containing C-S-H with a similar Si/Ca ratio but different Al contents. Pastes with three substitution levels of 5, 10 and 15% of metakaolin were cast with a water to binder (W/B) ratio (by weight) of 0.5. To obtain pastes with a similar Si/Ca ratio of the C-S-H but with minimal aluminium content, pastes were cast containing additions of silica fume to give the same content of reactive silica as in the metakaolin blends. To have the same overall level of substitution, and so the same effects of dilution, fine ground quartz (d50 = 7.6 µm, SSA = 1.6 m^2/g, assumed nonreactive) was added to these blends. The composition of the different blends is shown schematically in Figure 2.6. The type and the oxide composition of the different anhydrous phases are given in the Table 2.1.

The aggregates used were a Swiss reactive gneiss and a highly reactive North American river aggregate. The oxide contents of the two aggregates were analyzed by XRF and are given in Table 2.1. The petrography of the aggregates is presented in Table 2.2.

Table 2.1. Composition (XRF), d50, specific surface area and origin of raw materials

[%w]	**SiO_2**	**Al_2O_3**	**CaO**	**MgO**	**SO_3**	**K_2O**	**Na_2O**	**P_2O_5**	**MnO**	**TiO_2**	**Fe_2O_3**	**LOI**	**d50[µm] SSA[m^2/g]**	**Producer and type**
OPC	21.0	4.6	64.2	1.8	2.8	0.9	0.2	0.4	0.0	0.1	2.6	1.3	14.2 0.5	Holcim CEM I
Metakaolin	50.6	46.9	0.0	0.1	0.1	0.2	0.3	0.0	0.2	1.3	0.3	0.0	5.6 1.5	Burgess Optipozz
Silica fume	98.3	0.2	0.2	0.1	0.0	0.3	0.0	0.0	0.0	0.3	0.5	0.0	4.8 1.1	Elkem Micro-silica Grade983U
Swiss Alps agg.	78.9	10.1	0.7	0.8	0.1	5.2	0.5	0.0	0.0	0.3	2.0	1.0		
N. Am. agg.	79.2	9.2	1.4	0.5	0.0	3.0	2.3	0.0	0.1	0.3	2.2	1.2		

Table 2.2. Petrography of the a) Swiss reactive aggregate and b) North American reactive sand [25]

Aggregate	Rock type [%w]	Silicate [%w]	Silicate
Swiss Alps aggregate	Chlorite schist - 100	>95	Quartz, feldspar, chlorite >>> muscovite > biotite
N. American aggregate	Chert, volcanic - 100	>90	Chert, Granitic >> volcanic > quartzite > sandstone

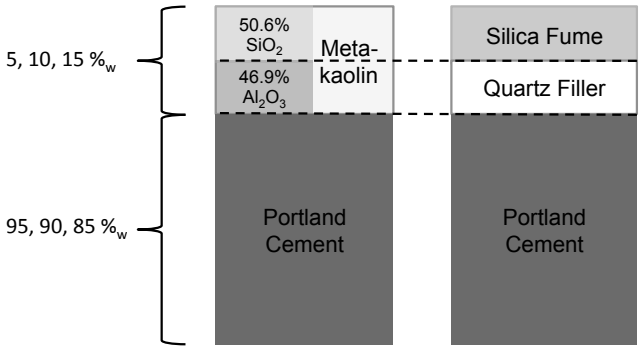

Figure 2.6. Schematic representation of the blended systems

2.2.2. Methods

2.2.2.1. Mortar expansion

Mortar bars (40 x 40 x 160 mm) containing the same blended pastes were cast with metallic measurement studs. The aggregate to cement ratio was 3. The mortars were first cured for 28 days at 20°C and 95% RH. The mortar bars were then put in an alkaline solution containing 0.6 molar NaOH at 38°C, in order to accelerate the expansion (3 bars in 1.5 liters soak solution). For this concentration of soak solution, alkalis will diffuse into the mortars and will eventually overwhelm the mitigating effects of the SCM.

2.2.2.2. EDS micro analysis

The C-S-H compositions in all blended pastes were measured by EDS micro analysis (Bruker AXS XFlash Detector 4030 133eV) in a Scanning Electron Microscope. The paste samples were cut at different times, immersed in isopropanol, to remove water and stop the hydration. They were then dried and impregnated with an epoxy resin. The samples were mechanically polished down to 1 micron. Around 100 measurement points were done for each of inner and outer C-S-H product (15 keV). These measurements give the composition of the C-S-H in term of calcium, silicon and aluminium in atomic percent.

2.2.2.3. Thermo gravimetric analysis

Thermo gravimetric analysis (Metler Toledo) was carried out on approximately 60 mg of stopped paste sample to measure the portlandite content of the different blends. The heating rate was 10°C per minute from 30°C to 900°C under an N_2 atmosphere. The portlandite content was calculated from the weight loss between 400°C and 500°C, using the tangent method to define the step size taking into account the C-S-H background.

2.2.2.4. XRD analysis

The XRD patterns of powdered pastes were collected using a PANalytical X'Pert Pro MPD diffractometer in a θ-θ coordination with CuKα radiation, with 2θ from 7° to 70°.

2.2.2.5. Pore solution extraction

A batch of pastes was cast in 200 ml sealed containers and stored at 20°C. They were pressed in an pore solution extraction device (following [26]) to extract the pore solution at several ages between 28 days and 2 years. The solutions obtained were analyzed by inductive coupled plasma (ICP-MS), to obtain their ionic concentrations.

2.3. Results

2.3.1. Accelerated expansion tests

Expansion curves for the various blends and the two aggregates are shown in Figure 2.7. It is seen that the highly reactive North American aggregate expands more and at a higher rate than the Swiss Alpine aggregate for all blends. The higher the substitution level, the slower and lower is the expansion. It is also visible that the systems containing alumina (metakaolin) show lower expansions over time.

The mortar bars studied here are exposed to more aggressive conditions than would be found in the field, with a soak solution of 0.6 M NaOH providing a reservoir of alkalis which can overcome the effects of the SCMs. Nevertheless higher levels of substitution are more effective in reducing expansion.

The soak solutions were analysed at 400 days. The difference in concentration from the starting solution is shown in Table 2.3. The decrease in alkalinity of the curing baths is similar in the metakaolin and silica fume – quartz systems, indicating a similar uptake of alkali for the two systems.

Due to the difference in temperature and alkalinity, the pore solutions and the expansion of the systems have to be compared with care. It is known that when C-S-H is *formed* at higher temperature it has a higher density [27]. However, the first 28 days curing at 95%RH is always at 20°C, during which time about 80% of the cement will react. The fact that most C-S-H is formed at the same temperature means that the C-S-Hs in the mortar and in the pastes studied below should be similar.

Table 2.3. Decrease in sodium concentration of the mortar expansion test curing solutions after 400 days. Start concentration: 600 mM NaOH. (mean error 10%)

	OPC	**10% MK**	**15% MK**	**10% SFQ**	**15% SFQ**
ΔNa [mM]	104.8	117.7	118.6	117.9	125.6

(a)

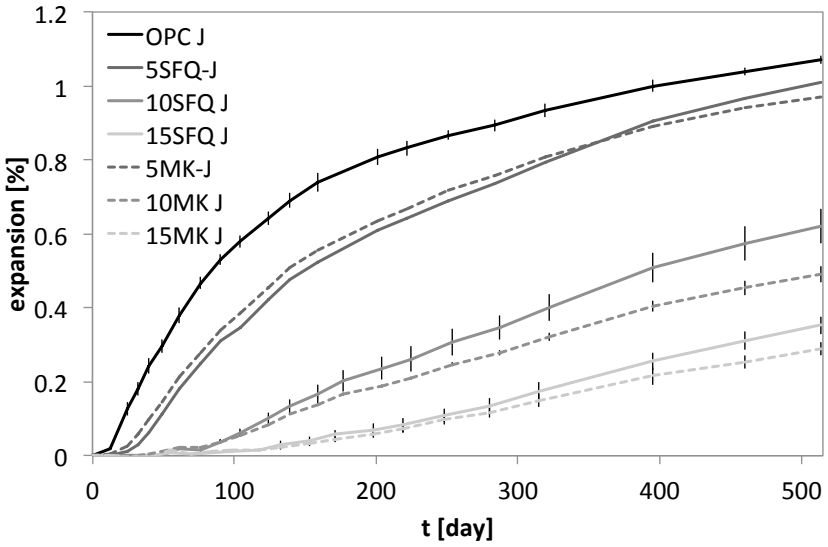

(b)

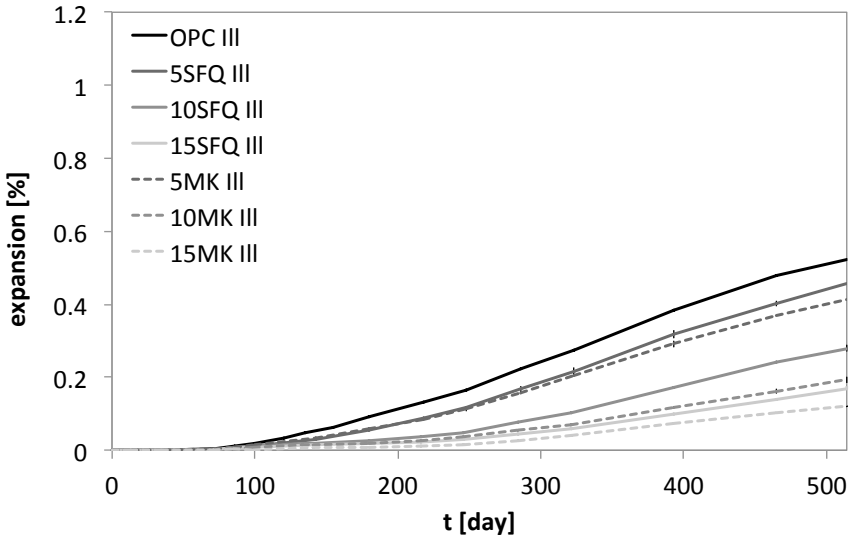

Figure 2.7. Expansion versus time of (a) a very reactive North American aggregate and (b) a reactive Swiss Alps aggregate – 38°C 0.6M NaOH solution. It is visible that the MK systems are more efficient against ASR for a same substitutions level.

2.3.2. C-S-H composition by SEM - EDS

The C-S-H compositions at 90, 300 and 500 days are shown as a function of Al/Ca vs Si/Ca in Figure 2.8 and Table 2.4 for inner and outer product. As expected, the higher the substitution level (silica fume or metakaolin); the higher is the Si/Ca ratio, due to the increase of added silica. It appears that the C-S-H in the metakaolin blended pastes has a similar distribution of Si/Ca ratios to the silica fume – quartz systems. However, as intended, the Al/Ca ratios of the metakaolin blended pastes increase with the substitutions level from 0.07 to 0.15, whereas the silica fume – quartz systems all have a similar Al/Ca ratio of approximately 0.06, independent of the substitution level.

Table 2.4. Al/Ca and Si/Ca of the different C-S-H at 300 days in atomic percent (from EDS analysis). Average value of approx. 60 measurement points.

	OPC	**5% MK**	**10% MK**	**15% MK**	**5% SFQ**	**10% SFQ**	**15% SFQ**
Al/Ca	0.05	0.07	0.10	0.17	0.05	0.06	0.08
strd error	0.003	0.003	0.004	0.009	0.002	0.001	0.001
Si/Ca	0.50	0.55	0.58	0.63	0.54	0.58	0.63
strd error	0.002	0.005	0.003	0.007	0.003	0.002	0.002

(a)

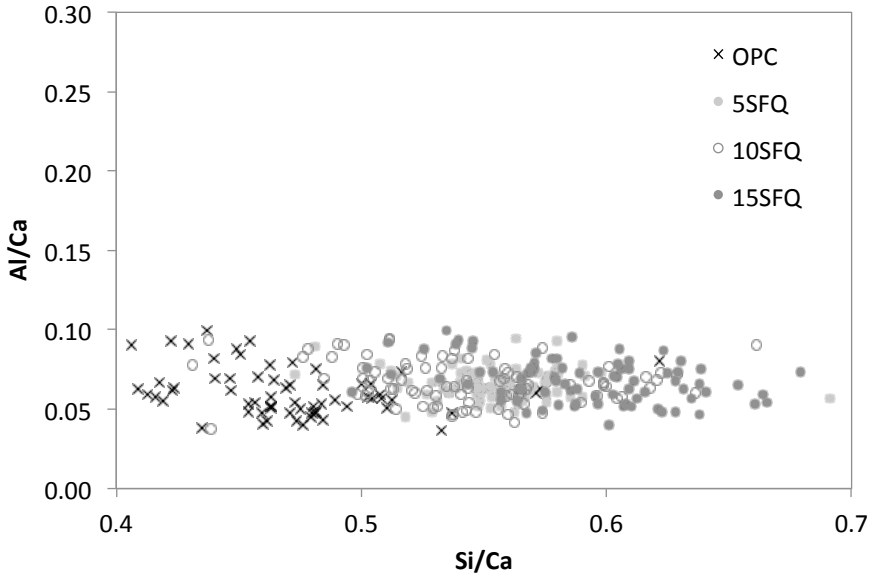

(b)

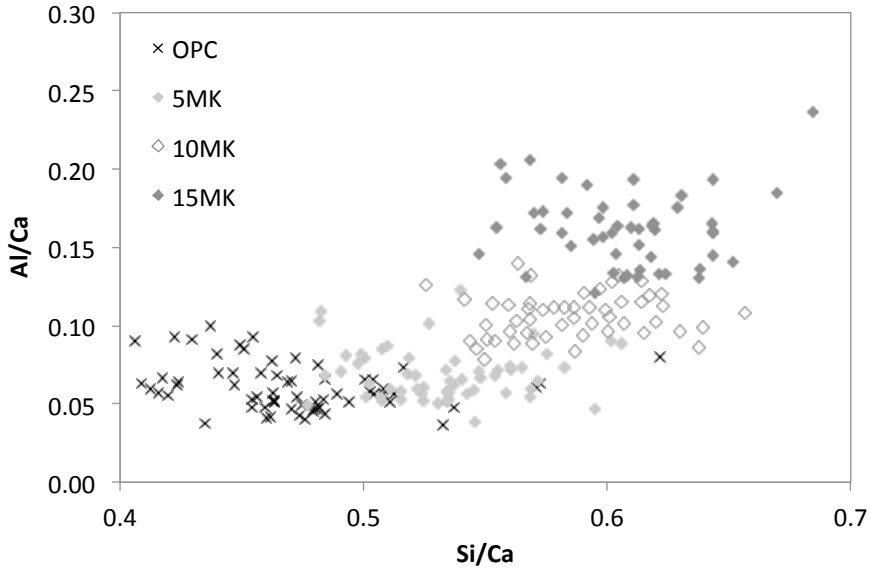

Figure 2.8. Caption next page

(c)

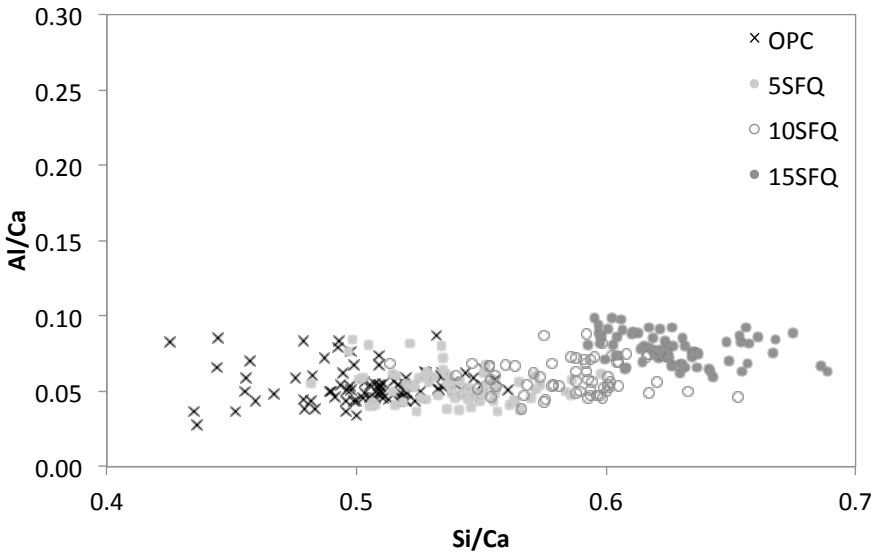

(d)

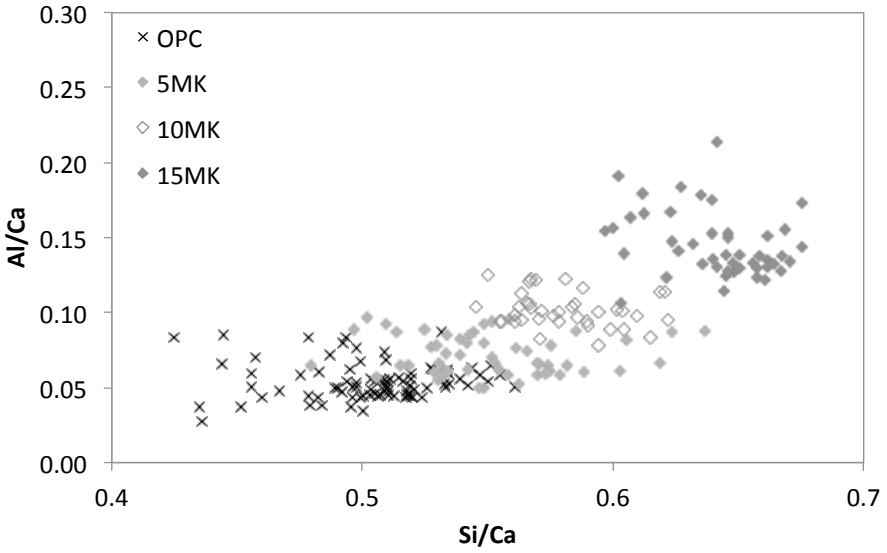

Figure 2.8. C-S-H composition of the different bends, at (a) SFQ 90 days, (b)MK 90 days (c) SFQ 300 days (d) MK 300 days for the outer product.

2.3.3. Thermo gravimetric analysis

Thermo gravimetric analyses were made on the blended pastes at 90 and 300 days. Thermo gravimetric curves are shown in Figure 2.9 for 10 % and 15 % of substitution at the two ages. In addition to the normal features, the peak around 180°C for the metakaolin substituted pastes is considered to be strätlingite (C_2ASH_8), as also indicated by XRD (peak at 7.066° 2θ) and previously found for such pastes [28]. The metakaolin systems have lower peaks around 30-150°C corresponding mainly to C-S-H, as some of the silicate reacting goes into the strätlingite. The tangent method was used to estimate the portlandite weight loss. Table 2.5 gives the total weight loss, between 30 and 550°C and the portlandite weight loss between 400 and 450°C. The total weight loss for the metakaolin systems are very similar to those of the silica fume – quartz systems, however the metakaolin systems have a lower Portlandite content as the reaction of both the silicate and aluminate components in the metakaolin consumes lime.

Table 2.5. TGA weight losses, calculated free water and free alkalis in mass percent of the blended paste at 90 and 300 days

		OPC	**10% MK**	**15% MK**	**10% SFQ**	**15% SFQ**
Total hydrates	90 days	21.0	21.2	21.5	20.3	19.9
[%w] +- 0.2	300 days	22.9	21.1	21.3	20.6	20.3
Portlandite	90 days	4.5	2.6	1.8	3.5	2.8
[%w] +- 0.2	300 days	4.4	1.6	1.7	3.0	2.7
C-S-H_{water} (30°C-150°C)	90 days	6.8	6.7	6.9	7.2	7.6
[%w] +- 0.2	300 days	7.8	6.9	6.9	7.8	8.0
Free water	90 days	12.3	12.1	11.8	13.0	13.4
[%w] +- 0.2	300 days	10.4	12.2	12.0	12.7	13.0
Free alkalis	90 days	3.9	2.5	1.6	2.1	1.6
[mmol/100g paste]	300 days	3.6	2.7	1.3	2.5	1.7

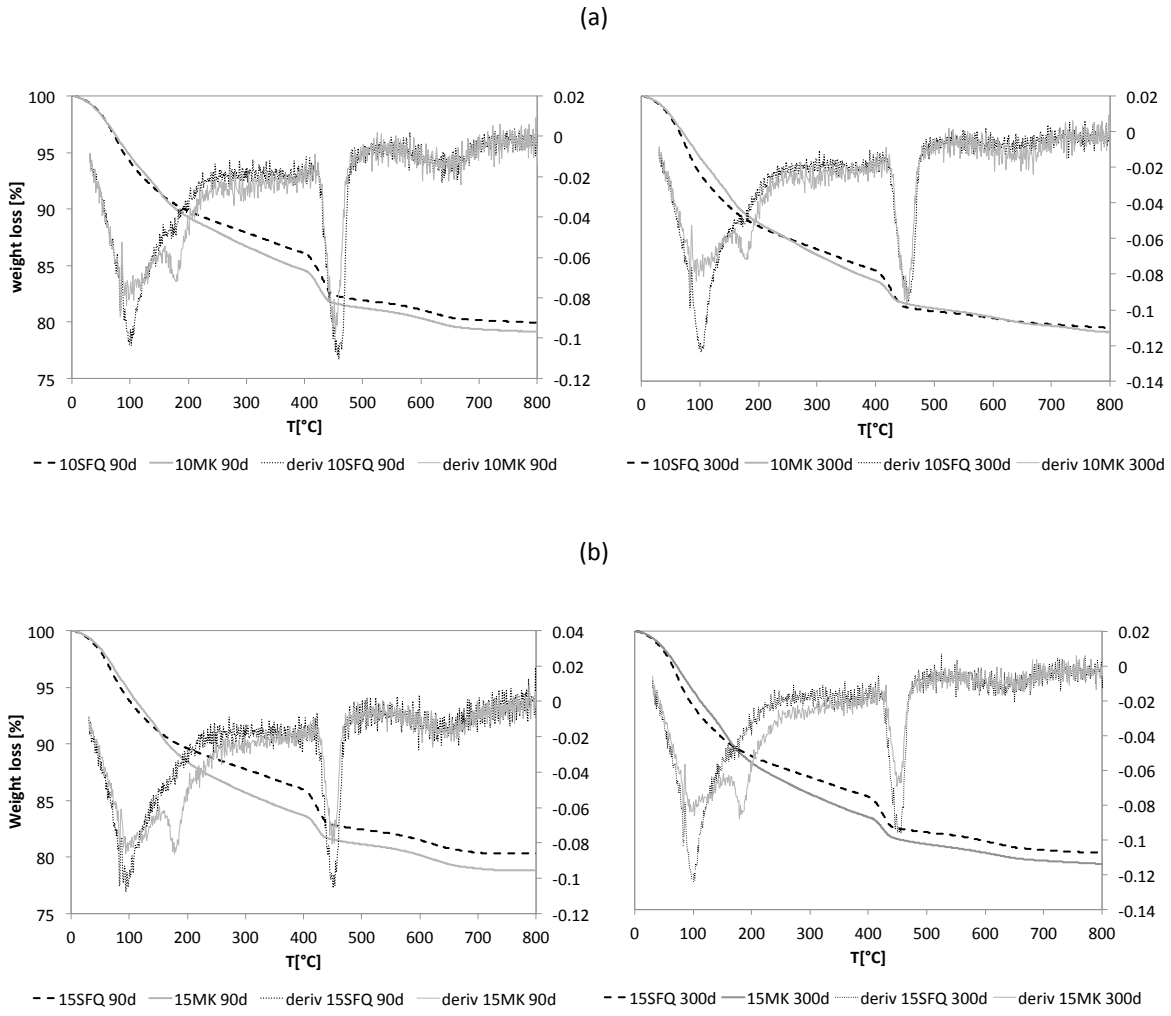

Figure 2.9. Thermogravimetric analysis of the (a) 10% and (b) 15% blended pastes and their derivatives at 90 and 300 days. Strätlingite peak it visible on MK systems at 190°C

2.3.4. Pore solution compositions

The analyses of sodium and potassium ions in the expressed pore solutions are shown in Figure 2.10. The concentrations of potassium and sodium are plotted as a function of time up to 2 years. The higher the substitution of SCM, the lower is the alkalinity of the pore solution at a given time. For 5 and 10% of substitution levels, the silica fume pastes have a bigger alkali decrease than the metakaolin systems. At 15% of substitution the evolution of alkalinity is similar for both systems.

After an initial decrease in the alkali content of the pore solution between 28 and 90 days, there appears to be a small increase for 300 days and 2 years. Similar increases are reported elsewhere [14]. This increase may be explained by the fact that the older pastes were pressed at a stress of 450 MPa, whereas the younger pastes were pressed at 225 MPa. Previous studies [29, 30], have shown that the extraction load has an effect on the pore solution concentration. To verify the magnitude of this effect, a 550 day old OPC cured at 20°C in a sealed container was cut into three pieces. The extraction pressures used were 230 MPa, 420 MPa and 800 MPa. The results are shown in Table 2.6. The ion concentrations measured increase with an increase of the load, in the same range as the increases between 90 and 300 days reported above.

The concentrations of aluminium, silicon and calcium are shown in Figures 2.11, 2.12 and 2.13. It is visible that for metakaolin pastes, the aluminium concentration increases with the substitutions level, until 2.7 mM at 28 days for the 15 % substitution. Silicon is present in low concentrations in the pore solution, but tends to increase slightly between 300 and 500 days. This increase is maybe due to a variation in the solution equilibrium due to a decrease in the pozzolanic reaction at these late ages. The increase remains however under the mM scale and has to be considered with reserve, taking into account the ICP measurement error (about +/- 0.5 mM).

The calcium concentration rapidly drops from 22 mM at 1 hour, corresponding to the saturation of portlandite in water, to less than one mM over the long term, despite the presence of portlandite as one sees in the TGA analysis. This is mainly due to the presence of alkalis in the system that increase OH^- concentration in the solution, so decreases the Ca^{2+} by common ion effect.

Table 2.6. Effect of load on the alkalis concentration. OPC paste at 550 days (E/C of 0.5)

load [Mpa]	Na [mM]	K [mM]
230	100	266
420	110	290
800	121	317

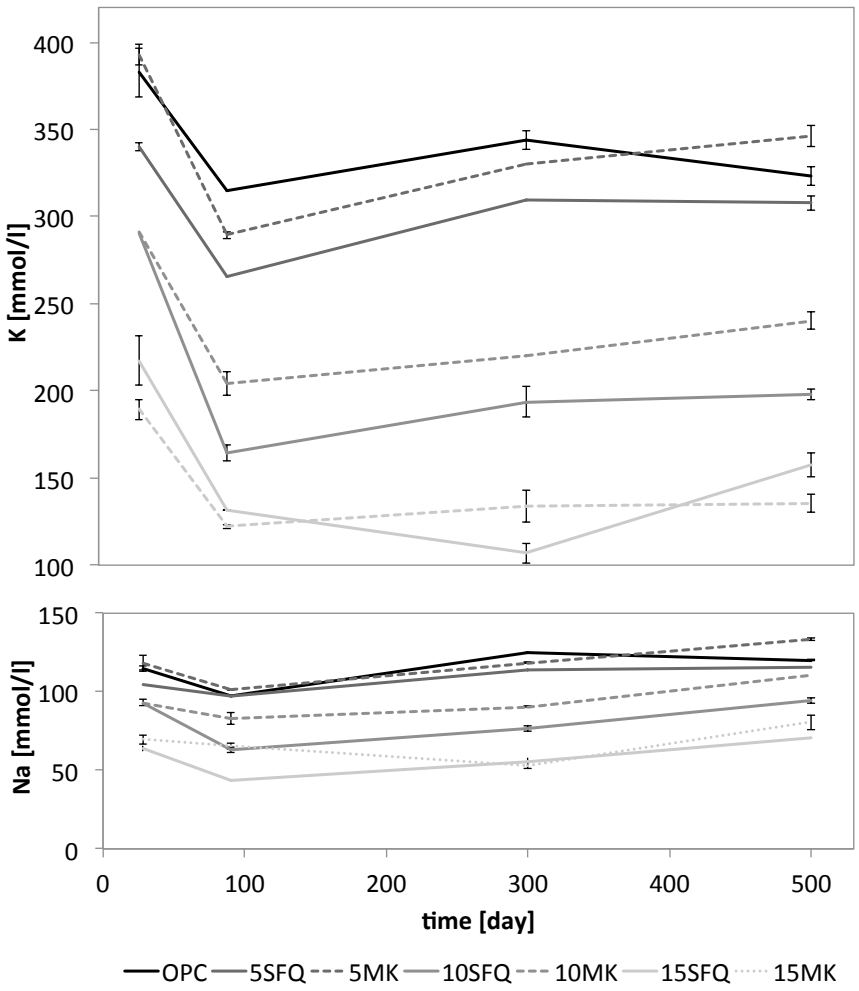

Figure 2.10. Potassium and sodium concentration of the different pore solutions over time.

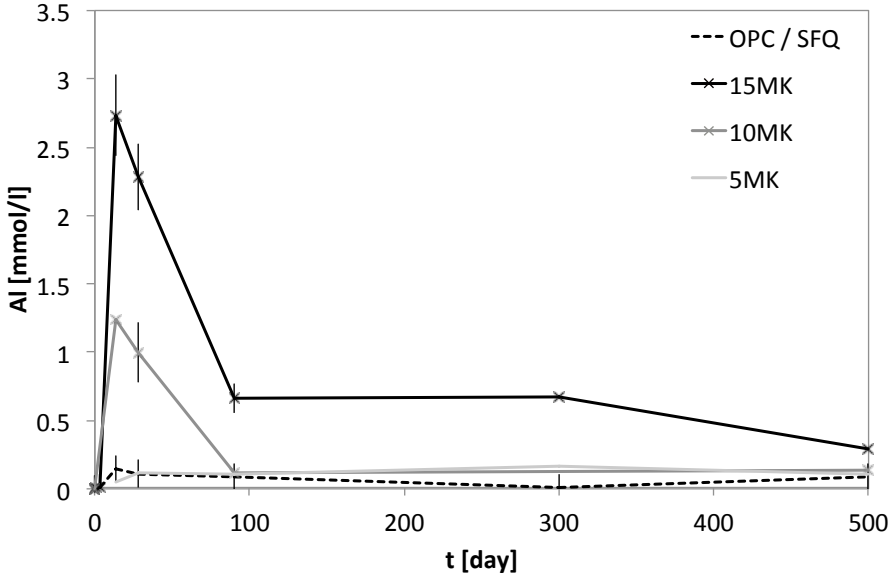

Figure 2.11. Aluminium concentration of the different pore solutions over time

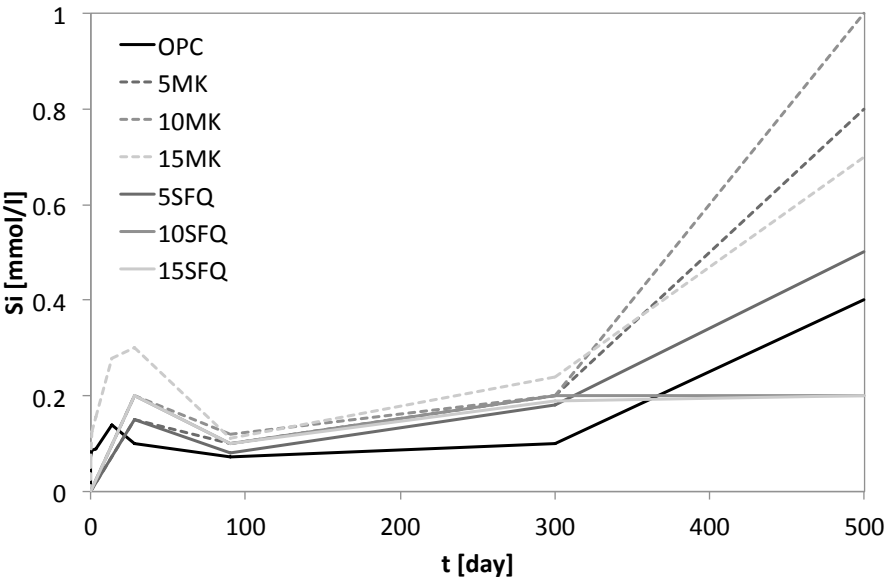

Figure 2.12. Silicon concentration of the different pore solutions over time

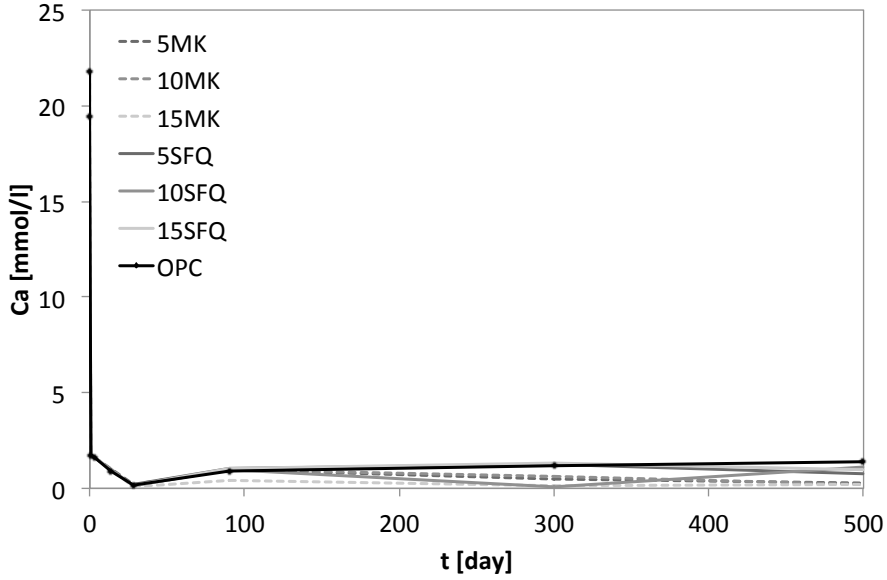

Figure 2.13. Calcium concentration of the different pore solutions over time

2.3.5. Estimation of the fixation capacity of the different C-S-H products

As mentioned in section 2.3.3, the TGA results show a difference in the amount of hydrates present in the systems and this must be considered to compare the fixation capacity of C-S-H. The alkalis fixed in the C-S-H phase can be estimated, if the amount of C-S-H and the amount of pore solution and its concentration are known. The real amount of C-S-H is difficult to define for such blended systems. However, a comparative analysis can be done by considering the bound water in C-S-H of each blend. To avoid interference from strätlingite, the comparison was made on the basis of the weight loss, between 30 and 150°C, before the dehydration of the AFm phases, assuming that this will be proportional to the total amount of C-S-H in each sample.

The amount of free water was estimated by subtracting the total measured bound water (up to 800°C) from the water added during mixing. The results of this analysis are shown in Table 2.5. From the pore solution analysis the free alkali are calculated, and this figure is subtracted from the total alkalis present in the system to give the "fixed" alkali. Finally the total amount of "fixed" alkali is divided by the C-S-H bound water (weight loss 30-150°C) to give a relative measure of the concentration of alkalis fixed by the C-S-H. These comparative values are shown in Figure 2.14 for 10% and 15% of SCM substitution at 90 and 300 days. Although there is quite a high error in these calculations, the trend is clear: more alkalis per unit C-S-H are fixed in the blended systems with the 15% systems showing higher values than the 10% systems. The values at 90 and 300 days are similar. Most importantly, there is no significant difference in the values of the metakaolin blends compared to the silica fume – quartz blends. This indicates that the aluminium enrichment of C-S-H does not increase its alkali fixation capacity.

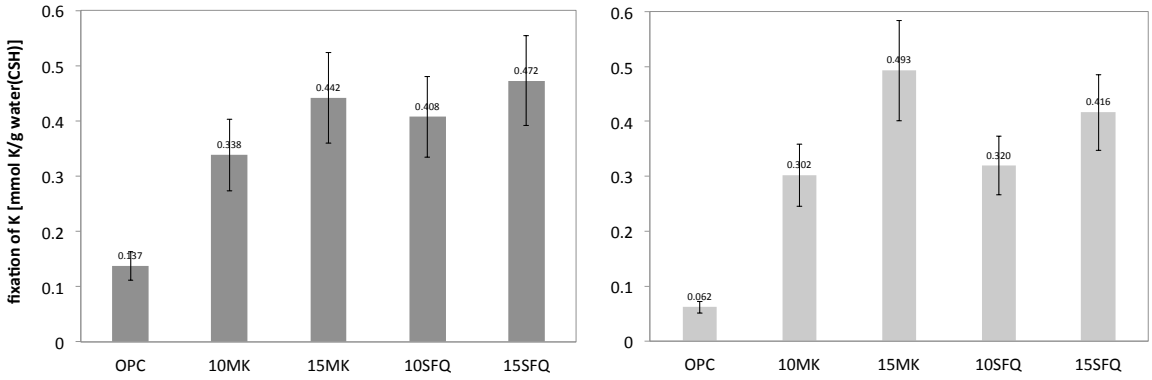

Figure 2.14. Estimation of the amount of fixed potassium at 90 and 300 days for the 10 and 15% blends per gramm of C-S-H water

2.4. Discussion

The results of this study confirm that SCM additions with aluminate can be more effective in reducing expansion due to alkali silica reaction, however this does not correspond to a greater reduction in the alkalinity of the pore solution. This indicates that a phenomenon other than alkali fixation is involved for alumina rich SCMs.

Although the C-S-H in the metakaolin systems clearly had a higher alumina content by EDS, the "fixation" capacity for alkalis appears to be similar to that of the C-S-H in the silica fume quartz systems. It is commonly assumed that the incorporation of alumina increases the fixation capacity of C-S-H due to the study of Hong and Glasser [22]. However, a closer examination shows that our results are not in disagreement with their study.

Figure 2.15 shows the results from the study of Hong and Glasser. There is a drastic reduction in the capacity for alkali absorption with an increase in the Ca/Si ratio of the C-S-H – the vertical scale on the graphs changes from left to right, a dotted line indicates the same value of 0.5 mM/g. The C-S-H of a 15% metakaolin paste at 28 days has a Ca/Si ratio of about 1.5, similar to the highest Ca/Si ratio synthesized C-S-H studied by Hong and Glasser. The alkali concentration of the OPC paste at 28 days is around 110 mM of sodium and 400 mM potassium (Figure 2.10), in the blended systems this is reduced 50 and 110 mM respectively. This range of concentrations is indicated by the grey zones in figure 2.15. It is clear that the effect of alumina on alkali absorption of synthesized C-S-H *at these concentrations* is extremely small. This supports our finding that alumina in C-S-H does not drastically change the alkalinity of the pore solution in real blended pastes.

An hypothesis can be proposed to explain the inefficiency of aluminium regarding alkali fixation in C-S-H: several researchers proposed that aluminium might substitute for calcium in the interlayer. Andersen and Skibsted observed by ^{27}Al and ^{29}Si MAS NMR investigation, that aluminium also substitute for calcium in the C-S-H [18]. Faucon et al. propose that above a Ca/Si ratio of 1.5, Al^{3+} doesn't only substitute Si^{4+} but also replaces Ca^{2+} in the CaO layer. This substitution of Ca^{2+} by Al^{3+} would generate a positive charge that increases the concentration of OH^- on the surface and repels positive alkali ions [24].

This study shows that the efficacy of alumina-containing SCMs in reducing expansion due to alkali silica reaction depends on some other mechanism.

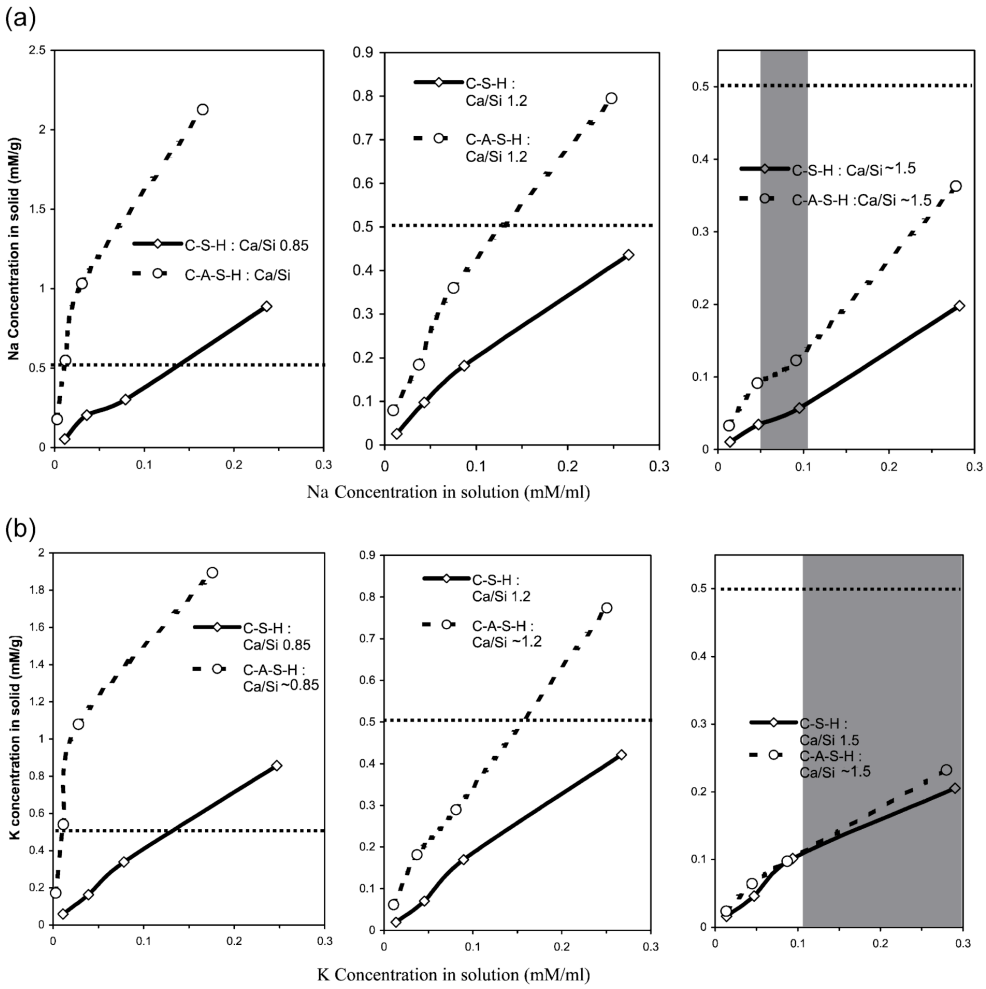

Figure 2.15. From [22]**.** Comparison of alkali binding between C-S-H and C-A-S-H gels. Solid lines and dashed lines indicate C-S-H and C-A-S-H gel, respectively. (In C-A- S-H gels, Si/Al = 16.2 (Ca/Si = 0.85), 14.1 (Ca/Si = 1.2) and 13.3 (Ca/Si = 1.5)). Na concentration in C-A-S-H gel (1 Na = 1 Al). (b) Comparison of alkali binding between C-S-H and C-A-S-H gels. Solid lines and dashed lines indicate C-S-H and C-A-S-H gel, respectively. (In C-A-S-H gels, Si/Al = 16.2 (Ca/Si = 0.85), 14.1 (Ca/Si = 1.2) and 13.3 (Ca/Si = 1.5)). K concentration in C-A-S-H gel (1 K = 1 Al).

2.5. References

[1] W. Stumm, Reactivity at the mineral-water interface:

dissolution and inhibition Colloids and surface, 120 (1996) 143-166.

[2] P.M. Dove, The dissolution kinetics of quartz in aqueous mixed cation solutions, Geochimica et Cosmochimica Acta, 63 (1999) 3715-3727.

[3] P.M. Dove, C.J. Nix, The influence of the alkaline earth cations, magnesium, calcium, and barium on the dissolution kinetics of quartz, Geochimica et Cosmochimica Acta, 61 (1997) 3329-3340.

[4] P.M. Dove, S.F. Elston, Dissolution kinetics of quartz in sodium chloride solutions: Analysis of existing data and a rate model for 25¬∞C, Geochimica et Cosmochimica Acta, 56 (1992) 4147-4156.

[5] H. Strandh, L.G.M. Pettersson, L. Söjberg, U. Wahlgren, Quantum chemical studies of the effects on silicate mineral dissolution rates by adsorption of alkali metals, Geochimica et Cosmochimica Acta, 61 (1997) 2577-2587.

[6] P.M. Dove, D.A. Crerar, Kinetics of quartz dissolution in electrolyte solutions using a hydrothermal mixed flow reactor, Geochimica et Cosmochimica Acta, 54 (1990) 955-969.

[7] M. Kawamura, K. Takemoto, Correlation between pore solution composition and alkali silica expansion in mortars containing various fly ashes and blastfurnace slags, International Journal of Cement Composites and Lightweight Concrete, 10 (1988) 215-223.

[8] M.D.A. Thomas, M.H. Shehata, S.G. Shashiprakash, D.S. Hopkins, K. Cail, Use of ternary cementitious systems containing silica fume and fly ash in concrete, Cement and Concrete Research, 29 (1999) 1207-1214.

[9] K.A. Gruber, T. Ramlochan, A. Boddy, R.D. Hooton, M.D.A. Thomas, Increasing concrete durability with high-reactivity metakaolin, Cement and Concrete Composites, 23 (2001) 479-484.

[10] I. Canham, C.L. Page, P.J. Nixon, Aspects of the pore solution chemistry of blended cements related to the control of alkali silica reaction, Cement and Concrete Research, 17 (1987) 839-844.

[11] A.M. Boddy, R.D. Hooton, M.D.A. Thomas, The effect of the silica content of silica fume on its ability to control alkali-silica reaction, Cement and Concrete Research, 33 (2003) 1263-1268.

[12] M.H. Shehata, M.D.A. Thomas, The effect of fly ash composition on the expansion of concrete due to alkali-silica reaction, Cement and Concrete Research, 30 (2000) 1063-1072.

[13] A.M. Boddy, R.D. Hooton, M.D.A. Thomas, The effect of product form of silica fume on its ability to control alkali-silica reaction, Cement and Concrete Research, 30 (2000) 1139-1150.

[14] J. Duchesne, M.-A. Bérubé, Long-term effectiveness of supplementary cementing materials against alkali-silica reaction, Cement and Concrete Research, 31 (2001) 1057-1063.

[15] W. Aquino, D.A. Lange, J. Olek, The influence of metakaolin and silica fume on the chemistry of alkali-silica reaction products, Cement and Concrete Composites, 23 (2001) 485-493.

[16] T. Ramlochan, M.D.A. Thomas, R.D. Hooton, The effect of pozzolans and slag on the expansion of mortars cured at elevated temperature: Part II: Microstructural and microchemical investigations, Cement and Concrete Research, 34 (2004) 1341-1356.

[17] I.G. Richardson, Tobermorite/jennite- and tobermorite/calcium hydroxide-based models for the structure of C-S-H: applicability to hardened pastes of tricalcium silicate, [beta]-dicalcium silicate, Portland cement, and blends of Portland cement with blast-furnace slag, metakaolin, or silica fume, Cement and Concrete Research, 34 (2004) 1733-1777.

[18] M.D. Andersen, H.J. Jakobsen, J. Skibsted, Incorporation of Aluminum in the Calcium Silicate Hydrate (C-S-H) of Hydrated Portland Cements: A High-Field 27Al and 29Si MAS NMR Investigation, Inorganic Chemistry, 42 (2003) 2280-2287.

[19] I.G. Richardson, The nature of C-S-H in hardened cements, Cement and Concrete Research, 29 (1999) 1131-1147.

[20] C.A. Love, I.G. Richardson, A.R. Brough, Composition and structure of C-S-H in white Portland cement-20% metakaolin pastes hydrated at 25°C, Cement and Concrete Research, 37 (2007) 109-117.

[21] S.-Y. Hong, F.P. Glasser, Alkali binding in cement pastes: Part I. The C-S-H phase, Cement and Concrete Research, 29 (1999) 1893-1903.

[22] S.-Y. Hong, F.P. Glasser, Alkali sorption by C-S-H and C-A-S-H gels: Part II. Role of alumina, Cement and Concrete Research, 32 (2002) 1101-1111.

[23] H. Stade, On the reaction of C-S-H(di, poly) with alkali hydroxides, Cement and Concrete Research, 19 (1989) 802-810.

[24] P. Faucon, A. Delagrave, C. Richet, J.M. Marchand, H. Zanni, aluminum incorporation in calcium silicate hydrates (C-S-H) depending on their Ca/Si ratio, The Journal of Physical Chemistry B, 103 (1999) 7796-7802.

[25] V. Villeneuve, Détermination de l'endommagement du béton par méthode pétrographique quantitative, in: Géologie et génie géologique, Laval, Quebed

c, 2011.

[26] K.J.Folliard. J.H. Ideker, B. Fournier and M.D.A. Thomas, The role of “non-reactive” aggregates in the Accelerated (60 °C) Concrete Prism Test, in: Proceedings from the Marc-André Bérubé Symposium on alkali–aggregate reactivity in concrete, 8th CANMET/ACI International Conference on Recent Advances in Concrete Technology, CANMET, Montreal, 2006, pp. 45-70.

[27] X. Zhang, quantitative microstructural characterisation of concrete cured under realistic temperature conditions, in: LMC, EPFL, Lausanne, 2007.

[28] R. Fernandez, F. Martirena, K.L. Scrivener, The origin of the pozzolanic activity of calcined clay minerals: A comparison between kaolinite, illite and montmorillonite, Cement and Concrete Research, 41 (2011) 113-122.

[29] B. Lothenbach, Thermodynamic equilibrium calculations in cementitious systems, Materials and Structures, 43 (2010) 1413-1433.

[30] C.Tremblay. M-A Bérubé, Chemistry of pore solution expressed under high pressure-influence of various parameters and comparison with the hot water extraction method, in: I.a.p.w.p. corporation (Ed.) ICAAR, Beijing, 2004, pp. 833-842.

CHAPTER 3* THE INFLUENCE OF ALUMINIUM IN SOLUTION ON THE DISSOLUTION OF AMORPHOUS SILICA

Several studies have shown that alumina-rich SCMs such as fly ash, metakaolin or slags are more efficient in preventing ASR expansion than pure silica additions [1-3].

It was shown in Chapter 2 through the study of C-S-H and pore solutions, that the incorporation of aluminium in C-S-H, contrary to silicon, had no measurable effect of lowering the alkali concentration of the cement paste pore solution for real blended pastes. It was proposed that another mechanism might control ASR in presence of additional alumina in blended concrete.

The aim of this study is to find out if the presence of additional aluminium provided by SCMs in the pore solution of cement pastes is able to reduce gel formation in reactive aggregates. This mechanism, observed in geology and marine chemistry studies, was investigated for concrete conditions. The incorporation mechanism of aluminium on amorphous silica and how it controls dissolution were studied. This mechanism has been investigated for highly alkaline, calcium-saturated systems and over periods of months to years. This study was realized in two main parts. First, the effect of aluminium in solution on reactive aggregates gel formation was studied. In a second part, a more fundamental study on amorphous silica plates gave information about the mechanism controlling silica dissolution in presence of aluminium in the pore solution.

* Basis of publications : 1) The influence of aluminium on the dissolution of amorphous silica and its relation to alkali silica reaction, T. Chappex, K. Scrivener, under review, 2) The effect of aluminium in solution on the dissolution of amorphous silica and its relation to cementitious systems, T. Chappex, K. Scrivener, under review.

3.1. State of the art

3.1.1. Dissolution mechanisms of minerals

The dissolution of crystalline matters is still subject to discussion. It was well reviewed in [4]. It will not be fully detailed here, however, some aspects are important to better understand the following study.

The dissolution of minerals is usually a surface controlled process, limited by the detachment of surface species. This results in the formation on the surface of kinks and edges.

Numerous studies observed the appearance of etch pits during dissolution, controlled by crystal defects e.g. [5]. Blum and Lasaga [6] proposed that the presence of these etch pits are sites of strong preferential dissolution. The "growth" of the pits exposes additional surface area to the solution. The pits are also evidence of surface-controlled dissolution, rather than diffusion or transport controlled [5]. Giovanoli et al. (from [5]) observed such pits on silicate minerals. For example, Figure 3.1 shows an SEM micrograph of a corroded Feldspar grain. The pits are present in subgrain boundaries and have narrow size distribution.

3.1.2. Dissolution mechanisms of amorphous silica

As already mentioned in section 2.1, ASR depends on the rate of dissolution of amorphous silica or poorly crystallized quartz e.g. [7]. Amorphous silica and silicates present in reactive aggregates are in contact with the pore solution. These phases dissolve and form an expansive gel.

The dissolution mechanism of amorphous silica is a complex process that is nowadays still discussed e.g. [8-10].

Dove et al. proposed a mechanism to explain the dissolution process of amorphous silica [8]. Considering the disordered structure of amorphous silica, they proposed a model based on

the etch-pit-driven dissolution, similar to crystalline silica. They proposed that amorphous minerals could be approximated as a disordered rumpled surface of differently coordinated Si groups without terraces, ledges or kinks, as shown shematically in Figure 3.2. It can be anticipated that the dissolution starts by removing species with lower coordination (Q2: tetrahedra with two coordinations to the surface). A rumpled Q3 surface results (tetrahedra with three coordinations to the surface).

Without electrolyte, the dissolution of Q3 species having higher coordination, the higher energy barrier is kinetically inaccessible. In the presence of electrolyte, this energy barrier is reduced, increasing the probability of removing Q3 units and creating new vacancy islands as the driving force increases. Each new vacancy island creates a new Q2 perimeter, the equivalent of new step edge on a crystal. The dissolution follows by the retreat of newly created Q2 step edges until the appearance again of a Q3 surface. These steps are represented in Figure 3.3.

On a real surface, dissolution will start at surface defects and high curvature zones, containing a high concentration of low coordinated species. The dissolution mechanism is proposed to be proportional to the energy barrier J needed to remove a unit of material:

$$J = A \exp\left(-\frac{\Delta G^{n}_{\mathrm{Crit}}}{kT}\right)$$

where A is a pre-exponential factor, ΔG_{Crit} is the free Gibbs energy barrier to nucleate 2D vacancies, k is the rate constant in $mol.m^{-2}.s^{-1}$ and T is the temperature. They calculate the rate R through the final expression:

$$\ln R = \ln(hS{\cdot}A) - \frac{\pi\alpha^{2}\omega h}{(kT)^{2}} \cdot \frac{1}{|\sigma|}$$

where h is the average height of a vacancy, S is the average area of the silica, ω is the specific volume of a molecule, α the local interfacial energy, and σ is the degree of undersaturation of the solution.

Following this expression, the rate of dissolution of amorphous silica is proposed to be proportional to three main parameters: the concentration of the solution, the temperature and the local interfacial free energy. This energy represents the increase in interfacial free energy per molecule that is created by removing material from the surface. In other words it is the energy needed to create new surfaces.

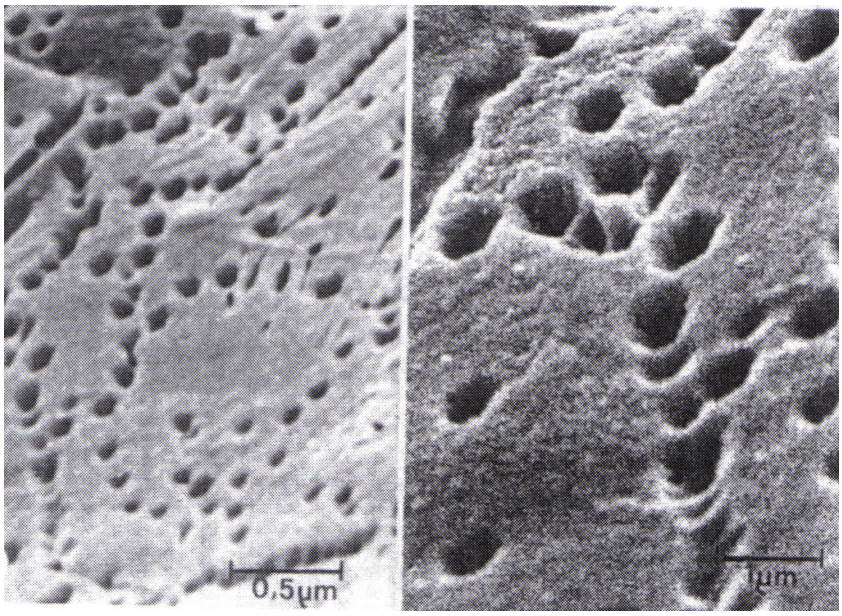

Figure 3.1. SEM micrograph of a corroded Feldspar grain (from [5]).

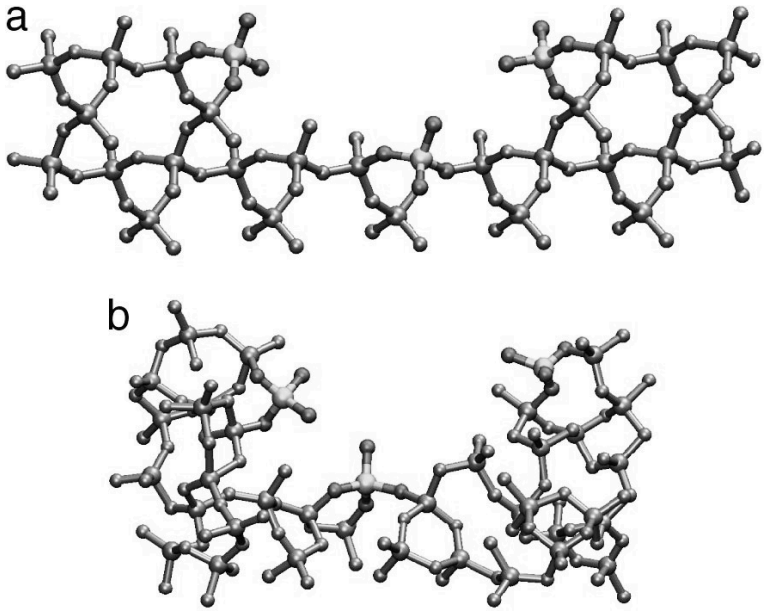

Figure 3.2. Illustration of quartz (a) and amorphous silica (b) showing Q2 and Q3 species as tetrahedra with two and three coordinations to the surface, respectively. The physical model holds that amorphous surfaces are repeatedly, atomically roughened at a length scale that is the average distance over which Q2 groups must be removed to return to a Q3-enriched SiO2 surface [8].

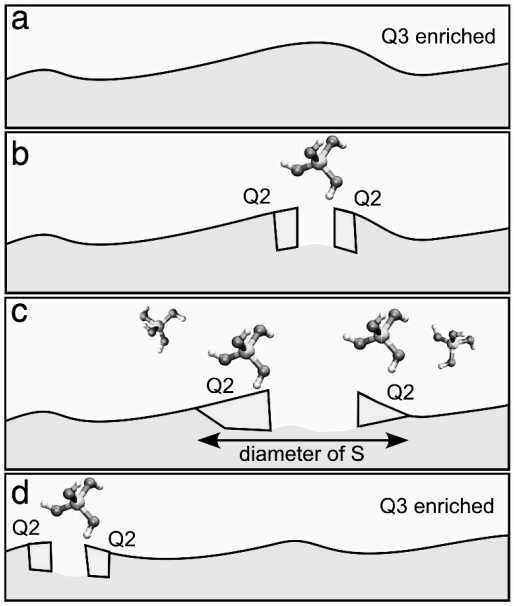

Figure 3.3. Illustration of amorphous silica dissolution by a simple rumpled structure concept. (a) After initial rapid dissolution of highly coordinated groups, a steady- state surface develops. (b) With each nucleated detachment of a highly coordinated Q3 species from the surface, a perimeter of higher-energy Q2 species is formed (Fig. 1b). (c) Reactive Q2 groups retreat over area, *S,* until (d) the affected surface returns to the lower-energy Q3-rich surface and the process regenerates new reactive vacancies [8].

3.1.3. The influence of aluminium on the dissolution of silica

In the fields of geology and marine chemistry, the question of dissolution of amorphous silica has been studied for many years.

It was proposed in the 50's [11], that the presence of magnesium, iron, aluminum or other polyvalent cations in solution had an impact on the dissolution rate of amorphous silica. It was first proposed that these species produce a passive layer of insoluble silicates on the surface of silica, decreasing the dissolution rate of the silica.

Lewin [12] showed in 1960, that milli-molar concentration of metal ions and particularly of aluminium in sea water (at pH 8-9) were able to reduce or even stop the dissolution of amorphous silica, more specifically of silica frustules of diatoms. Iler [13] calculated, from experiments with silica in aluminium containing solutions, that much less than one atomic layer of aluminium was incorporated on the silica surface. This was enough to significantly reduce silica dissolution (Figure 3.4). 112 ppm of added alumina in the solutions was enough to stop silica dissolution after 2 days and during 30 days.

Koning et al. [14] studied the incorporation of aluminium in diatom frustules in sea water with various amount of aluminium (from 2 to 500 nM Al) with batch and flow through experiments. They observed an incorporation of aluminium on the frustule surface within 14 days. The rate of dissolution of frustules put in 100 nM Al seawater was 20 % lower than in the aluminium free seawater at 30 days, as seen in Figure 3.5. They could define, using Al K-edge XANES analysis, that aluminium was incorporated mainly in tetrahedral sites inside the silica framework of frustules skeletons in seawater. Stone et al. [15] also found out that aluminium was mainly incorporated in tetrahedral sites on the silica surface. However, a part of the species remains surface adsorbed as octahedral sites. It was proposed [16] that only the framework-incorporated species was able to influence the dissolution of the silica, by blocking the edge and kink sites of higher energy on the surface of silica.

It was also proposed that the number of incorporated aluminium species was dependent on the number of reactive sites on the surface of silica, which depends on the silica type and the ageing of the surface e.g. [14, 17]. Considering the aluminium avoidance principle, or

Loewenstein rule [18], it can be assumed that the aluminium preferentially binds to silicon through oxygen and avoids Al-O-Al linkage.

Bickmore et al. [19] studied the effect of $Al(OH)_4^-$ on the dissolution kinetics of quartz in highly alkaline environment, up to pH 13.1 and 80 °C. They were able to confirm the reducing effect of aluminium on quartz dissolution under these conditions. They made the assumption that inhibition of dissolution was related to the adsorption of $Al(OH)_4^-$ to silanol sites. They demonstrated that the reduction of the dissolution rate of quartz due to the presence aluminium species was less as the pH increased.

Labrid and Duquerroix [20] calculated that at 30°C and pH 11.5, approximately 4 $Al(OH)_4^-$ per nm^2 sorbed on quartz sand. This value corresponds approximately to the amount of silanol sites on quartz surface. They proposed a mechanism of incorporation of $Al(OH)_4^-$ species on silica in highly basic conditions. They suggest that $Al(OH)_4^-$ would co-adsorb with Na^+ to compensate the negatively charged SiO^- at the surface of quartz:

$$>SiO^- - Na^+ + Al(OH)_4^- \leftrightarrows >SiOAl(OH)_3^- - Na^+ + OH^- \quad (3.1)$$

where > correspond to a surface functional group.

This mechanism of binding was further supported by McCormick et al. [21]. They could show through NMR spectroscopy that aluminosilicates were formed in alkaline solutions. They proposed that the ion pairing between Na^+ and the anions species Si and Al enhance the formation of aluminosilicates, similarly to the mechanism proposed by Bickmore, by enhancing the sorption of $Al(OH)_4^-$ on the negatively charged silica species by pairing with Na^+.

The effect of aluminium on the dissolution rate of amorphous silica and quartz has been already widely studied, however mainly for marine environments, and only occasionally in highly alkaline conditions. The evidence of incorporation and of dissolution inhibition is needed to understand if this mechanism is applicable in concretes to control ASR.

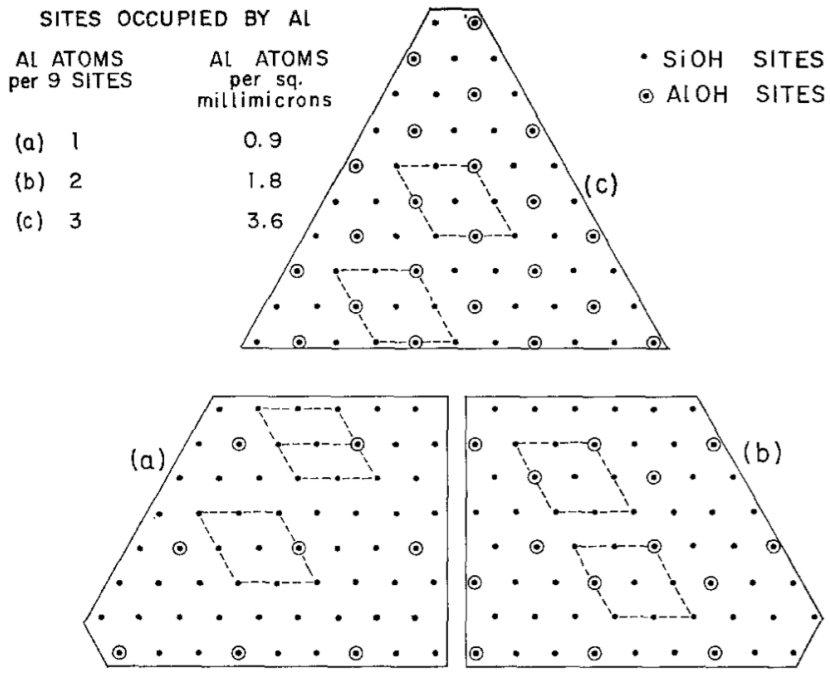

Figure 3.4. Iler's schematic representation of different degrees of coverage of silica surface by aluminosilicate sites, controlling silica dissolution [13]

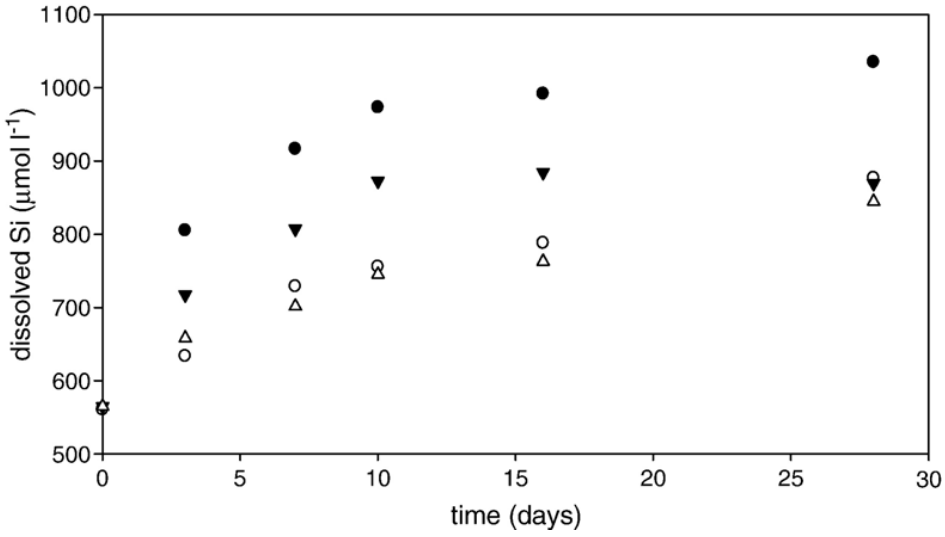

Figure 3.5. Dissolution as a function of time of frustules in seawater and in seawater with added dissolved aluminum. Closed circles: Ashed frustules, open triangles: ashed frustules with 100 nM Al added [14]

3.2. Study of reactive aggregates

3.2.1. Materials and methods

3.2.1.1. Mortar expansion

A set of mortar bars made with plain portland cement following the procedure described in 2.2.2. was immersed in a soak solution saturated in aluminium hydroxide in addition to the same alkali concentration of 0.6 M NaOH, to simulate the pore solution of alumina rich SCMs.

3.2.1.2. Reactive aggregates in simulated pore solutions

The same Swiss reactive gneiss already described in 2.2.1 was used as reactive aggregates in a grain size distribution of 0.315 to 0.65 mm, exposed in solutions.

To simulate the aggregates in contact with different pore solutions, reactive aggregate samples of 40 g crushed to 315 – 630 µm were immersed in 120 ml of simulated pore solutions at 38 °C and 60 °C. These solutions were prepared as follows: solutions of sodium hydroxide (0.6 and 0.3 M) with excess calcium hydroxide were put at 60 °C in an oven for 4 days. Aluminium hydroxide (5.6 g of hydrargillite powder) was added to each of three batches (120 ml) of the solution after one day, three days and 2 hours before the end respectively, to obtain different concentrations of aluminium in solution. The temperature of 60°C was chosen to increase the kinetics of dissolution of the aluminium hydroxide powder. All the solutions were cooled down to 20 °C and filtered through a 0.45 µm filter. Part of the batch, to which aluminium hydroxide had been added at three days, was left unfiltered, so it had a continuous supply of solid aluminium hydroxide. Excess portlandite (3.55 g) was then added back to each batch to provide a calcium source for the ASR. Without a calcium source, the alkalis are quickly depleted in solution. In the presence of solid portlandite, Ca^{2+} exchanges for alkali ions in the reaction gel, forming C-S-H and returning alkali ions to

solution. An aliquot of each batch was analysed by ICP-MS to confirm the ion concentrations at 20 °C. The solutions containing aggregates were then stored at 60 °C or 38 °C. Table 3.1 gives the compositions of all the solutions at 20 °C before adding the aggregates and at the end of the test, after 300 or 550 days respectively. As the solubility of $Al(OH)_3$ increases with temperature, the amount in solution is assumed to stay constant for the solutions with limited addition of aluminium. The concentration at equilibrium at the testing temperature for each solution was calculated with Gems © [22] to have information about the stability of the solutions. The results are given in the Table 3.1.

The alkali concentration of 0.6 M was chosen to be the same as the soak solutions for the mortar bars, and 60 °C to speed up the reaction. However, considering that C-S-H can fix alkalis and so lower the alkalinity of the pore solution, the condition 0.3 M at 38 °C was also studied.

Three to five grams of aggregates sand were extracted at different times from the simulated pore solutions, washed with isopropanol, dried and embedded in an epoxy resin. The samples were mechanically polished to 1 µm and examined with backscattered electrons in the SEM. A high-resolution montage of 144 pictures at a magnification of 400x was acquired to analyse a representative amount of aggregates, approximately comprising 350 aggregate particles. The amount of degradation in the aggregates was quantified by the image analysis method developed by Ben Haha et al. [23]. First, the aggregate particles are identified by a combination of grey level and shape. Then the dark areas, corresponding to cracks and gel in the aggregates are thresholded and measured (see Figure 3.6).

Table 3.1. Composition and conditions of the simulated pore solutions used for the aggregates degradation test

Solution	Testing T [°C][8]	Na [mM]	Al start [mM]	Al end of test [mM]	Portlandite	At Equilibrium (Gems©) [mM]
1	60	600	0	0.3	in excess	Al 52 / Ca 0.005 / Na 600
2	60	600	3.9	0.3	in excess	Al 52 / Ca 0.005 / Na 600
3	60	600	10.7	0.3	in excess	Al 52 / Ca 0.005 / Na 600
4	60	600	34.5	0.5	in excess	Al 52 / Ca 0.005 / Na 600
5	60	600	(in excess) 5	(in excess) 48	in excess	Al 52 / Ca 0.005 / Na 600
6	38	300	0	0.1	in excess	Al 52 / Ca 0.03 / Na 200
7	38	300	(in excess) 1	(in excess) 1	in excess	Al 52 / Ca 0.03 / Na 200

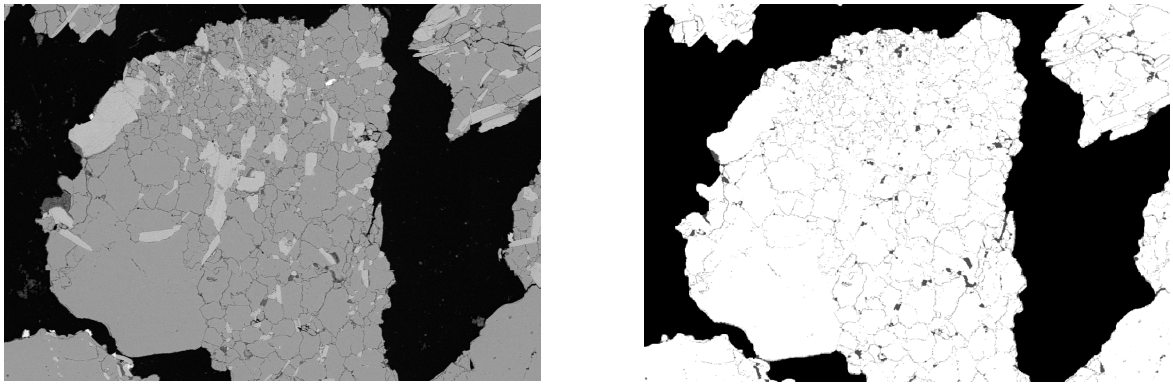

Figure 3.6. Analysis of a reacted aggregate (a). (b) segmented image: in grey, the gel pockets and cracks. Image width 360 microns.

3.2.2. Results

3.2.2.1. Mortar expansion

The PC mortar in the solution saturated with respect to aluminium is shown in Figure 3.7. The presence of aluminium results in 15 % less expansion compared to the reference PC mortars at 500 days.

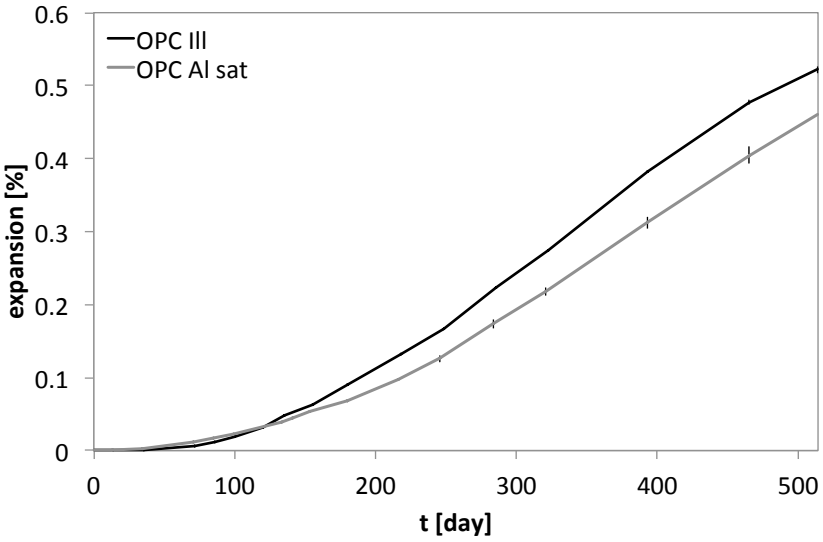

Figure 3.7. Accelerated expansion tests at 38 °C in 0.6 M NaOH curing solution (a) excess aluminium hydroxide in the curing solution and (b) blended mortars

3.2.2.2. Reactive aggregates in simulated pore solutions

The aggregates from the simulated pore solutions were studied in the SEM. The total damage, including the cracks and the gel pockets measured by image analysis, is shown in Figure 3.8. (a) shows the results up to 300 days for the five different solutions at 0.6 M NaOH at 60 °C: without aluminium, with 3.9, 10 and 35 mM of aluminium, and saturated in aluminium hydroxide.

The results show a clear effect of aluminium on the deterioration of the aggregates. The system containing only 3.9 mM aluminium, corresponding approximately to the 15 %

metakaolin paste pore solution, shows a reduction in reacted fraction of 42 % at 300 days, while the aggregate exposed in the solution saturated with aluminium shows a reduction of 63 %.

Figure 3.9 shows the state of degradation of the aggregates at the end of the test for the aluminium free solution and the aluminium saturated solution, compared to the original state of the aggregates. The system with no aluminium is completely disintegrated, while that in saturated aluminium hydroxide shows very little visual deterioration over 300 days.

Figures 3.8 (b) shows the results for the aggregates tested in less aggressive conditions with 0.3 M NaOH at 38 °C, with no aluminium and saturated in aluminium up to 550 days. After 550 days in these conditions, the aggregates in solution without aluminium show an increase of the damage of 5 %, while those in the aluminium saturated solution only 1.5 %.

As reported in table 3.1, the three solutions at 60 °C with limited addition of aluminium (solutions 2, 3 and 4) have almost no more aluminium species in solution at the end of the test. The aluminium must be adsorbed on the aggregates or incorporated in the products of the reaction. It is also seen that the systems without aluminium at the start of the test contain some aluminium species at the end. This is due to the dissolution of some aluminosilicate phases in the aggregates (see tables 2.1). The solution with an excess of aluminium hydroxide had 5 mM aluminium at the start of the test, and this had 48 mM after 300 days at 60 °C. At 38 °C, the aluminium concentration remains at 1 mM during 550 days.

(a)

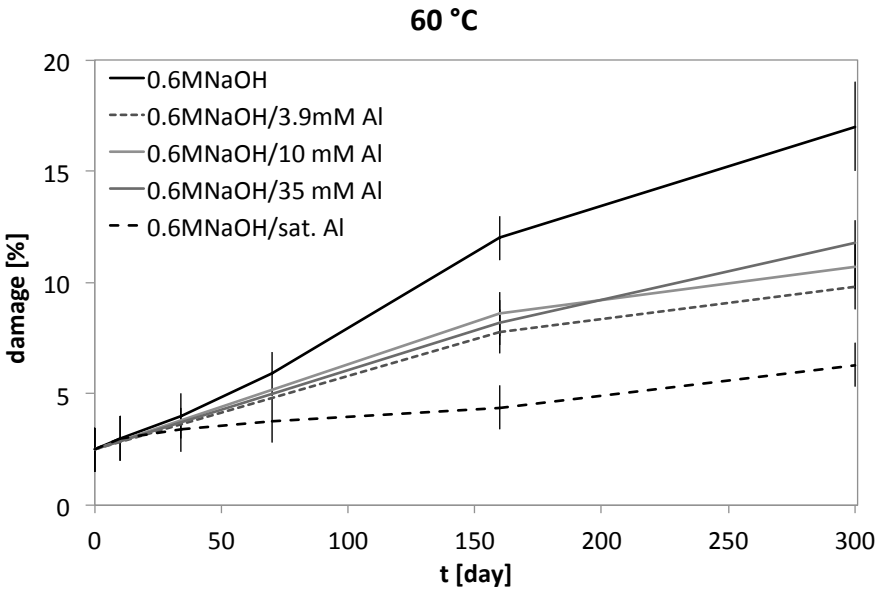

(b)

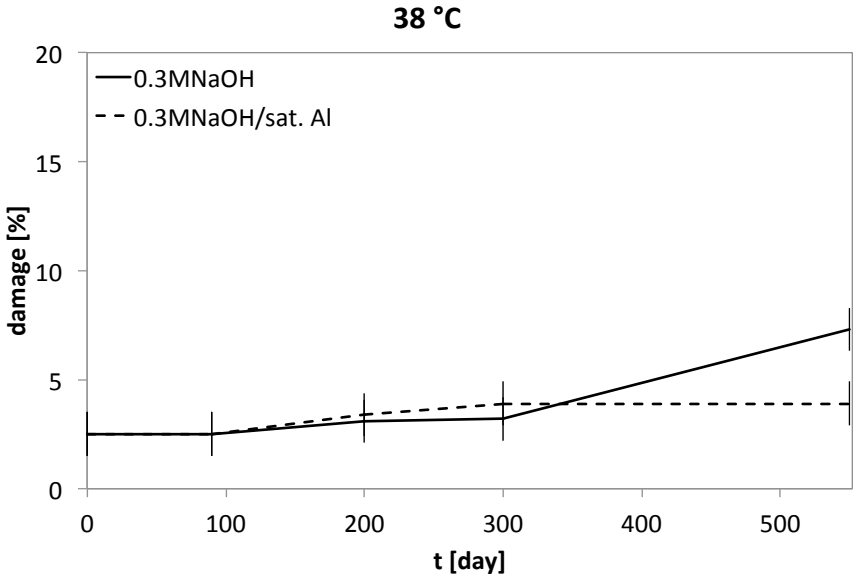

Figure 1.8. Reacted fraction analysis over time of the reactive aggregates in simulated pore solutions (a) 60 °C, 0.6M NaOH (b) 38 °C, 0.3 M NaOH (see table 3.1)

(a)

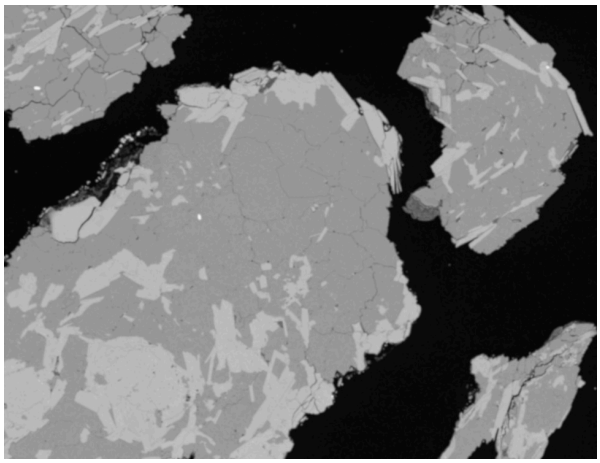

(b)

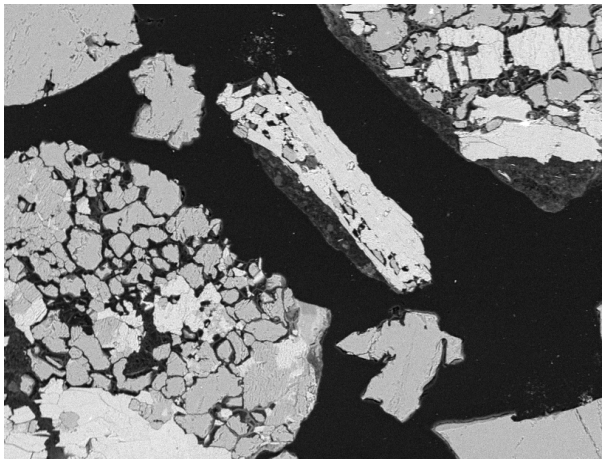

(c)

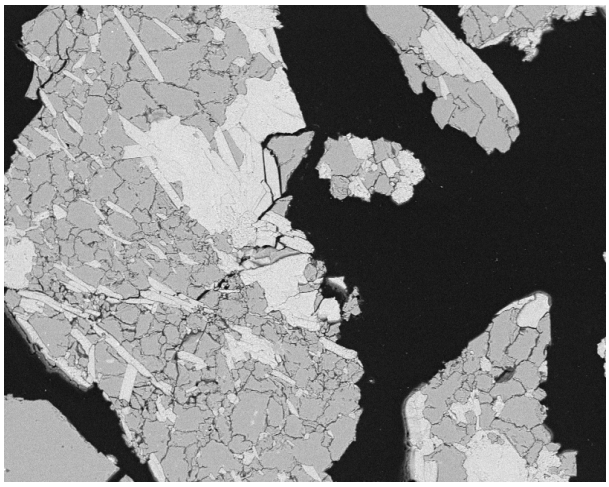

Figure 3.9. Aggregate state (a) before testing, (b) in aluminium free solution after 300 days in simulated pore solution at 60°C and (c) in aluminium saturated solution after 300 days in simulated pore solution at 60°C (image width 360 microns)

3.3. Fused silica study

3.3.1. Materials and methods

Pure polished amorphous silica plates (Producer: Lanno Quartz, 99.9 % amorphous SiO_2) were used. The plates were mechanically polished, originally for optical purpose. They have a diameter of 25 mm and a thickness of 2 mm.0

The fused silica plates were immersed in simulated pore solutions at 20°C in an N_2 environment to limit carbonation. They were taken out of the solution at different times up to 120 days, rinsed one minute with deionized water and put in isopropanol during 3 minutes in an ultrasonic bath. The plates were then air dried and analysed by X-ray photoelectron spectroscopy (XPS). XPS data were collected by Axis Ultra (Kratos Analytical, Manchester, UK) under ultra-high vacuum condition (<10-8 Torr), using a monochromatic Al Ka X-ray source (1486.6 eV), in the Surface Analysis Laboratory of CIME at EPFL. The source power was maintained at 150 W (10 mA, 15kV). The emitted photoelectrons were sampled from a square area of 750*350 µm. Gold (Au 4f7/2) and copper (Cu 2p3/2) lines at 84.0 and 932.6 eV, respectively, were used for calibration, and the adventitious carbon 1s peak at 285 eV as an internal standard to compensate for any charging effects. For quantification, relative sensitivity factors from the supplier were used.

The amounts of incorporated aluminium found by XPS analysis are presented as recalculated values, assuming that the incorporation of aluminium happens only in the first atomic layer of silica e.g. [13]: The interaction volume of the XPS on the fused silica plates corresponds approximately to a 350 x 750 µm surface over a penetration depth of 50 Å. By estimating the thickness of an SiO_2 layer at 2.7 Å, approximately 18.5 SiO_2 layers are analysed. The amount of incorporated aluminium can be recalculated. The obtained spectra were renormalized to a carbon binding energy of 285 eV to get comparable results.

The plates were also analysed by scanning electron microscope (SEM, Philips XLF 30 FEG) with secondary electrons and a topographic image was obtained for certain samples by atomic force microscopy (AFM).

The simulated pore solutions contain different alkali and aluminium concentrations, in a range corresponding to the concentrations that can be present in blended cement systems. Certain systems were calcium saturated before filtering.

These solutions were prepared as follows: solution of sodium hydroxide (0.05, 0.3 and 0.6 M) (some of them with excess calcium hydroxide) were put at 60 °C in an oven for 4 days. As the kinetic of dissolution of $Al(OH)_3$ powder increases with temperature, aluminium hydroxide (2.8 g in 0.6 M NaOH and 5.6 g in 0.2 and 0.05 M NaOH solutions) was added to each batch (120 ml) of the solution at different times, from 3 days to 1 hour before cooling down, to obtain different concentration of aluminium in solution. All the solutions were cooled down to 20 °C in an N_2 environment at 20°C and filtered with a 0.45 µm filter. The solutions were in this case not CH saturated again, in order to ensure a clean surface of the fused silicas for the XPS study. An aliquot of each batch was analysed by ICP-MS to confirm the ion concentrations at 20 °C. Table 3.2 gives the compositions of all the solutions. As for cement paste pore solutions, the concentration of Ca^{2+} is very low, due to the presence of alkalis in the pore solution.

Table 3.2. Composition of the simulated pore solutions of the fused silica systems by ICP-MS

Alkali conc. [mM]	aluminium [mM]	calcium [mM]
50	3.6	Ca free
50	7.2	Ca free
50	8.3	Ca free
200	1.5	0.2
200	16.4	0.1
200	19.2	0.1
200	27.5	0.1
200	4.9	Ca free
200	21.6	Ca free
200	31.1	Ca free
200	37	Ca free
600	1.9	0.3
600	2.4	0.2
600	3.7	0.3
600	9.4	0.1
600	19.1	0.1
600	25.8	0.1
600	34.4	0.1
600	2.4	Ca free

3.3.2. Results

3.3.2.1. XPS analysis of fused silica plates

XPS shows the presence of aluminium on the surface of silica exposed to the aluminium containing solutions. Figure 3.10 shows the aluminium incorporation as an average Al/Si ratio for the solution concentrations 1.5 - 15 mM Al, as a function of the exposure time in the simulated pore solution. For both alkalinities, 0.2 and 0.6 M NaOH, the aluminium incorporation is stable after 28 days. The kinetics of incorporation seems to be similar for both alkalinities. Similar observations were made for the higher aluminium concentrations.

Preliminary tests showed that no aluminium incorporation was detected at 20 days (at least, the XPS signal was too low for quantification). This shows that the aluminium incorporation is slow in conditions similar to this found in concrete and occurs mainly between 20 and 28 days.

Figure 3.11 shows the Al/Si ratio on the surface, as a function of the concentration of aluminium in the simulated pore solution. The graphs give the incorporation from 28 to 120 days, for 0.2 and 0.6 M of NaOH. At 60 days, an additional third alkali concentration of 0.05 M NaOH is also shown. It appears that the amount of incorporated aluminium tends to a constant value (even for low concentrations of aluminium in the solution), which depends mainly on the alkalinity. These values of Al/Si are 0.4- 0.5 at 0.2 M of NaOH and 0.3- 0.35 at 0.6 M NaOH. The reason for higher levels of incorporation at lower alkalinity is not totally clear, but probably related to the fact that the solubility of aluminium increases with alkalinity so the solution becomes relatively less saturated, increasing the energy for incorporation on the surface.

Previous work on aluminosilicates has shown that the binding energies of silicon and oxygen decrease when the Al/Si ratio increases [24-26]. This is a complex phenomenon and was proposed to be due to changes in the covalency/ionicity in the silicate bonds [24]. Therefore to check to what extent aluminium is really incorporated in the silica structure, the Si2p and O1s binding energy peaks were plotted as a function of Al/Si ratio for all the systems, Figure

3.12. This clearly confirms the decrease in binding energies O1s and Si2p with increasing Al/Si ratio on the surface of silica, strongly supporting the conclusion that aluminium observed on the surface of the silica plates is not just surface adsorption but a framework incorporation creating Al-O-Si bonds.

Figure 3.13 shows an example of a deconvoluted O1s binding energy peak. Following the aluminosilicate literature e.g. [27], the secondary peak (here at 530.5 eV) corresponds to an Si-O-Al binding energy, whereas the main one corresponds to the Si-O-Si bonds. Figure 4b) shows the evolution of this second oxygen peak as a function of the aluminium incorporation. It was found that the area of this second peak increased in direct proportion to the aluminium incorporation with a ratio of approximately 3/1. This supports the assignment of this second peak to Al-O-Si bonds.

Studies on aluminosilicates also report another peak in the deconvolution of the Si2p binding energies, such a peak was not seen in this work. Considering the small amount of aluminium incorporated compared to bulk aluminosilicates, it is possible that this secondary peak is too small to be detected.

Figure 3.14 shows the impact of calcium concentration on the Al/Si ratio as a function of the aluminium ion concentration in the pore solution for the 0.2 M NaOH systems. There is no difference between the two conditions in terms of incorporated aluminium, which is perhaps not surprising considering the very low concentration of calcium in solution. It is clear from Figure 3.12 that the presence of low concentration of calcium in the solution doesn't change the binding energy of silicon and oxygen as a function of the incorporated aluminium.

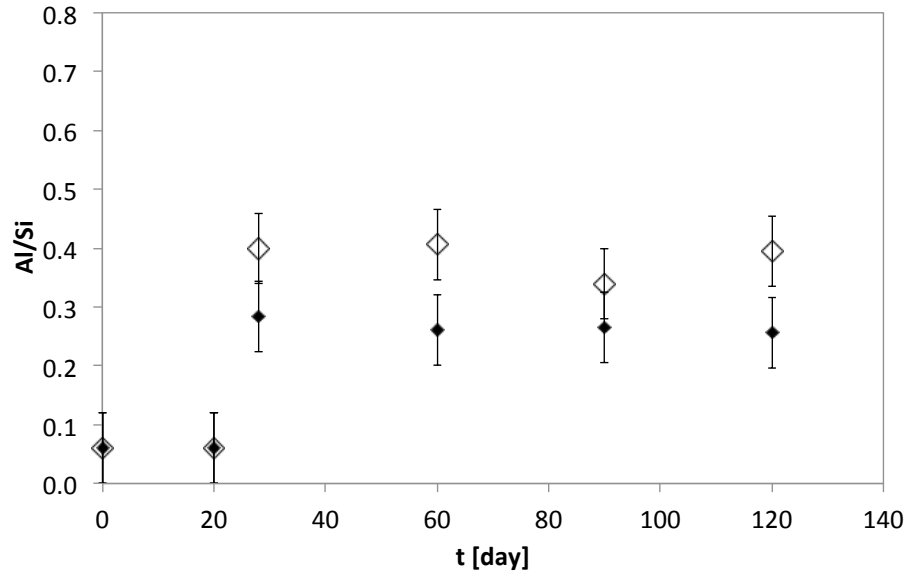

Figure 3.10. Average aluminium incorporated in surface of silica in the range 1.5 to 15 mM Al. Al/Si as a function of time for 2 alkalinities of 0.2 and 0.6 M NaOH.

(a)

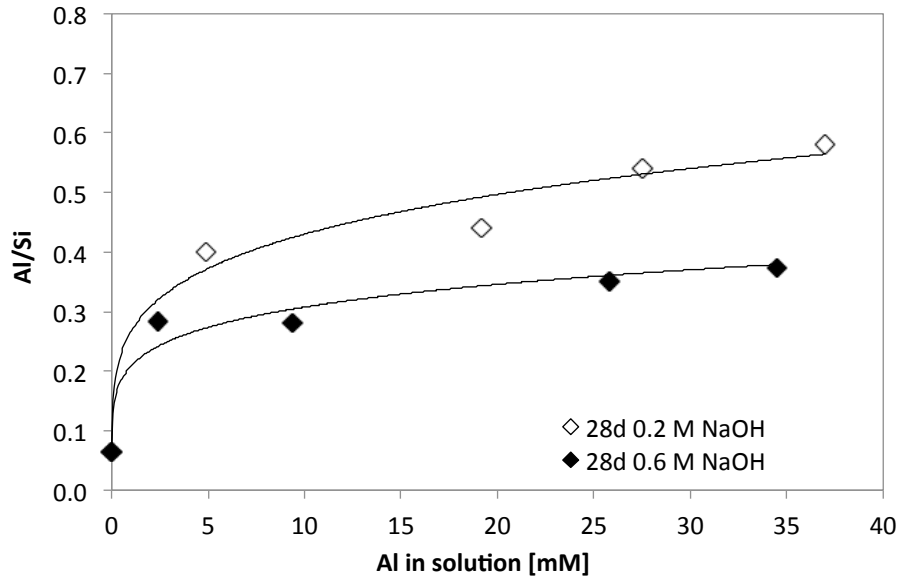
0.8
0.7
0.6
0.5
0.4
0.3
0.2
0.1
0.0
Al/Si
0
5
10
15
20
25
30
35
40
Al in solution [mM]
28d 0.2 M NaOH
28d 0.6 M NaOH

(b)

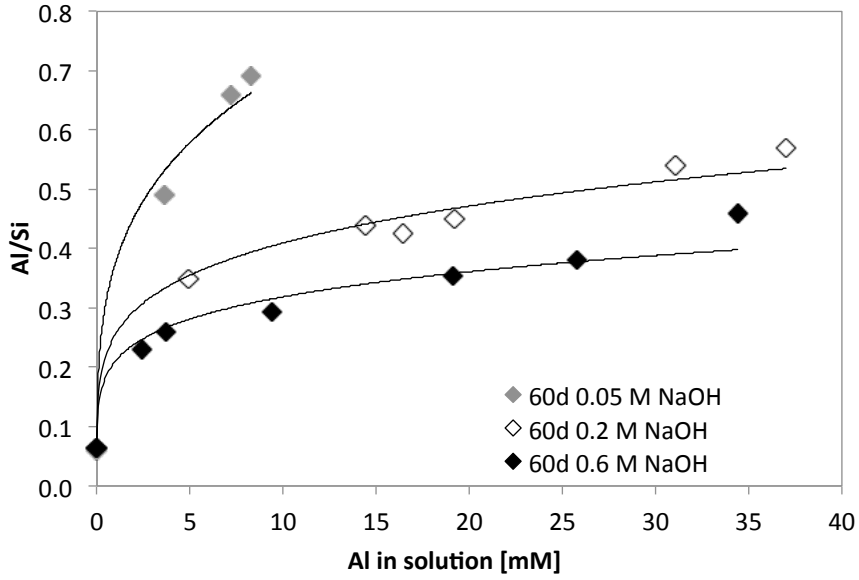
0.8
0.7
0.6
0.5
0.4
0.3
0.2
0.1
0.0
Al/Si
0
5
10
15
20
25
30
35
40
Al in solution [mM]
60d 0.05 M NaOH
60d 0.2 M NaOH
60d 0.6 M NaOH

(c)

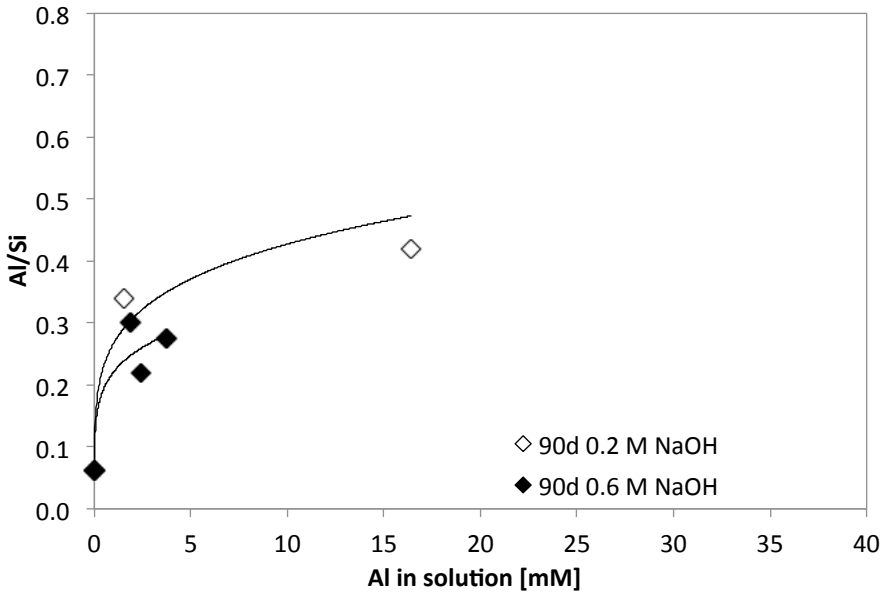

(d)

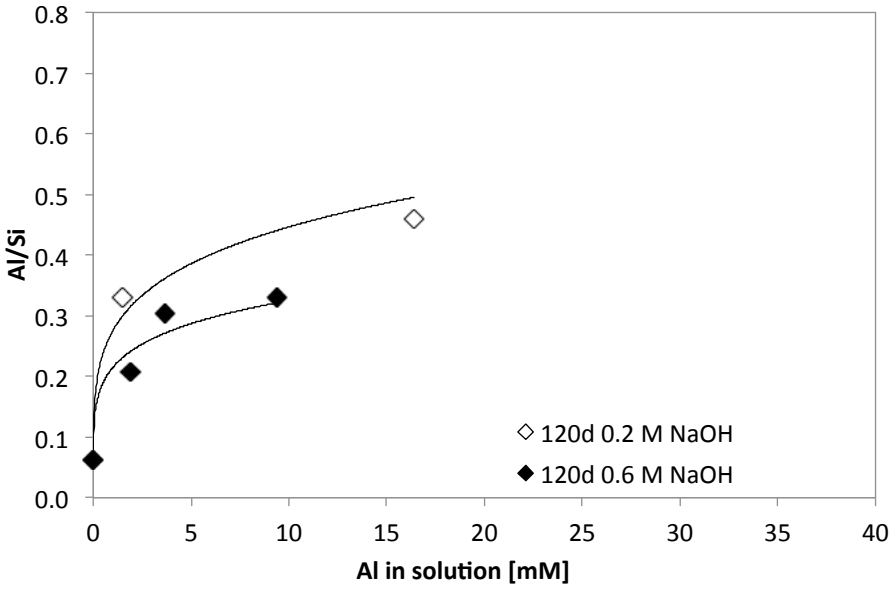

Figure 3.11. Incorporated aluminium on the surface of silica; Al/Si as a function of the aluminium in solution. At 4 different times: (a) 28 days, (b) 60 days, (c) 90 das and (d) 120 days. For different alkalinities: 0.05 (at 60 days only), 0.2 and 0.6 M NaOH.

(a)

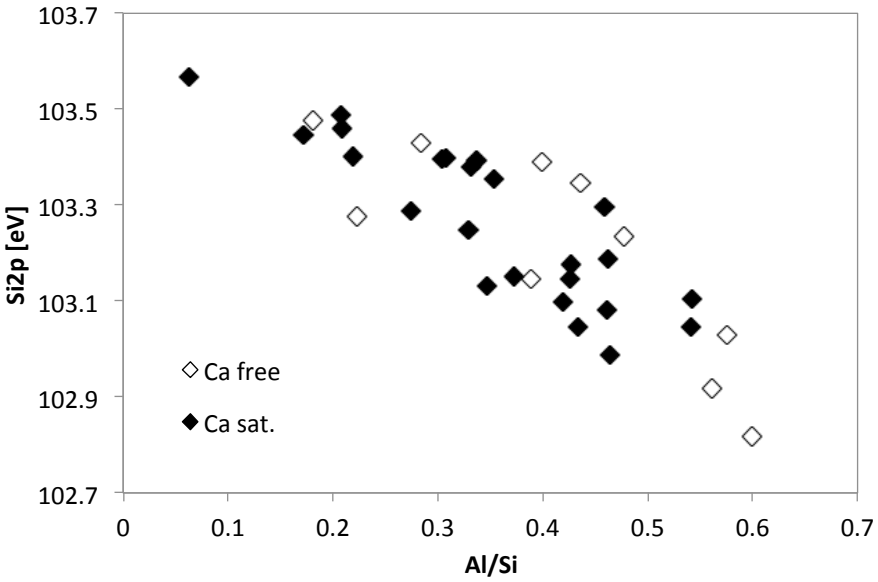

(b)

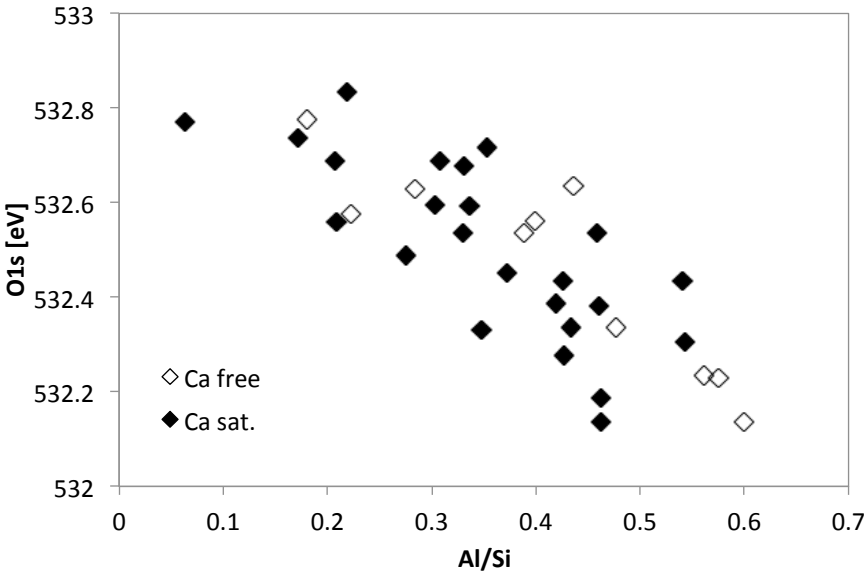

Figure 3.12. Evolution of the binding energies Si2p and O1s as a function of the incorporated aluminium. For calcium saturated and calcium free systems.

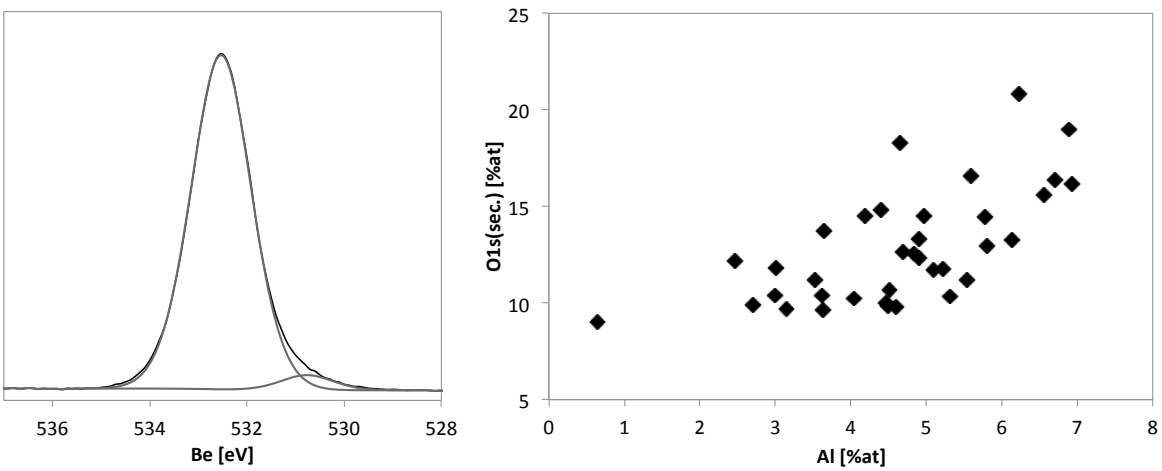

Figure 3.13. Deconvoluted O1s peak and evolution of the amount of secondary O1s peak (at 530.5) as a function of the incorporated aluminium on the surface of silica.

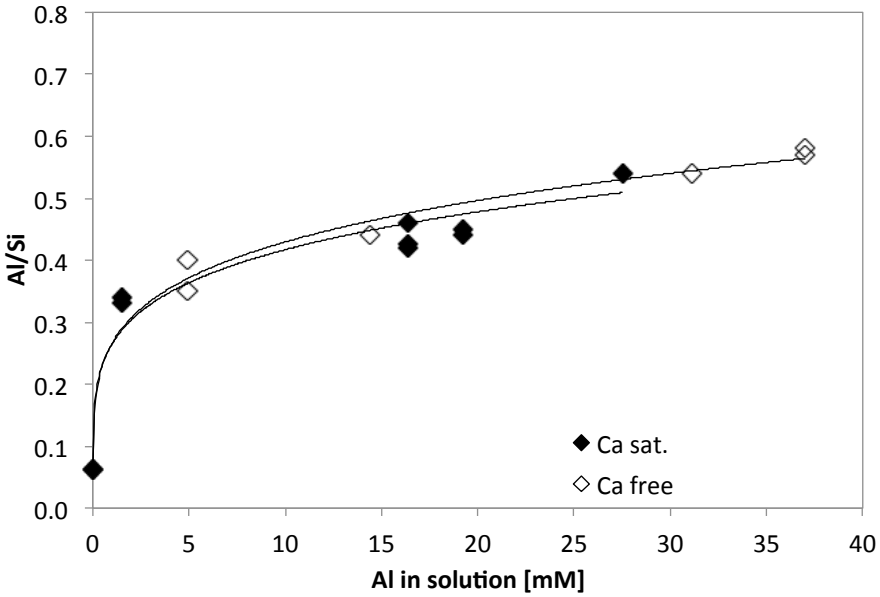

Figure 3.14. Incorporated aluminium on the surface of silica; Al/Si as a function of the aluminium in solution. For calcium saturated and calcium free systems.

3.3.2.2. SEM imaging of the fused silica plates

Figure 3.15 shows the state of the silica plates after 90 days in the simulated pore solutions. The surfaces of the plates that were in solutions containing aluminium all have less surface roughness than the aluminium free system. Dissolution results in pits all over the surface, compared to the original surface state.

Some plates were exposed to four different conditions in four quarters to ensure the same surface state at the beginning of the test (Figure 3.16). One half of the plate was immersed in a 30mM aluminium solution at 0.2 M NaOH for 90 days. The plate was then taken out of the solution and rinsed with water. It was then turned 90 degrees and put in an 0.6 M NaOH solution to attack the surface. The four surfaces were observed under the SEM at 60, 90 and 120 days. The results after 60, 90 and 120 days are shown in Figures 3.17 to 3.19. The aluminium-treated quarter shows less dissolution than the untreated side, even when second exposure was in an alkaline solution containing no aluminium. The pre-treatment with aluminium was enough to stabilize the surface of silica over this time.

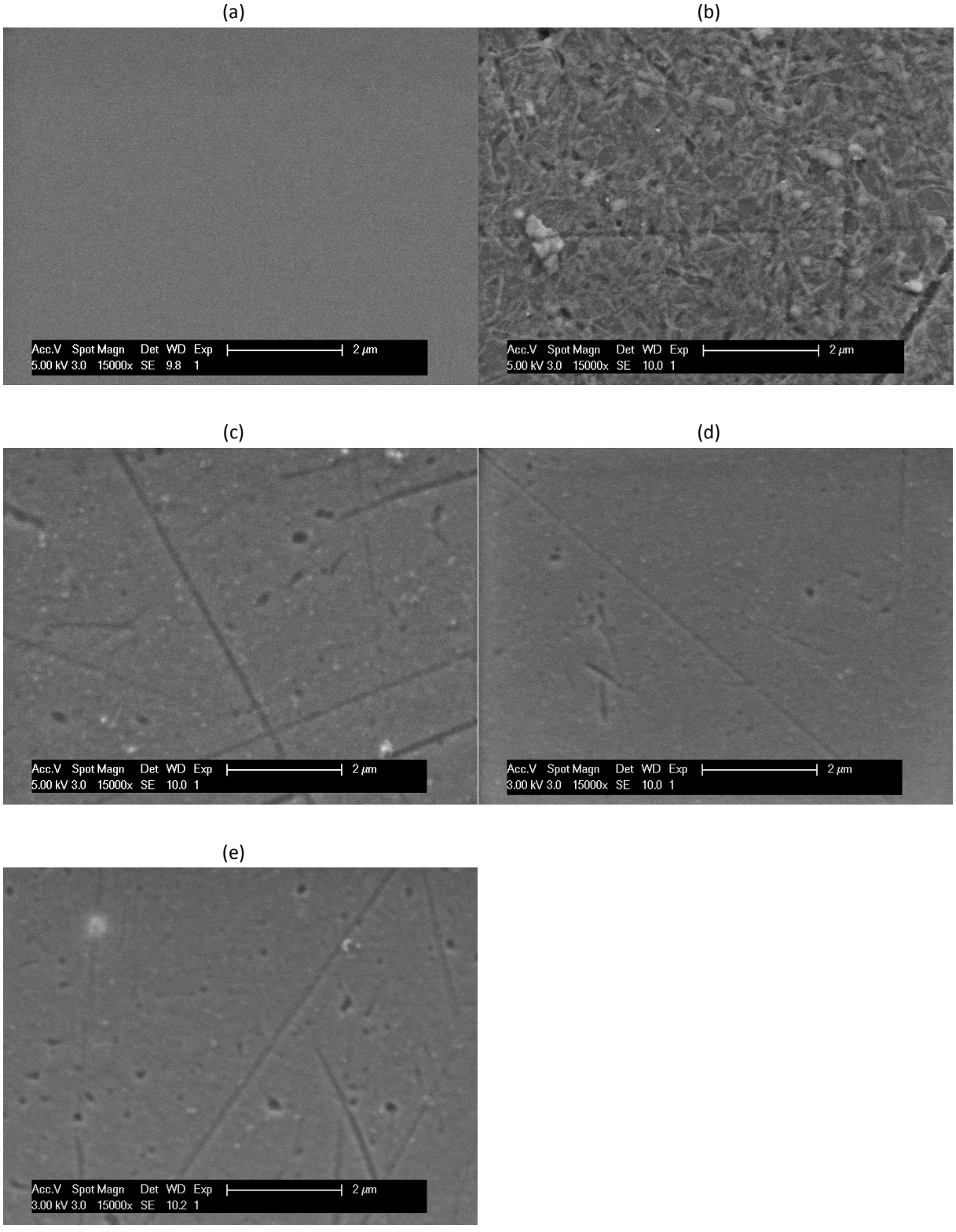

Figure 3.15. SEM backscattered images of the fused silica plates – (a) Silica surface state before treatment, (b) FS plate in 0.6 M NaOH during 90 days, (c) FS plate in 0.6 M NaOH and 1.9 mM Al 90 days, (d) FS plate in 0.6 M NaOH and 2.5 mM Al 90 days, (e) FS plate in 0.6 M NaOH and 19 mM Al 90 days. The images are representative parts of the FS surfaces.

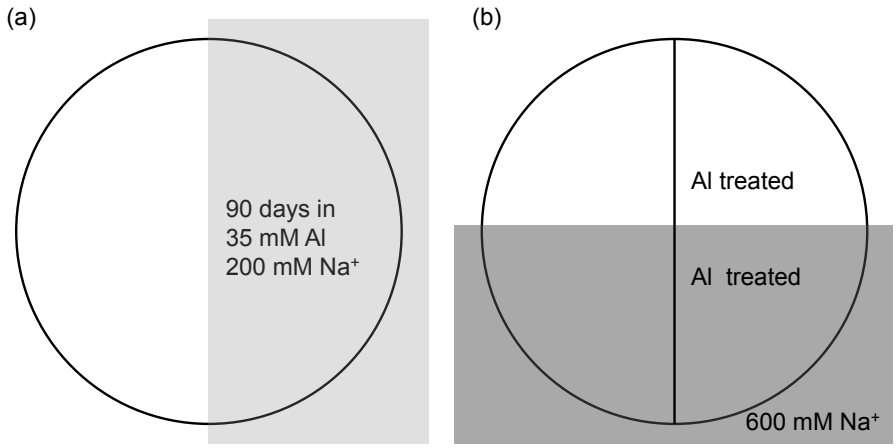

Figure 3.16. Schematic representation of the 4 quarter test:

a) 90 days pre-treatment with 35 mM aluminium and 200 mM sodium solution
b) post treatment in 600 mM sodium solution up to 120 days

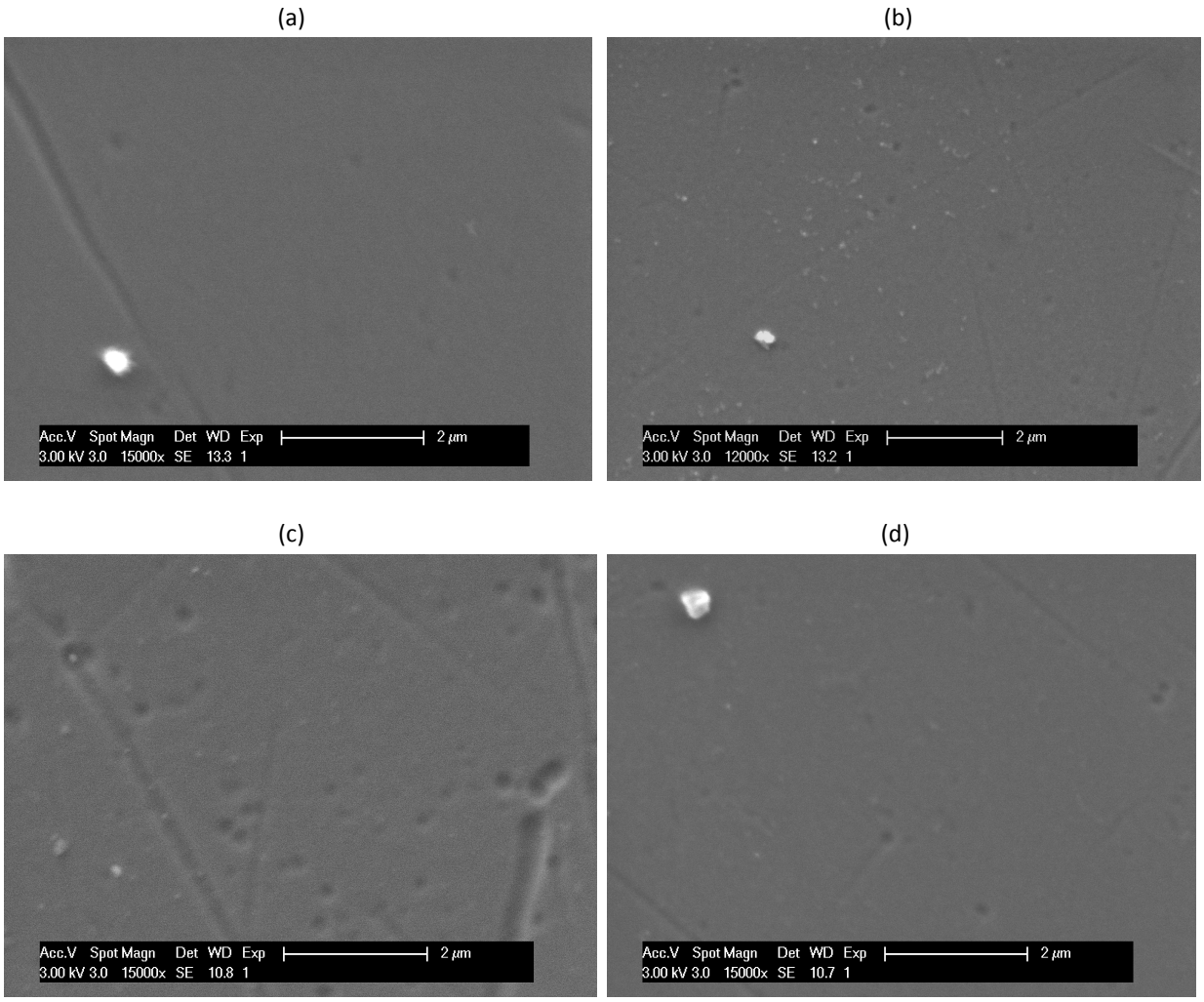

Figure 3.17. SEM backscattered images of the 4 quarter test after 60 days of post treatment – (a) untreated surface, (b) surface treated in 0.2 M NaOH and 30 mM Al during 90 days, (c) same as a with 60 days post treatment in 0.6 M NaOH solution, (d) same as b with 60 days post treatment in 0.6 M NaOH solution

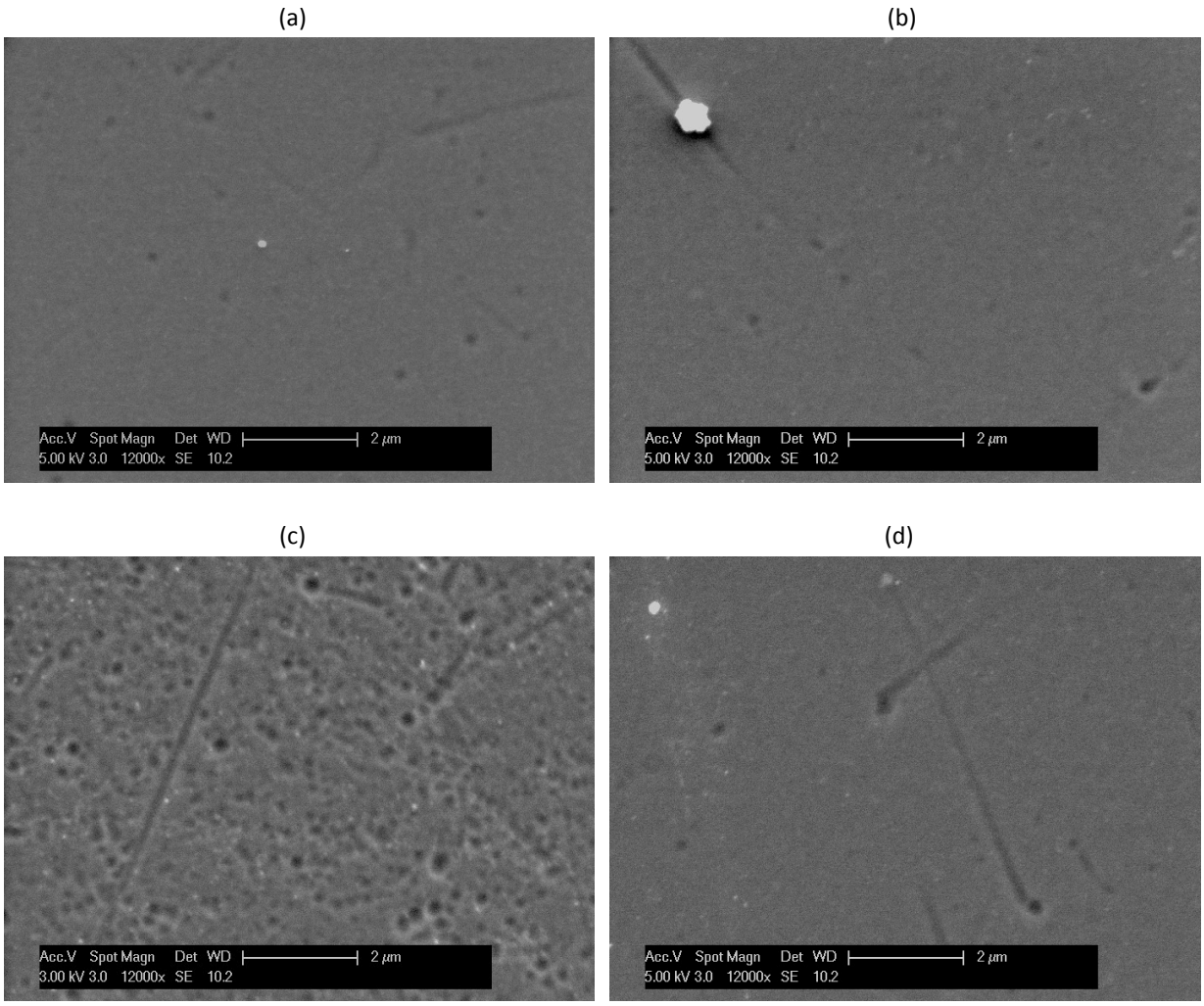

Figure 3.18. SEM backscattered images of the 4 quarter test after 90 days of post treatment – (a) untreated surface, (b) surface treated in 0.2 M NaOH and 30 mM Al during 90 days, (c) same as a with 90 days post treatment in 0.6 M NaOH solution, (d) same as b with 90 days post treatment in 0.6 M NaOH solution

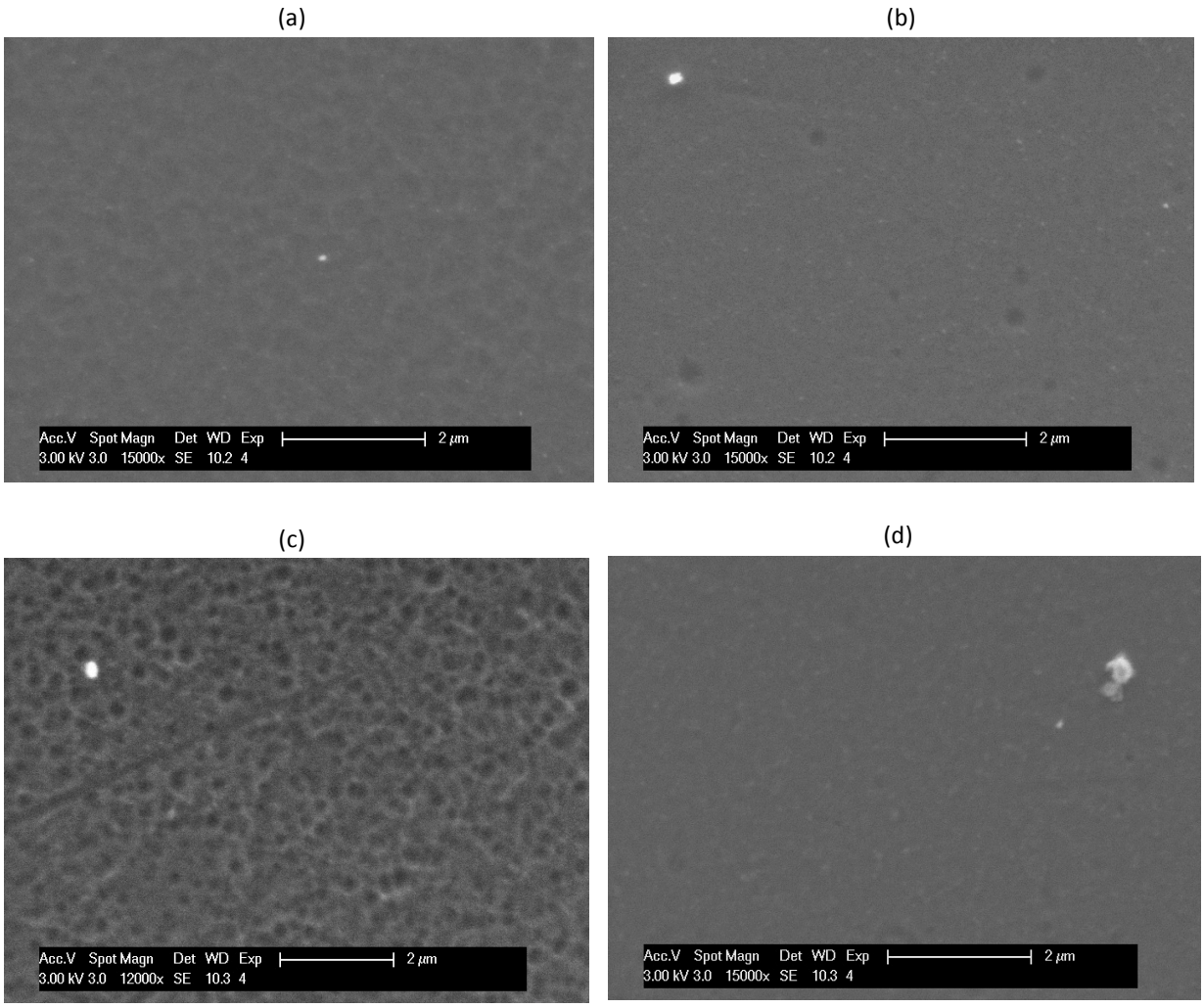

Figure 3.19. SEM backscattered images of the 4 quarter test after 120 days of post treatment – (a) untreated surface, (b) surface treated in 0.2 M NaOH and 30 mM Al during 90 days, (c) same as a with 120 days post treatment in 0.6 M NaOH solution, (d) same as b with 120 days post treatment in 0.6 M NaOH solution

3.3.2.3. AFM imaging of the fused silica plates

The Figure 3.20 shows the 3D surface representation of a 10 × 10 µm section for 3 different cases: untreated/unexposed, after 90 days in a calcium-saturated 0.6 M NaOH solution, and after 90 days in the same solution but with 2.5 mM aluminium. It confirms the SEM observations, the plate cured in the solution containing aluminium has less degradation. Some preferential attack along polishing scratches and defects are visible on the surface of the samples. Roughness profiles are shown in Figure 3.20. The position of the line profile is shown on the 3D images by the grey line for each plate. As the original height of the surface is unknown, it is difficult to quantify the amount of attack. The higher degradation in system (b) is indicated by the amplitude of the roughness and the amount of pits. The aluminium free system has a surface roughness of 0.03 µm whereas the aluminium containing system has approximately 0.01 µm.

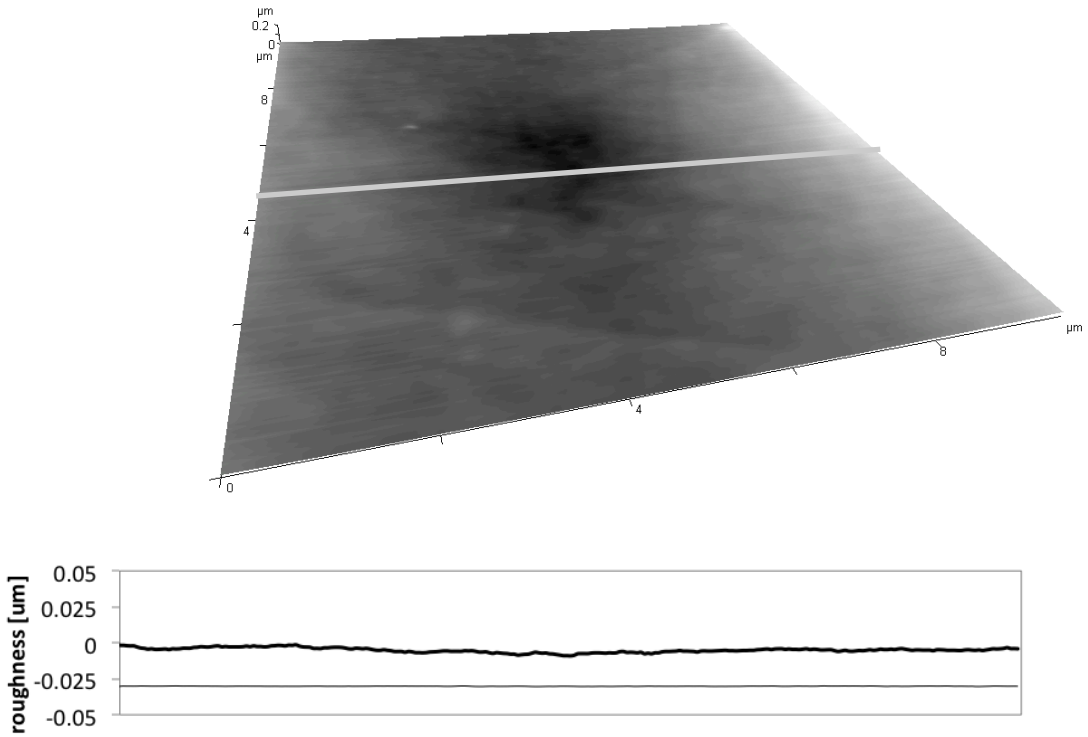

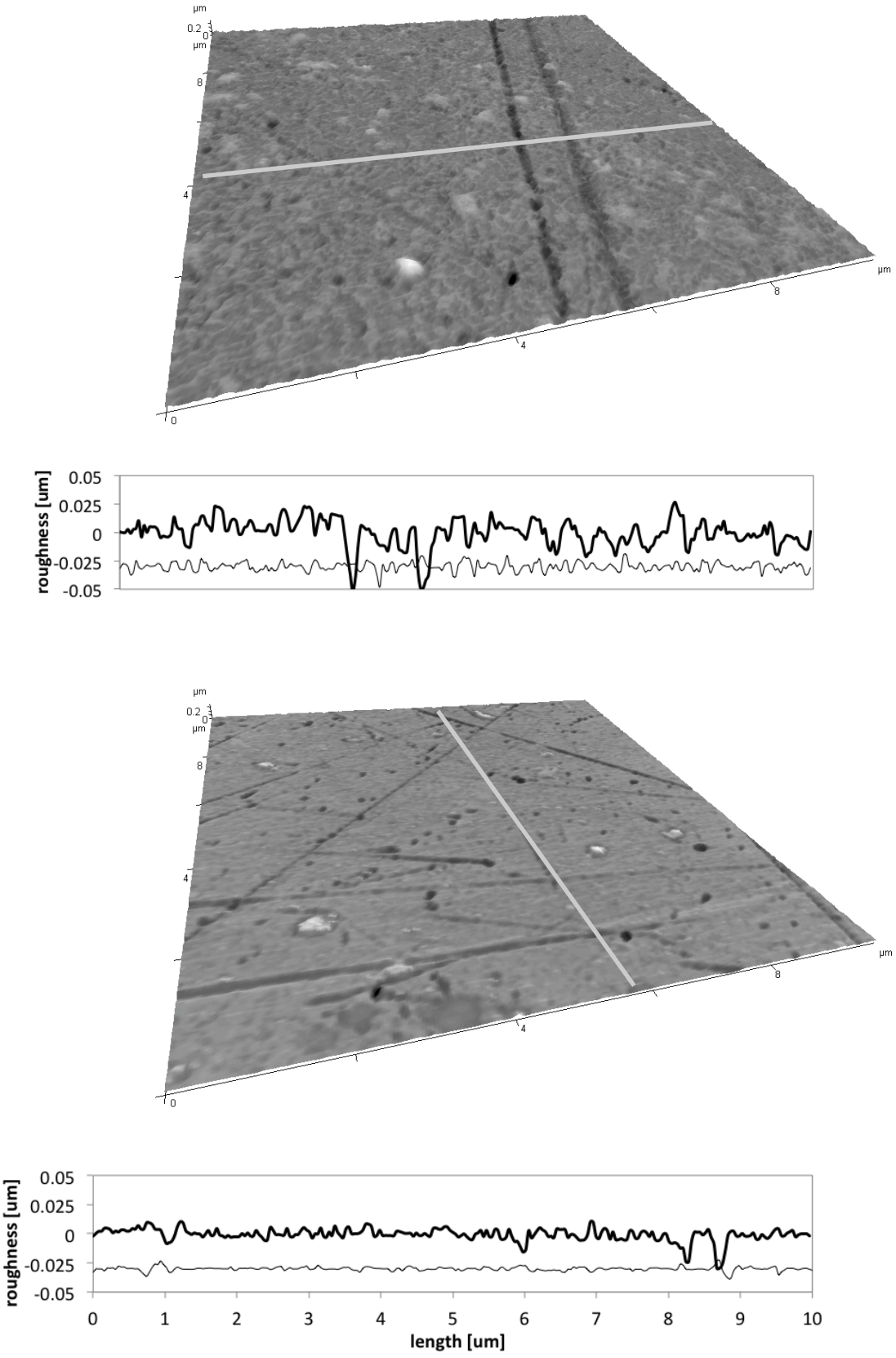

Figure 3.20. AFM 3D representations and roughness profile for 3 different cases: a) before testing, b) 90 days in a 0.6 M NaOh calcium saturated solution c) 90 days in a 0.6 M NaOH solution calcium saturated and with 1.5 mM aluminium. The grey line show the profile.

3.4. Discussion

As reported in the chapter 2, systems with SCMs containing alumina expand less due to ASR than those containing only additions of silica. The addition of silica lowers the Ca/Si ratio of the C-S-H in both systems, which increases the absorption of alkalis, but despite aluminium being incorporated in the C-S-H this does not further contribute to alkali fixation by the C-S-H. Systems containing alumina rich SCM have higher contents of aluminium in their pore solutions. When reactive aggregates are exposed in alkaline solutions with different concentration of aluminium, the presence of aluminium clearly reduces the amount of reaction of the aggregates.

Only 3.9 mM of aluminium was enough to significantly reduce the aggregate deterioration due to alkali gel formation over 300 days at 60 °C. However there is no significant difference in aggregate damage for aluminium concentrations in the range 3.9 to 35 mM. On the other hand a solution with an excess of aluminium hydroxide leads to a dramatic reduction in the amount of damage. This experiment clearly shows that aluminium in solution can reduce the dissolution of disordered silica even in high pH solutions and indicate that it is important to have a continuous reserve of aluminium.

XPS analysis shows, that the aluminium species are incorporated in the silica framework of amorphous silica (not just surface adsorbed) even at the high alkalinities found in cement paste. Under these conditions, the incorporation of the aluminium species on silica is a relatively slow process that happens between 20 and 28 days, after which the amount of incorporated aluminium stabilizes. The level of aluminium incorporation does not depend on the concentration of aluminium in solution. This confirms the findings on reactive aggregates: The reduction of degradation of reactive aggregates was the same regardless the aluminium concentration in the solution between 2.5 and 35 mM.

The importance of a long-term aluminium source in concretes and mortars can be understood considering the long-term reactivity of aggregates: A reactive aggregate which reactivity is slow down by the presence of SCMs, may let appear new reactive zones due to cracking. The presence of aluminium over the long term may control the surface of these new reactive zones of the aggregates.

The incorporation of aluminium on the surface of silica probably follows equation 3.1 (section 3.1). Labrid and Duquerroix [20] proposed that the negative aluminium hydroxide $Al(OH)_4^-$ present in high pH environment would co-adsorb with Na^+ to balance the negative charge. Ca^{2+} could also by co-adsorbed.

If aluminium species are incorporated in the silica framework at the reactive sites like kinks and edges (e.g. [14, 17]), they increase the interfacial free energy and slow down silica dissolution. The AFM and SEM analyses clearly confirmed that the presence of aluminium on the surface of silica reduces its dissolution. The pre-treatment experiment confirms that it is the aluminium incorporation, which is important in controlling the dissolution of silica and not just the presence aluminium species in solution. The etch pits present on the fused silica surfaces look similar to the pits observed by Giovanoli et al. on granitic gneiss (from [5]). The presence of these etch pits shows that defects on the surface of silica are sites of strong preferential dissolution. The pits are also an indication for a surface controlled dissolution reaction [5]. The aluminium treated surface presents less etch pits and this is evidence of a stabilisation of the preferential dissolution sites at the atomic scale.

The degree of aluminium incorporation does depend strongly on the alkalinity – increasing as the concentration of NaOH decreases. It was shown in chapter 2, that pozzolanic addition containing reactive silica reduce the Ca/Si ratio of the main binding phase C-S-H, which then absorbs more alkali ions and lowers the pH of the pore solution. From this perspective, it is important to consider the effect of alkalinity on the aluminium incorporation. At 60 days, at 5 mM of aluminium in the solution, which is typical of the conditions found in blended pastes, the incorporation of aluminium in the 0.2 M NaOH solution (typical to that found in blended pastes) is 40% higher than in the 0.6 M NaOH solution (close to that found in unblended Portland cement systems).

3.5. Conclusions

This study demonstrates that a chemical mechanism already well known in geology and marine chemistry is probably operating in concretes prone to alkali silica reaction. It was shown that the presence of aluminium in solution in mM concentrations (similar to those found in blended cement paste pore solutions) is able to incorporate into a silica surface. This incorporation reduces the dissolution of amorphous silica, even in highly alkaline and calcium saturated environments similar to those found in cement pastes.

In terms of the alkali silica reaction, this work supports the conclusion that the incorporation of reactive aluminosilicates may have two effects. First, the presence of reactive silica in the aluminosilicates changes the composition of the C-S-H hydrate and so lowers the pH of the pore solution. This slows down the rate of dissolution of susceptible phases in the aggregates. Secondly, reactive alumina may absorb directly on the surface of the susceptible silica containing phases in the aggregates and slow down their dissolution. There is also likely to be a synergy between these two effects, as a lowering of the pH will increase the absorption of aluminium on the surface of susceptible phases.

The presence of low concentrations of calcium in solution (as present in the pore solutions of mature cement paste) does not influence the incorporation of aluminium species on the silica surface.

3.6. References

[1] J. Duchesne, M.-A. Bérubé, Long-term effectiveness of supplementary cementing materials against alkali-silica reaction, Cement and Concrete Research, 31 (2001) 1057-1063.

[2] W. Aquino, D.A. Lange, J. Olek, The influence of metakaolin and silica fume on the chemistry of alkali-silica reaction products, Cement and Concrete Composites, 23 (2001) 485-493.

[3] T. Ramlochan, M.D.A. Thomas, R.D. Hooton, The effect of pozzolans and slag on the expansion of mortars cured at elevated temperature: Part II: Microstructural and microchemical investigations, Cement and Concrete Research, 34 (2004) 1341-1356.

[4] P. Juilland, Early hydration of cementitious systems, in: STI IMX LMC, EPFL, Lausanne, 2009.

[5] W. Stumm, Reactivity at the mineral-water interface:

dissolution and inhibition Colloids and surface, 120 (1996) 143-166.

[6] A.C. Lasaga, A.E. Blum, Surface chemistry, etch pits and mineral-water reactions, Geochimica et Cosmochimica Acta, 50 (1986) 2363-2379.

[7] L.S. Dent Glasser, N. Kataoka, The chemistry of 'alkali-aggregate' reaction, Cement and Concrete Research, 11 (1981) 1-9.

[8] P.M. Dove, N. Han, A.F. Wallace, J.J. De Yoreo, Kinetics of amorphous silica dissolution and the paradox of the silica polymorphs, Proceedings of the National Academy of Sciences, 105 (2008) 9903-9908.

[9] J.P. Icenhower, P.M. Dove, The dissolution kinetics of amorphous silica into sodium chloride solutions: effects of temperature and ionic strength, Geochimica et Cosmochimica Acta, 64 (2000) 4193-4203.

[10] Niibori, Dissolution rates of amorphous silica in highly alkaline solution, Journal of nuclear science and technology, 37 (2000) 349-357.

[11] R.K. Iler, The colloid chemistry of silica and silicates, Cornell University Press, Ithaca, New York, (1955).

[12] J.C. Lewin, The dissolution of silica from diatom walls, Geochimica et Cosmochimica Acta, 21 (1961) 182-198.

[13] R.K. Iler, Effect of adsorbed alumina on the solubility of amorphous silica in water, Journal of Colloid and Interface Science, 43 (1973) 399-408.

[14] E. Koning, M. Gehlen, A.M. Flank, G. Calas, E. Epping, Rapid post-mortem incorporation of aluminum in diatom frustules: Evidence from chemical and structural analyses, Marine Chemistry, 106 (2007) 208-222.

[15] W.E.E. Stone, G.M.S. El Shafei, J. Sanz, S.A. Selim, Association of soluble aluminum ionic species with a silica-gel surface: a solid-state NMR study, The Journal of Physical Chemistry, 97 (1993) 10127-10132.

[16] S. Dixit, P. Van Cappellen, A.J. van Bennekom, Processes controlling solubility of biogenic silica and pore water build-up of silicic acid in marine sediments, Marine Chemistry, 73 (2001) 333-352.

[17] S. Dixit, P. Van Cappellen, Surface chemistry and reactivity of biogenic silica, Geochimica et Cosmochimica Acta, 66 (2002) 2559-2568.

[18] W. Loewenstein, The distribution of aluminium in the tetrahedra of silicates and aluminates, Am Mineral, 39 (1954) 92-96.

[19] B.R. Bickmore, K.L. Nagy, A.K. Gray, A.R. Brinkerhoff, The effect of $Al(OH)_4^-$ on the dissolution rate of quartz, Geochimica et Cosmochimica Acta, 70 (2006) 290-305.

[20] J. Labrid, J.P. Duquerroix, Aspects thermodynamiques et cinetiques de la dissolution des melanges quartz-kaolinite par les alcalis, Oil & Gas Science and Technology - Rev IFP, 46 (1991) 41-58.

[21] A.V. McCormick, A.T. Bell, C.J. Radke, Evidence from alkali-metal NMR spectroscopy for ion pairing in alkaline silicate solutions, The Journal of Physical Chemistry, 93 (1989) 1733-1737.

[22] D. Kulik, GEMS-PSI 3.0, PSI, Villigen, Switzerland, 2002 (available at http://les.web.psi.ch/Software/GEMS-PSI/), in.

[23] M.B. Haha, E. Gallucci, A. Guidoum, K.L. Scrivener, Relation of expansion due to alkali silica reaction to the degree of reaction measured by SEM image analysis, Cement and Concrete Research, 37 (2007) 1206-1214.

[24] T.L. Barr, The nature of the relative bonding chemistry in zeolites: An XPS study, Zeolites, 10 (1990) 760-765.

[25] B. Herreros, H. He, T.L. Barr, J. Klinowski, ESCA Studies of Framework Silicates with the Sodalite Structure: 1. Comparison of Purely Siliceous Sodalite and Aluminosilicate Sodalite, The Journal of Physical Chemistry, 98 (1994) 1302-1305.

[26] V. La Parola, G. Deganello, S. Scirë, A.M. Venezia, Effect of the Al/Si atomic ratio on surface and structural properties of sol-gel prepared aluminosilicates, Journal of Solid State Chemistry, 174 (2003) 482-488.

[27] B.P. McGrail, J.P. Icenhower, D.K. Shuh, P. Liu, J.G. Darab, D.R. Baer, S. Thevuthasen, V. Shutthanandan, M.H. Engelhard, C.H. Booth, P. Nachimuthu, The structure of Na2O-Al2O3-SiO2 glass: impact on sodium ion exchange in H2O and D2O, Journal of Non-Crystalline Solids, 296 (2001) 10-26.

CHAPTER 4 THE INFLUENCE OF ALKALIS ON ASR

In this chapter, the influences of alkali type and concentration on ASR are studied. It is known that the evolution of ASR strongly depends on the alkali concentration. ASR accelerated expansion tests are usually done by increasing the temperature and the alkalinity of the mixing or soaking water, to increase the kinetics of the reaction and provide an excess of reactant in the system. The impact of the ionic species, and the effect of concentration, has to be further investigated to better understand accelerated expansion tests. Some non-linear behaviour was observed in such tests, and special attention was given to the differences between sodium and potassium addition. The study of mortars and pastes with various sodium and potassium concentration were analysed.

Some additional studies were made on the effect of lithium. At this stage the results are inconclusive and are given in Annex 1.

4.1. State of the art

4.1.1. Influence of sodium and potassium on ASR

4.1.1.1. Context

Frequently, sodium hydroxide is used to accelerate ASR in tests, either in external soak solution or in in the mixing water. The potassium present in cement is often converted as equivalent Na_2O in the mixing solution (equation 1). It corresponds to the transformation of the K_2O concentration present in anhydrous cement into the same molar quantity of Na_2O.

$$[Na_2O_{equ}] = [Na_2O] + 0.658[K_2O] \quad (4.1)$$

This simplification implies that the effect of sodium and potassium are equivalent on ASR. However, several studies show that this is not the case [1-5].

4.1.1.2. The effect of alkali type on ASR

Following the gel formation mechanism proposed in 1.1, saying that sodium and potassium migrate into the disrupted silica structure to neutralize negative anion charges, the presence of both ions would appear to behave similarly with respect to ASR. However, there are some studies showing that alkali cations have different effects on the dissolution of silica [1, 5].

The value of enthalpy of hydration $\Delta H°_{hydr}$ is lower for sodium than potassium, as shown in the Table 4.1 [6]. Cations present in a hydrous solution are surrounded by a shell of oriented water molecules, this difference in the enthalpy of hydration may lead to a stronger binding of the water shell on Na^+ than on K^+.

Depasse and Watillon [7] showed by spectrophotometric measurements of colloidal silica particles in solution, that above a certain pH value, sodium was able to coagulate colloidal silica particles within some seconds, whereas potassium completely dissolves them, as shown in Figure 4.1. It was also shown that above a certain Na/K ratio, silica coagulated in high pH solutions. This suggest that potassium disrupts more the silica structure compared to sodium, which tends to allow the binding of silica species together. It leads to the coagulation of the colloidal silica particles.

Others studied directly the effect of the alkali type on the ASR:

Leeman and Lothenbach [4] studied two different cements with similar Na_2O_{eq} but different K/Na ratios. The reactive mortars cast with these cements showed very different expansion behaviour and different pore solution compositions (Figure 4.2). The pore solution of both pastes had a similar silicon concentration up to 10 weeks, whereas the two reactive mortars did not. The mortar containing the lower K/Na ratio had double the amount of silica in the pore solution, after 10 weeks.

Hou et al. [2, 3] studied synthesized alkali silica gels by Si NMR spectroscopy and X-ray diffraction. They showed that Na^+ and K^+ behave similarly to form gel, but that gels with K^+ may have a more disordered structure than gels with Na^+.

Prezzi et al. [8, 9] proposed a swelling mechanism of the silica gel particles based on the Gouy-Chapman model of double layer theory. They supported this theory with gel EDS analyses of different expansive mortars using different SCMs substitutions. They proposed that the valence of the ions determines the double-layer thickness, which determines the water uptake and the repulsive force, resulting in a higher pressure. The more Na^+ and K^+ were contained in the gel product compared to Ca^{++}, the more expansive were the mortar bars. They proposed that the expansion of gel increased following this order: $Ca^{2+} < Mg^{2+} < K^+ < Na^+$.

Table 4.1. Radius and enthalpy of hydration of the principal alkalis [6, 10]

	Li^+	Na^+	K^+
Radius [Å]	0.68	0.97	1.33
$\Delta H°_{hydr}$/kJmol^{-1}	-519	-406	-322

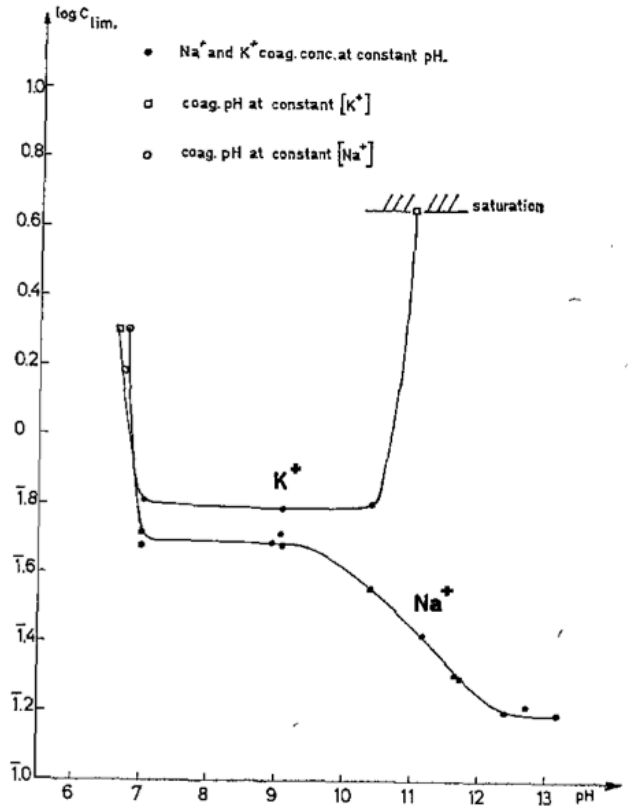

Figure 4.1. Limiting concentration of coagulation byKCl and NaCl as a function of the pH. [7]

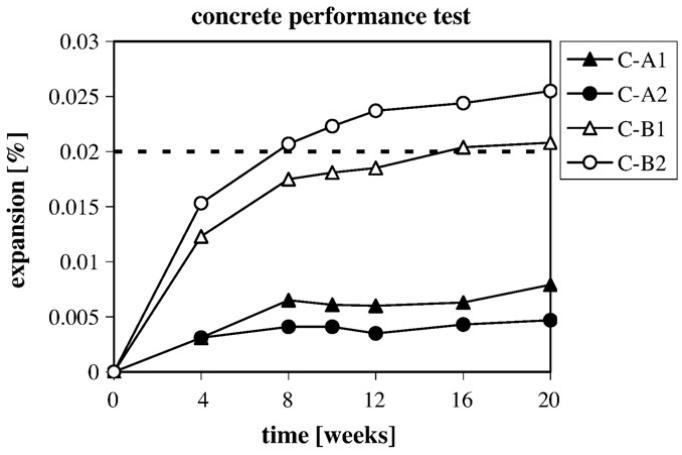

Figure 4.2. Expansion of concrete prisms with reactive aggregates, A1: K/Na=3.95, A2: K/Na=3.95, B1: K/Na=2.41, B2: K/Na=2.83 (ratios based on molar concentrations) [4]

4.1.1.3. The effect of alkali concentration on ASR

The alkali concentration plays an important role in ASR expansion. Several accelerated expansion test protocols reduce the testing time by increasing the molarity of alkali in the soak solution. Certain tests are even done with 1 M NaOH solutions (e.g. ASTM 1260). However, it seems that an increase of the alkali concentration is not always synonymous with an increase in expansion. For example, Folliard et al. [11] measured a decrease of the final expansion of certain reactive mortars above a certain alkalinity, as shown in Figure 4.3. The reasons for this effect are unknown and are surprising, considering that the dissolution of quartz and silicate phases, which are directly responsible of the ASR expansion rate, was shown to increase with an increase of the pH and alkaline ionic strength e.g. [1, 12, 13] and described in section 2.1.2.

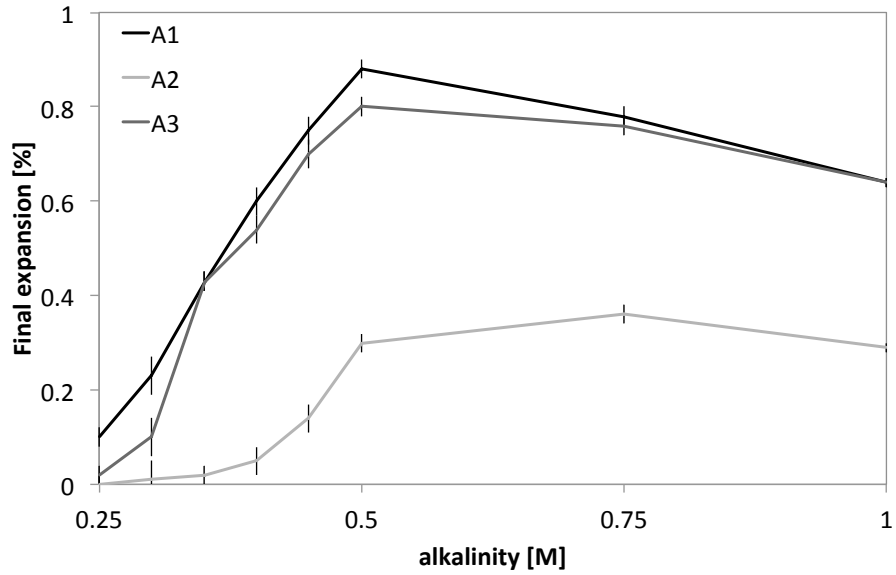

Figure 4.3. Non-linear relation of the final expansion with the alkalinity of the testing solution [11]

4.2. Materials and methods

The cement, the aggregates and the ratios of the pastes and mortars are the same as presented in 2.2.1. The accelerated expansion test, the pore solution extraction and the EDS micro analysis are described in 2.2.2.

Table 4.2 shows the systems studied. Mortars for pore solution extraction (PSE) used for the comparison between sodium and potassium were mixed with various concentrations of alkalis in the mixing water as detailed in Table 4.2. To be able to see changes in the pore solution over time, it was impossible to apply the same external curing in alkaline solution as for expansion mortars. The EDS analyses of the systems with various potassium concentrations were done on expansion samples.

Table 4.2. Mortars and pastes: comparison study of NaOH and KOH addition

[M]	Alkali in curing bath at 38° C after 28 days in 95% RH at 20° C	Alkali addition in the mixing water. Cured at 38° C after 28 days at 20° C
Expansion mortar N. American highly reactive aggregates	NaOH: 0 / 0.35 / 0.6 / 0.9 KOH: 0 / 0.35 / 0.6 / 0.9	
Expansion mortar Swiss reactive aggregate	NaOH: 0 / 0.35 / 0.6 / 0.9	
EDS mortars N. American highly reactive aggregates	KOH: 0.35 / 0.6 / 0.9	
PSE Pastes		KOH: 0.35 / 0.6 / 0.9
PSE mortar N. American highly reactive aggregates		KOH: 0.35 / 0.6 / 0.9
PSE mortar Swiss reactive aggregate		KOH: 0.35 / 0.6 / 0.9

4.3. Results

4.3.1. Accelerated expansion test

Figure 4.4 shows the expansion of PC mortars with highly reactive North American aggregate in curing baths containing NaOH or KOH at 0, 0.35, 0.6 or 0.9 M. The effect of alkali type is shown. The expansion rate of mortars in KOH soak solution is higher than in NaOH. However, the final expansion is nearly the same at each concentration. These observations are in contrast with the observations done by Leeman and Lothenbach. [4].

Figure 4.5 shows the evolution of the expansion of PC mortars with highly reactive North American aggregate in curing baths containing 0, 0.35, 0.6 and 0.9 M NaOH or KOH. Figure 4.6 shows the expansion as a function of time for the Swiss reactive gneiss in 0.35, 0.6 and 0.9 M NaOH solutions. The effect of alkali amount is shown. All mortars start with an expansions rate proportional to the amount of added alkalis. However, the mortars with highly reactive aggregates show a crossover between 0.9 and 0.6 M of alkalis, after around 100 – 200 days immersion. The mortars in the 0.9 M NaOH and KOH solutions show less final expansion than in the 0.6 M solution.

The Swiss gneiss shows a lower degree of expansion in this test, as already mentioned in chapter 2. The expansion seems to increase with the increase of alkalinity. Although, it has to be noted that the reaction is not finished and a crossover may appear later as observed for the North American aggregate. However, the 0.6 and 0.9 M systems seem to separate with time contrary to the systems of Figure 4.5, suggesting that this aggregate doesn’t show the non-linearity of final expansion as a function of alkalinity.

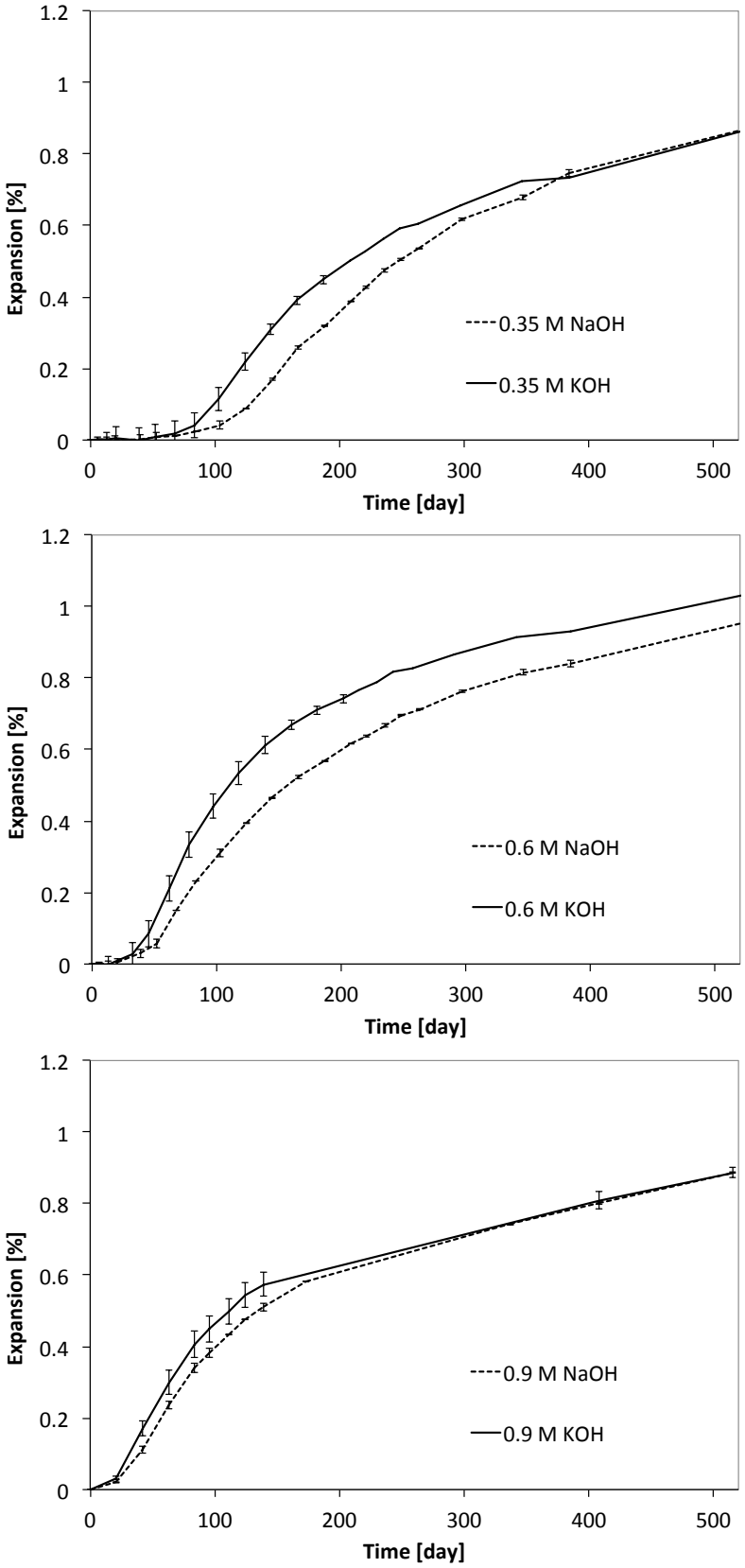

Figure 4.4. The effect of alkali type on ASR. Expansion as a function of time of the highly reactive North American aggregate for 3 alkali concentrations, a) 0.35, b) 0.6 and c) 0.9 M NaOH and KOH.

(a)

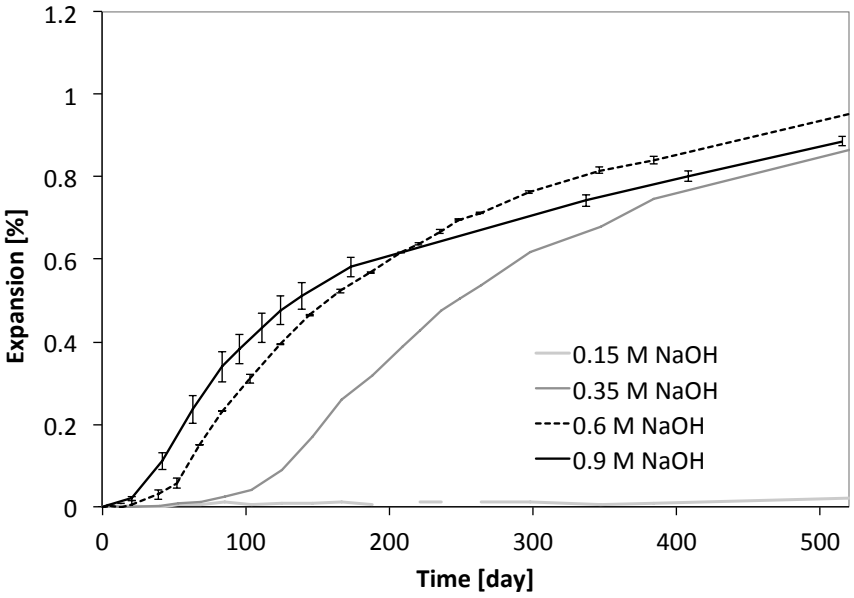

(b)

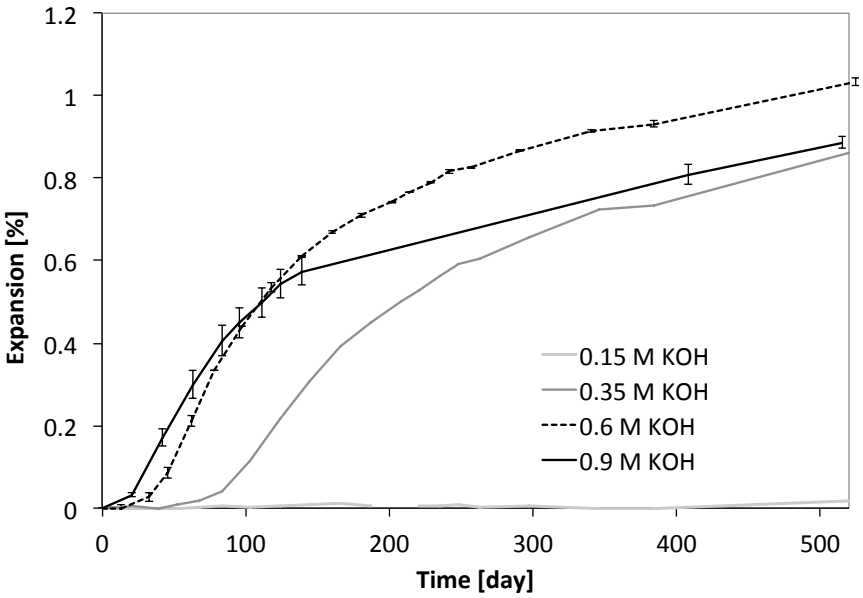

Figure 4.5. Expansion versus time of mortars with the North American highly reactive aggregates cured at 38° C in (a) sodium solution (b) potassium solution.

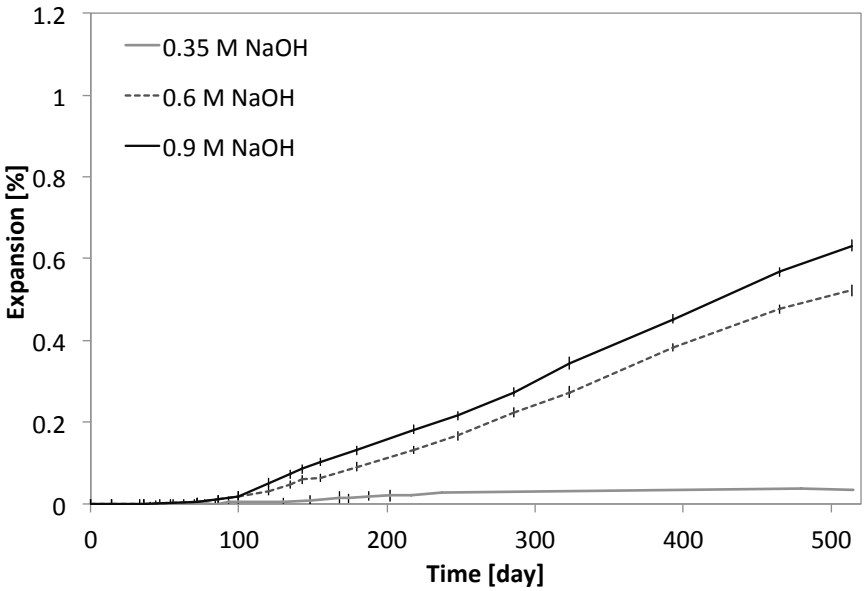

Figure 4.6. Expansion versus time of mortars with the Swiss reactive gneiss cured at 38° C in sodium solution.

4.3.2. Pore solution compositions

The analysis of the pore solution was made only with potassium hydroxide addition, because the general pattern with increasing concentration is similar for both alkalis. Moreover, the KOH systems show a higher expansions rate than with NaOH.

The Table 4.3 shows the concentrations of the main ions present in the pore solutions of the systems studied at 14, 28 and 70 days. It was impossible to obtain any pore solution later than 70 days. It is probably because the batches were cured at 38° C after 20 days to mimic the conditions of the mortars monitored for expansion. This may result in a higher hydration [14], or increase partial evaporation from the bottles, reducing the amount of pore solution available.

The evolution of the potassium, silicon and aluminium concentrations is plotted in Figure 4.7. It appears that the concentration of potassium stays constant over 70 days for the paste and the reactive gneiss, similar to the concentration added in the mixing water. However, the highly reactive aggregate shows a large decrease of alkali concentration over three months. It is visible that the higher the mixing potassium concentration is, the higher the decrease is.

In the 0.35 M KOH, the mortar fixes 0.22 M K^+, in the 0.6 M KOH, 0.40 M K^+ and in the 0.9 M KOH, 0.54 M K^+. This corresponds to a drop of approximately 70 % of the alkali concentration for the 0.9 M KOH mortar, which is in the same order of magnitude as the drop induced by the 15 % substitution blends studied in chapter 2. This comparison is however to be taken with care, considering that the starting alkali and the temperature are different in each system. This drop in alkali concentration seems to be much faster in the pore solution of sealed mortars (28 days) than in the expansion mortars in soak solution (100-200 days). This value can be estimated from the expansion results, considering the drop in expansion rate, probably corresponding to a lack of alkalis. As already mentioned in 2.2, three expansion bars are immersed in 1.5 liters of soak solution, providing a much larger alkali reservoir than only the mixing water.

The silicon concentration of the highly reactive aggregate shows a net increase compared to the two other systems. It is also visible that between 28 and 70 days, the concentration of silicon at 0.9 M KOH becomes lower than at 0.6 M KOH.

The aluminium concentration shows no clear dependence on the alkali concentration for reactive gneiss mortars. It is however visible that the concentration in aluminium increases with the alkalinity in the highly reactive aggregate mortar pore solution. This shows that the highly reactive aggregate, composed mainly of silicate and aluminate phases (see Table 2.1) is dissolved by the presence of alkaline species.

Table 4.3. Ionic concentration of the pore solutions at 3 different alkalinities of 0.35, 0.6 and 0.9 M KOH

	[mM]	Na			K			Ca			Si			Al		
	[day]	14	28	70	14	28	70	14	28	70	14	28	70	14	28	70
Paste	0.35	132.7	127.0	149.6	486.1	449.7	488.6	1.7	0.9	1.5	0.3	0.3	0.4	0.1	0.1	0.2
	0.6	127.4	129.7	145.3	680.5	689.0	700.9	1.3	0.9	1.4	0.3	0.4	0.4	0.1	0.2	0.2
	0.9	122.2	124.3	143.5	900.5	912.8	972.1	1.2	0.8	2.1	0.5	0.5	0.6	0.2	0.2	0.2
Swiss reactive gneiss	0.35	73.1	135.5	115.7	486.1	452.3	411.9	1.7	0.9	0.2	0.4	0.5	1.4	0.1	0.2	0.4
	0.6	142.7	132.4	126.1	706.1	664.4	639.5	1.2	0.7	0.1	0.5	1.0	2.6	0.1	0.2	0.4
	0.9	134.0	133.1	106.6	897.9	896.7	877.5	1.1	0.6	0.3	0.7	1.2	3.0	0.2	0.3	0.4
N. Amercan highly reactive agg.	0.35	134.8	124.9	138.8	163.7	136.6	129.7	1.0	0.04	0.1	0.3	4.4	17.8	0.1	0.1	0.3
	0.6	131.4	104.4	140.5	278.8	199.3	192.6	0.1	0.02	0.1	4.7	16.0	52.7	0.2	0.2	0.3
	0.9	132.2	120.4	139.6	427.2	360.5	271.2	0.1	0.02	0.2	12.6	21.8	40.2	0.2	0.3	0.3

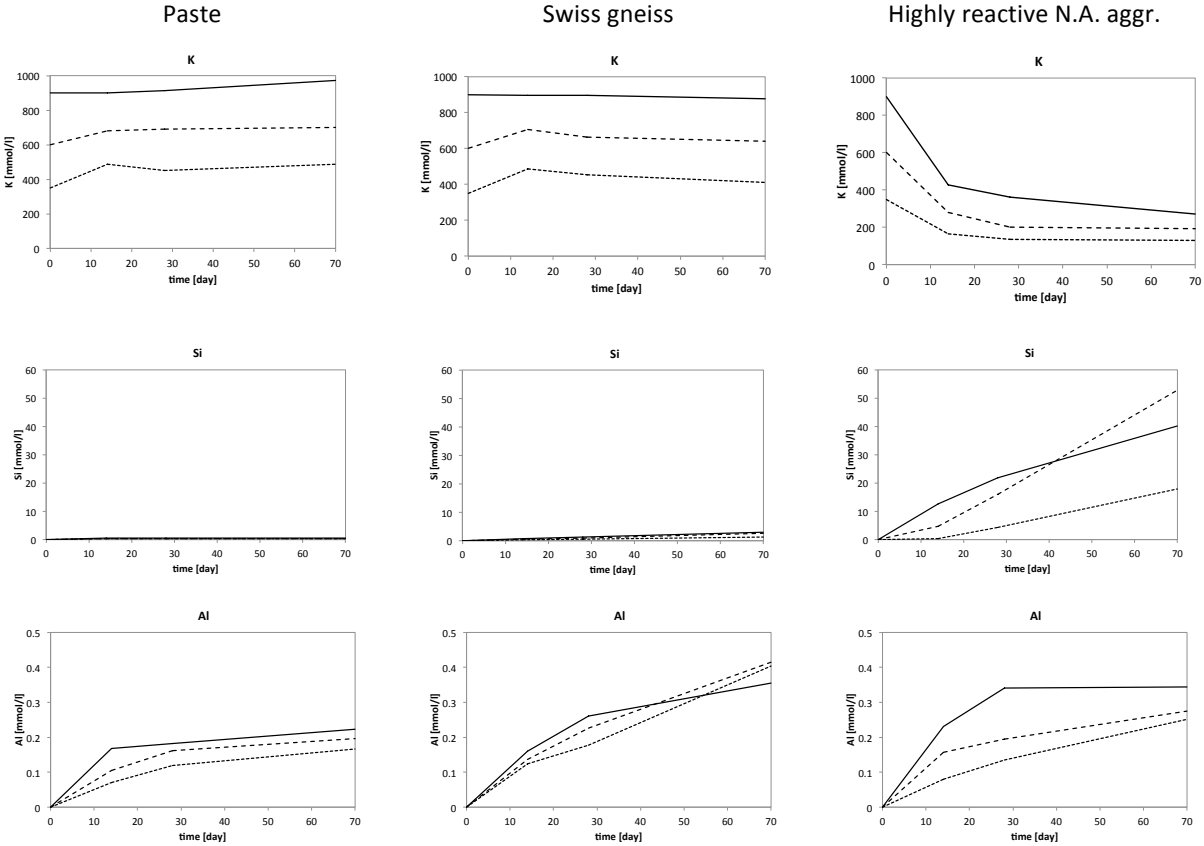

Figure 4.7. Graphic representation of potassium (average standard dev. 6 mM), silicon (average standard dev. 0.4 mM) and aluminium (average standard dev. 0.1 mM) concentration of the pore solutions over time. Pointed line: 0.35 M KOH, dotted line: 0.6 M KOH, line: 0.9 M KOH

4.3.3. Saturation indices of tobermorite and portlandite

The saturation index (SI) is an index indicating whether a mineral is precipitating or dissolving in a solution. The value is positive when the mineral is precipitating and negative when it is dissolving. Zero corresponds to the equilibrium state. The SI is the log of the ratio of the ion activity product IAP and the solubility product K_{SP}, following equation 4.2:

$$SI = \log(IAP/K_{SP}) \qquad 4.2$$

The saturation indexes of the main phases present in the pastes were calculated with the help of the thermodynamic simulation program PhreeqC © [15]. Tobermorite is a mineral

with composition close to C-S-H. The SI of tobermorite and portlandite for the pastes and the two reactive mortars are shown in the Table 4.4 at 28 and 70 days as a function of the added alkali concentration. Figure 4.8 shows the evolution of the SI at 70 days.

The SI of portlandite remains close to equilibrium at each alkali concentration in the paste pore solution at 28 and 70 days. The tobermorite is also close to equilibrium but remains however in the oversaturation regime.

The SI of the two phases for the Swiss gneiss mortars pore solutions is very close to the SI of the paste. Only the portlandite tends to drop into the dissolution regime at 28 days for two alkalinities. The absolute values are however very low and may be considered as being at equilibrium, considering standard errors of the ICP measurement (e.g. pore solution dilution).

The SI of portlandite is however in a dissolution regime in the highly reactive North American aggregate mortars. The tendency increases until 70 days. In parallel, the SI of tobermorite is very high and shows a tendency to the supersaturation at both ages too, increasing with the alkali concentration.

Table 4.4. Saturation indexes at 28 and 70 days of the pore solutions of the pastes, Swiss gneiss mortars and North American highly reactive aggregates mortars.

		KOH [M]	**0.35**	**0.6**	**0.9**
Paste	28 days	Tobermorite	2.4	1.7	3.0
		Portlandite	0.4	0.5	0.8
	70 days	Tobermorite	0.9	0.9	0.7
		Portlandite	0.1	0.3	0.3
Swiss gneiss	28 days	Tobermorite	1.9	1.2	3.4
		Portlandite	-0.6	-0.7	-0.1
	70 days	Tobermorite	2.1	2.8	2.3
		Portlandite	0.1	0.2	0.2
Highly reactive N. American agggregate	28 days	Tobermorite	7.8	10.5	11.0
		Portlandite	-1.2	-1.2	-0.8
	70 days	Tobermorite	2.7	4.3	4.2
		Portlandite	-1.5	-1.9	-1.7

(a)

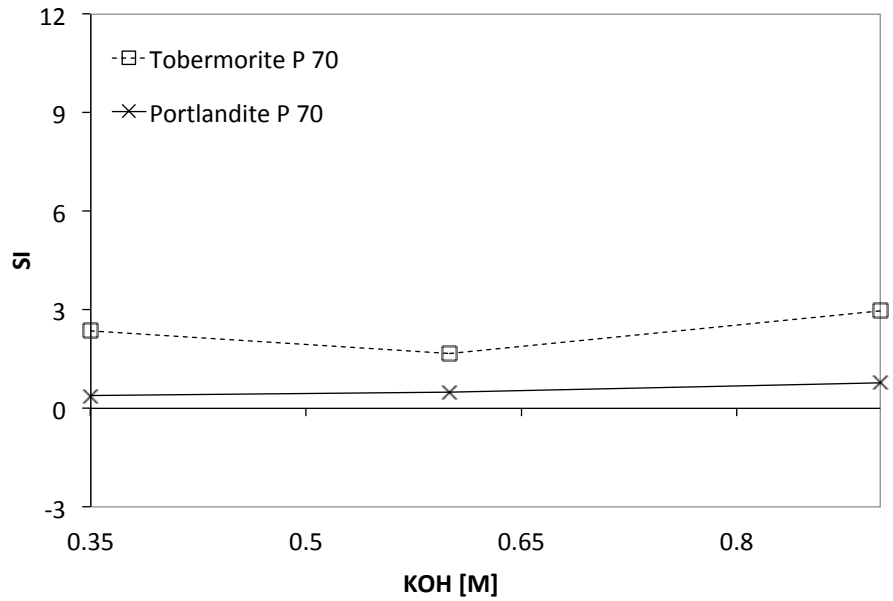
12
9
6
3
0
-3
SI
Tobermorite P 70
Portlandite P 70
0.35
0.5
0.65
0.8
KOH [M]

(b)

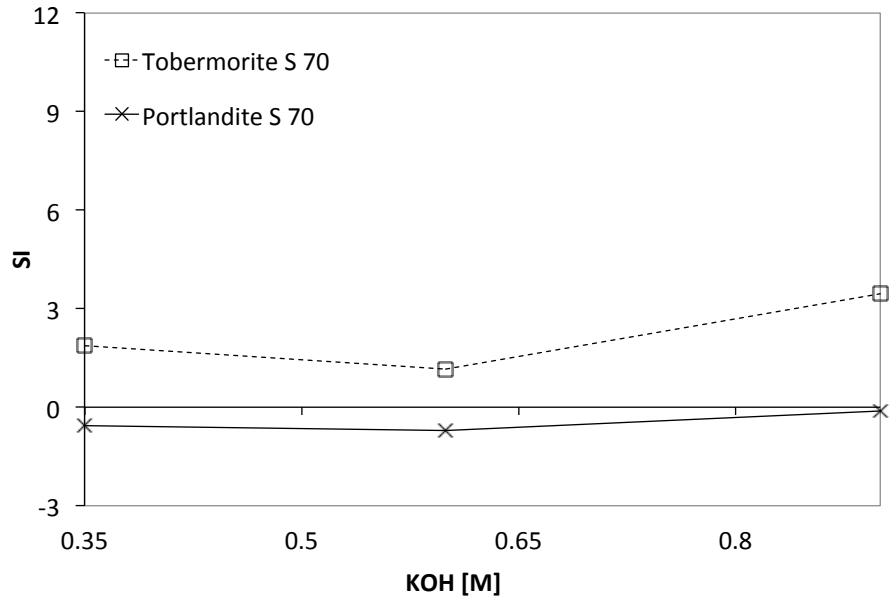
12
9
6
3
0
-3
SI
Tobermorite S 70
Portlandite S 70
0.35
0.5
0.65
0.8
KOH [M]

(c)

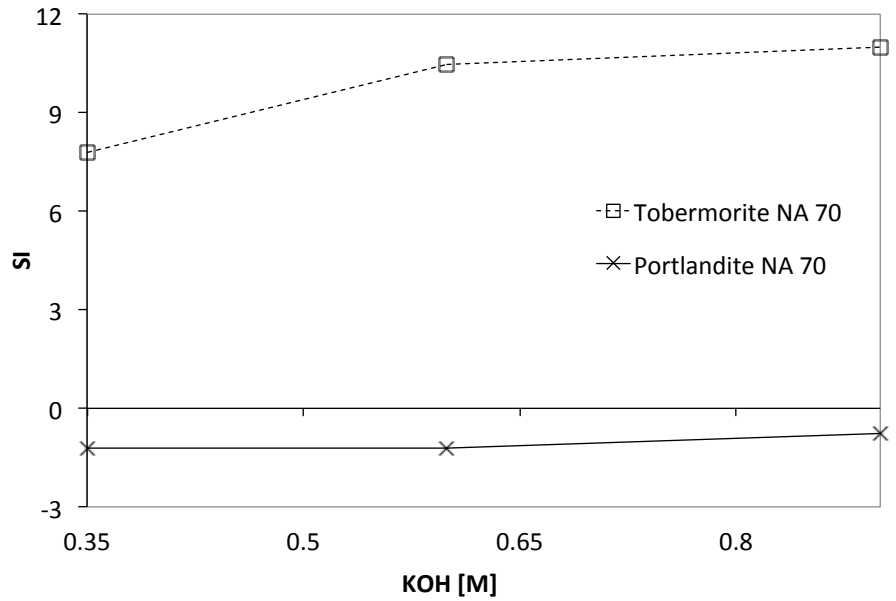

Figure 4.8. Saturation indexes at 70 days for (a) the paste, (b) the Swiss gneiss and (c) the north American highly reactive aggregate at three different alkalinities.

4.4. Discussion

The mortars put in KOH soak solutions had a higher expansion rate than the ones in NaOH solutions. The final expansion was however similar. As discussed, K^+ ions have a lower enthalpy of hydration than Na^+ (Table 4.1). Consequently, potassium more easily releases the water shell adsorbed on its surface, which can be expected to facilitate bind on terminal silanol bonds. This tends to enhance the disintegration of the silica structure, facilitating dissolution and so on ASR gel formation. This behaviour is supported by the coagulation effect observed by Depasse [16], showing less dissolution of silica in NaOH solution than in KOH solutions.

Secondly, it is possible that the radius of the ions also play a role; the higher radius of K^+ (Table 4.1) may results in a greater disruption of the silica framework as observed by Hou et al. [2, 3], allowing more water to penetrate the gel.

It was observed that the highly reactive mortars in 0.9 M soak solutions had a lower final expansion than the ones in the 0.6 M solutions. This was not observed in the Swiss reactive gneiss mortars. This crossover of the final expansion between both alkali concentrations is difficult to explain and was not elucidated in this work. Some conjections can be made:

In the highly reactive mortars immersed in alkaline soak solution, the undersaturated state of portlandite and the oversaturated state of tobermorite suggests consumption of portlandite to form C-S-H. The dissolution of the highly reactive aggregates results in a high silicon concentration in the pore solution, which supports the formation of additional C-S-H in these conditions. This may reduce the source of calcium present in the system, accelerating the alkali depletion due to consumption by ASR gel and C-S-H.

Secondly, the aggregates have different mineralogy and morphology. The highly reactive aggregate is mostly amorphous, rapidly reacting on its surface. The Swiss gneiss is a poly-phased mineral. Its phases are basically non-reactive except some reactive zones inside the aggregate, at the phase interfaces. This results in a very slow reactivity, with a confined gel formation. Considering that the reactive phases and the kinetic of gel formation are different for both aggregates, it is possible that the viscosity, and subsequently the mobility of the gels are different. The rapid gel formation on the surface of the highly reactive aggregates in

the 0.9 M soak solution may result in a low viscosity gel, applying fewer stresses to the matrix.

The increase of alkali concentration in highly reactive mortars also increases the aluminium concentration in the pore solution. The concentration remains very low and the difference in aluminium in solution is marginal, considering the error of measurement of ICP. However, this small but constant source of aluminium may also have an impact on ASR, reducing the silica dissolution over the long term. Coupled to the reduction of alkalinity, this aluminium may have an effect on gel formation. A threshold ratio between the decrease of the alkali concentration of the pore solution and a sufficient amount of aluminium ions could stabilize the gel formation of highly alkaline systems over the long-term.

4.5. References

[1] P.M. Dove, The dissolution kinetics of quartz in aqueous mixed cation solutions, Geochimica et Cosmochimica Acta, 63 (1999) 3715-3727.

[2] X. Hou, Structural investigations of alkali silicate gels, Journal of the American Ceramic Society, 88 (2005) 943-949.

[3] X. Hou, L.J. Struble, R.J. Kirkpatrick, Formation of ASR gel and the roles of C-S-H and portlandite, Cement and Concrete Research, 34 (2004) 1683-1696.

[4] A. Leemann, B. Lothenbach, The influence of potassium-sodium ratio in cement on concrete expansion due to alkali-aggregate reaction, Cement and Concrete Research, 38 (2008) 1162-1168.

[5] W.L. Marshall, J.M. Warakomski, Amorphous silica solubilities--II. Effect of aqueous salt solutions at 25∞C, Geochimica et Cosmochimica Acta, 44 (1980) 915-917, 919-924.

[6] J. Burgess, Metal ions in solution, 1978.

[7] J. Depasse, A. Watillon, The stability of amorphous colloidal silica, Journal of Colloid and Interface Science, 33 (1970) 430-438.

[8] M. Prezzi, The alkali reaction part 1: Use of the double-layer theory to explain the behaviour of the reaction product gels, ACI Mater, 94 (1997) 10-17.

[9] M. Prezzi, The alkali silica reaction - part 2: the effect of chemical admixtures, ACI Mater, 95 (1998) 391-401.

[10] d. McPhee, Activation of SCMs: some chemical perspectives, in: Supplementary cementitious materials, Lausanne, EPFL, 2010.

[11] K.J. Folliard, R. Barborak, T. Drimalas, L. Du, Garber, S., J. Ideker, T. Ley, S. Williams, M. Juenger, M.D.A. Thomas, B. Fournier, Preventing ASR/DEF in New Concrete: Final Report, The University of Texas at Austin, Center for Transportation Research (CTR), CTR 4085-5, (2006).

[12] P.M. Dove, S.F. Elston, Dissolution kinetics of quartz in sodium chloride solutions: Analysis of existing data and a rate model for 25¬∞C, Geochimica et Cosmochimica Acta, 56 (1992) 4147-4156.

[13] J.P. Icenhower, P.M. Dove, The dissolution kinetics of amorphous silica into sodium chloride solutions: effects of temperature and ionic strength, Geochimica et Cosmochimica Acta, 64 (2000) 4193-4203.
[14] X. Zhang, quantitative microstructural characterisation of concrete cured under realistic temperature conditions, in: LMC, EPFL, Lausanne, 2007.
[15] D.L. Parkhurst, C.A.J. Appelo, User's guide to PHREEQC (Version 2)—A computer program for speciation, batch-reaction, one-dimensional transport, and inverse geochemical calculations, in: US Geological Survey Water-Resources Investigations, 1999, pp. 312 pp.
[16] J. Depasse, Coagulation of Colloidal Silica by Alkaline Cations: Surface Dehydration or Interparticle Bridging?, Journal of Colloid and Interface Science, 194 (1997) 260-262.

CHAPTER 5 CONCLUSIONS AND PERSPECTIVES

5.1. Conclusions

The aim of this thesis was to better understand the mechanisms controlling ASR expansion in presence of SCMs. Special attention was given to the role of aluminium. The common theory to explain the role of aluminium addition on ASR was contradicted. A new mechanism was proposed and experimentally confirmed.

It was shown in a first part of this work that SCMs containing silica and alumina lowered expansion of reactive mortars more than those containing only silica. Both silicon and aluminium provided by SCMs entered the C-S-H structure. However, the alkalinity of the pore solution of blended pastes with aluminosilicates SCMs was not lower than blended pastes with only silica addition at a similar substitution level. Even by recalculating the amount of alkalis fixed as a function of the amount of C-S-H, it was observed that the presence of aluminium in C-S-H doesn't significantly change the alkali fixation capacity of this phase in the range of compositions of classical blended pastes. The observations are consistent with the results obtained by Hong and Glasser [1], if the composition of the C-S-H is taken into account.

These new results showed that the presence of aluminium has a beneficial impact on the ASR expansion, but this is not due to the higher alkali fixation of aluminium rich C-S-H as usually thought.

The addition of aluminosilicates SCMs, like metakaolin, gives some mM of aluminium in the pore solution.

In marine hydrous and geo-chemistry, the effect of aluminium in solution on the reduction of silica dissolution is already well known. Evidence of a similar effect in cementitious systems was found in this work. When reactive aggregates were immersed in simulated pore solutions containing similar concentrations of aluminium to those seen in blended pastes, the amount of degradation was clearly reduced. The role of aluminium in solution was further investigated with a more fundamental study on fused silica plates. The presence of

some mM of aluminium in solution was able to control the surface dissolution of these amorphous silica plates. The aluminium is incorporated into the silica framework and is not merely surface-adsorbed. Furthermore, when a plate was first immersed in a solution containing aluminium, and then subsequently in an aluminium free alkaline solution, the dissolution was still inhibited. It is proposed that aluminium is incorporated at high-energy sites, reducing the removal of surface species. It was observed that a lower pH level allows more aluminium to incorporate on silica surface.

This study brings new insights into the main mechanisms controlling ASR. The presence of both silica and alumina in SCMs seems to be important to control ASR over the long-term. The presence of silica decreases the alkalinity of the pore solution. This has a double effect. First, the lower pH reduces the dissolution rate of the reactive silica and secondly, the lower pH supports the aluminium incorporation on the surface of reactive phase. Alumina is important as it adsorbs directly on the surface of reactive silicates, inhibiting their dissolution. Both mechanisms seem to work in synergy ensuring a control of ASR over the long-term.

Some new insights were obtained to understand accelerated testing. This work tries to better understand the different effect of KOH and NaOH addition on ASR expansion.

Despite a relatively similar final expansion, the rate of expansion of mortars immersed in KOH soak solutions was higher than with NaOH. This difference was though to be due to the different ionic properties of both alkalis, such as enthalpy of hydration and radius, which means that it is easier for potassium to penetrate reactive silicates and break silanol bonds.

The mortars with highly reactive aggregates in 0.9 M alkaline solutions show a lower final expansion than in 0.6 M solutions. This phenomenon was not fully understood, but may have several reasons: the higher consumption of portlandite in highly alkaline solutions probably reduces the amount of calcium ions buffering ASR. It could also result in a formation of more C-S-H fixing alkalis from the solution. Aluminium in solution provided by the early aggregates dissolution may have a reducing effect on the long-term aggregate dissolution. Finally, the gel composition and viscosity may change and have an impact on the internal stresses in the aggregates, resulting in a lower final expansion despite the higher alkalinity.

5.2. Perspectives

This work gives new insights into the mechanisms controlling ASR in presence of SCMs. Future work should focus on the improvement of testing methods and modeling of ASR degradation in presence of SCMs. If testing methods can be improved, this will facilitate the design of ASR resistant concretes. The improvement of testing methods is only possible by considering the entire picture of ASR expansion. A schematic representation is shown in Figure 5.1.

The expansion of reactive concrete depends first on the dissolution rate of the aggregates. The dissolution rate is influenced by several factors:

- The mineralogy of the reactive phase; chalcedony, feldspars, biotite and muscovite are typical reactive silicate phases. Their different composition, atomic structures and amorphous fraction leads to different dissolution rates. Petrographic analysis is able to find out what reactive phases are present in potentially reactive aggregates and at which quantity. It may also be possible to asses this with studies of aggregates in simulated pore solutions.
- The pH of the pore solution is the main parameter influencing the dissolution rate of silicates phases in reactive concrete (for a given reactive phase). The solution pH can be reduced by the presence of silica rich SCMs. The kinetics of hydration and the composition of the C-S-H have important impact on the pore solution pH over the long term. In this study, the amount of sodium and potassium fixed per gram of C-S-H bound water was calculated for a given phase composition. Further investigations would able to more accurately calculate the alkali fixation per gram of C-S-H. Furthermore, the understanding of the kinetic of hydration of blended cement pastes would help quantifying alkali fixation.
- The presence of mM of aluminium in the pore solution was shown to reduce or even stop the dissolution rate of silica over the long term. As shown in this work, MK blends provide enough aluminium over at least two years to stabilize silica phases. A wider matrix of blends should be analyzed to get more idea about the amount of aluminium dissolved in solution for different SCMs, which can control ASR. For example, Annexe 2 shows a parallel study of fly ash blended mortars. 20% of PC

substitution by class F fly ash was able to fully control ASR expansion at 38°C over two years, and the pore solution of the paste had an alkalis decrease of 65% compared to PC, and contained 0.5 mM of aluminium over one year.

- The K/Na ratio of the pore solution was shown to have an influence on the dissolution rate. This parameter is a function of the PC and SCM type as already known.

The synergy between silica and alumina addition has to be studied more in detail, to be able to select the optimal SCM or a combination of SCM as a function of reactivity, silica and alumina concentration.

The mineralogy of reacting systems has to be investigated, to get more information about the composition and viscosity of the formed gel. Sodium and potassium hydroxide concentration may also influence the viscosity and mobility of the gel, resulting in variation of expansion.

Finally, the structure of the aggregate can change the expansion. A multi-phased aggregate, as for example the Swiss reactive gneiss studied in this work, contains only a small fraction of reactive phases. The existing micro-cracking allows the ions and water to penetrate the aggregate and reach the reactive phase. It results in a slow but significant expansion, continuing over many years. Furthermore, cracking of the aggregates, exposes more reactive phases. This remains to be investigated, but is probably one of the reason why a long-term aluminium source is important in concretes, to stabilize reactive aggregates over the long term. In a mono-phased amorphous aggregate, as for example the North American aggregate studied in this work, the pore solution is directly in contact with the reactive surface of the aggregate. The gel has a tendency to form at the interface aggregate-cement paste and the reaction may exhaust itself earlier.

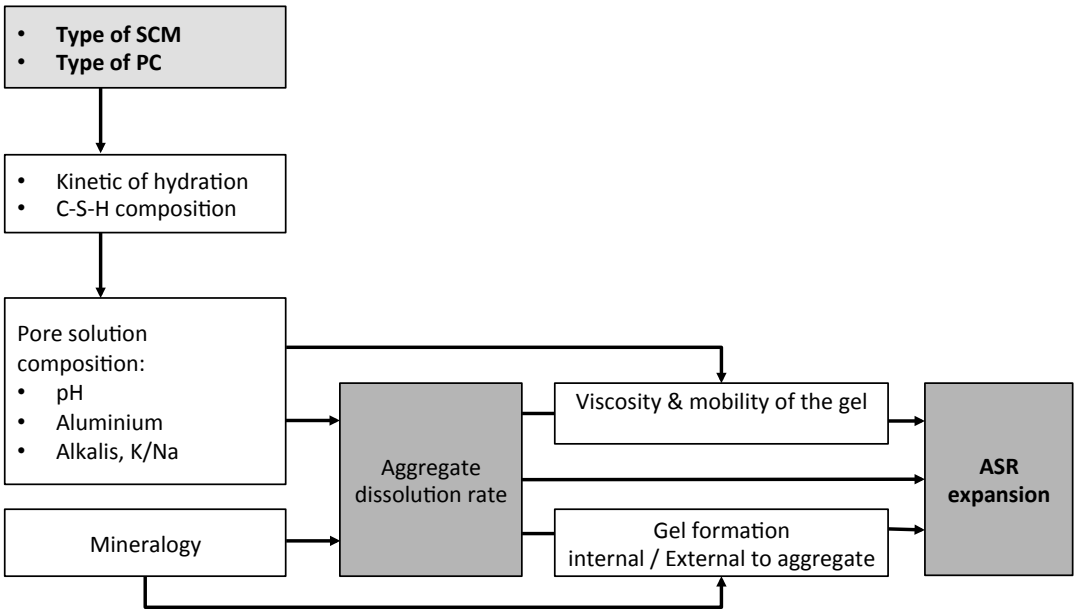

Figure 5.1. Schematic representation of the parameters influencing and controlling ASR

5.3. References

[1] S.-Y. Hong, F.P. Glasser, Alkali sorption by C-S-H and C-A-S-H gels: Part II. Role of alumina, Cement and Concrete Research, 32 (2002) 1101-1111.

ANNEX 1 THE INFLUENCE OF LITHIUM HYDROXIDE ON ASR

This work focuses on the impact of lithium, and mainly lithium hydroxide on ASR. More especially, the effect of LiOH on the dissolution of silicates and its impact on the pore solution and hydrates was observed.

1. State of the art

1.1. Context

It is known that the addition of lithium in several forms in the batch water of reactive concrete and mortars is able to reduce the expansion due to ASR e.g. [1, 2]. McLoy and Caldwell [3] found in the 50's that the use of different type of lithium based compounds were promising in suppressing ASR. This is a troubling observation, considering that lithium hydroxide, for example, is known to increase the dissolution of silicates and quartz, which should increase the gel formation rate e.g. [4].

At least 11 types of lithium salts (LiF, LiCl, LiBr, LiOH, LiOH-H_2O, $LiNO_3$, $LiNO_2$, Li_2CO_3, Li_2SO_4, Li_2HPO_4, Li_2SiO_3) show some reducing effect regarding ASR if they are present at an appropriate dosage [1].

1.2. The mechanisms controlling ASR in presence of lithium compounds

The mechanisms controlling ASR through the use of lithium salts are still being discussed. Different directions were proposed: Certain works focused on the ASR gel repolymerization. Kurtis and Monteiro [5] observed dissolved silica in solutions with and without lithium

chloride with X-ray imaging. The repolymerization of the dissolved silica was less evident in lithium free systems. It also seems that lithium promotes the aggregation of larger particles, having lower surface charge density. These mechanisms tend to lower the expansion of the ASR gel, as proposed by Prezzi et al. [6, 7].

Others propose [8] that the suppressive effect of $LiNO_3$ regarding ASR could be attributed to the passivation of the silica reactive zone of the aggregates by a layer of Li-Si crystal and a low calcium dense gel product, as shown in Figure 1. This results in the reduction of the dissolution rate of silica, forming less expansive gels.

Feng et al. [1] observed that the amount of lithium added to the batch was reduced to about half of the original concentration. Hydration products of the cement paste, such as C-S-H, but also the passivation layers, may probably adsorb the lithium ions.

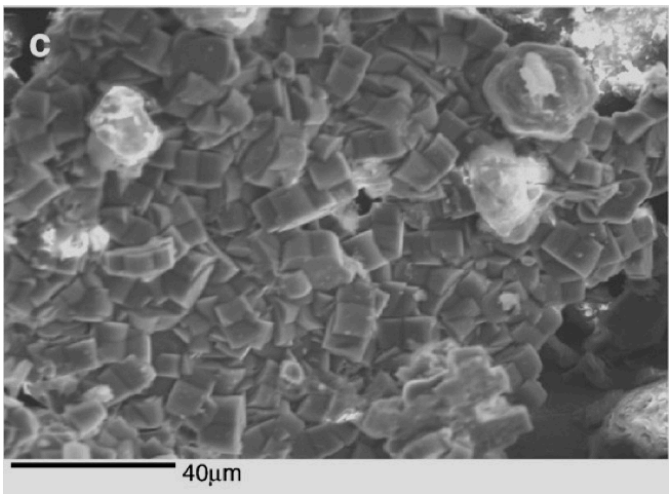

Figure 1. SEM BSE image of a Vycor glass disk immersed in a 1M NaOH + 0.74M $LiNO_3$ solution during 120 days at 38°C. The Li-Si crystals are covering the surface. [8]

1.3. Contradictory results

The mechanisms described above most probably play a role in controlling ASR, at least under certain conditions. Some works show however unexplained behaviour, showing that the picture is not fully understood. Feng et al. [1] conclude in their critical review, that findings on the influence of lithium salts on ASR was contradictory.

The nature of the reactive aggregate seems to play an important role. Several researchers showed that the efficacy of lithium compounds was greatest with highly reactive aggregates. Lane [9] observed that for a similar lithium dosage, highly reactive pyrex glass was better controlled than the less reactive Virginia quartz aggregate. He also observed that the effect of lithium compounds was higher in highly accelerated conditions. Durand [10] observed that the minimum amount of compound necessary to reduce expansion below the limit given in standards at two years (CSA) varies according to the lithium salt type and the reactivity of the aggregate. Following these studies, it seems that principally LiOH and $LiNO_3$ are more effective with highly reactive aggregates than with slowly reacting aggregates.

Sakagushi et al. [11] showed through pore solution studies, that the concentration of sodium and potassium stayed nearly constant, whereas the concentration of lithium clearly dropped. This was in contradiction with lithium free systems where sodium and potassium concentration dropped, as also observed in the chapter 2.

Berra et al. [12] discovered a linear relation between the dosage in $LiNO_3$ needed to mitigate ASR and the amount of Na + K. The amount of alkalis in the aggregates also tends to have an impact on the $LiNO_3$ threshold.

Geology studies proposed that the presence of lithium ions may substitute for 6-coordinated elements like Al, Fe, Cr, Sc, and V in minerals [13]. Goguel [14] mentioned that lithium may replace aluminium in silicate phases, and that this mechanism may increase with temperature. He also proposed that an insoluble lithium silicate could form in the minerals.

2. Materials and methods

PC expansion mortars with the North American highly reactive aggregate were cast. In parallel, three types of pastes were mixed with 0.55 M LiOH: a PC paste, a 10 % MK and a 10 % SFQ (as described in 2.2). To make a comparative study with different alkalis, similar pastes were cast with 0.55 M NaOH and 0.55 M KOH (Table 6.1). The experimental batch focused on how the evolution of hydration products and pore solution in blended systems depended on the alkali type.

Table 1. Pastes: study of the effect of lithium hydroxide addition

[M]	Alkali addition in the mixing water
Expansion mortar N. American highly reactive aggregates	LiOH: 0.55
EDS paste	20°C: KOH(P): 0.55 NaOH(P): 0.55 LiOH (P): 0.55
PSE pastes	20°C: KOH(P): 0.55 NaOH(P): 0.55 LiOH (P): 0.55

The accelerated expansion test, the pore solution extraction and the EDS micro analysis are described in 2.2.2.

3. Results

3.1. Accelerated expansion test

Figure 6.2 shows the expansion versus time of PC mortars containing highly reactive North American aggregate in two different curing solutions of 0.35 and 0.6 M NaOH. In each solution, a batch of mortars was mixed with 0.55 M LiOH. The mortars containing the LiOH do not expand during 1 year at 38° C in both curing solutions.

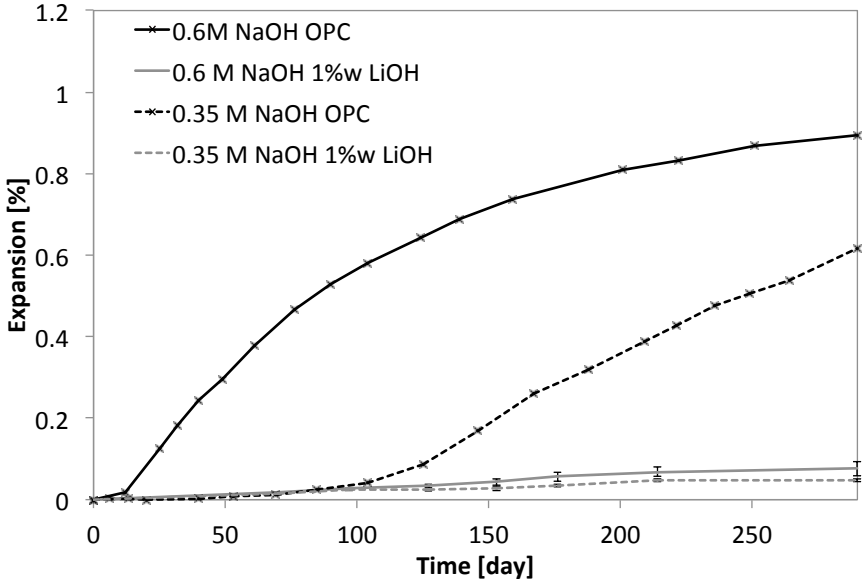

Figure 6.2. Expansion versus time of PC mortars with 0.55 M LiOH. Two different curing solutions: 0.35 and 0.6 M NaOH at 38° C

3.2. Pore solution composition

The Table 2 shows the ionic concentration of the PC pastes and 10 % blends up to 300 days, at 0.55 M of NaOH, KOH or LiOH.

The silicon concentration over time for the SFQ blend is shown in Figure 3. The silicon concentration is significantly increased by the NaOH addition. Then to a lower extent by KOH and LiOH.

The evolution of the silicon and aluminium concentrations over time for the 10 % MK blend is shown in Figure 6.4. It is visible that the concentration of silicon is increased by alkalis, mainly by the LiOH. The aluminium concentration is clearly increased by the presence of lithium, followed by sodium and potassium hydroxide.

Table 2. Pore solution concentration of the PC pastes and blends with 0.55 M of different alkalis

	[mM]	time	Na	K	Li	Ca	Si	Al
	PC	0	0.0	0.0		0.00	0.00	0.00
		28	115.0	382.7		0.17	0.10	0.11
		90	97.4	314.6		0.94	0.07	0.09
		300	125.0	344.0		1.16	0.10	0.01
	10MK	0	0.0	0.0		0.00	0.00	0.00
		28	92.5	291.0		0.13	0.20	1.00
		90	83.0	204.2		0.95	0.10	0.12
		300	90.4	220.4		0.60	0.20	0.14
	10SFQ	0	0.0	0.0		0.00	0.00	0.00
		28	93.0	290.7		0.17	0.20	0.11
		90	63.0	164.2		0.95	0.10	0.09
		300	76.6	193.7		0.08	0.20	0.01
NaOH	PC	0	550	0.0		0.00	0.00	0.00
		28	400.2	355.6		1.63	0.23	0.15
		90	382.8	370.9		1.45	0.17	0.07
		300	0.1	0.3		0.00	0.00	0.00
	10MK	0	550	0.0		0.00	0.00	0.00
		28	210.1	167.8		0.86	0.45	1.73
		90	231.4	167.8		0.86	0.30	0.83
		300	43.4	31.2		0.12	0.10	0.21
	10SFQ	0	550	0.0		0.00	0.00	0.00
		28	198.8	155.5		0.17	39.89	0.17
		90	278.0	163.5		0.05	7.41	0.12
		300	0.0	0.1		0.00	0.00	0.00
KOH	PC	0	0.0	550		0.00	0.00	0.00
		28	112.2	560.3		1.53	0.23	0.13
		90	129.2	754.7		1.41	0.18	0.08
		300	81.8	335.1		1.18	0.20	0.17
	10MK	0	0.0	550		0.00	0.00	0.00
		28	80.5	284.0		0.74	0.67	1.42
		90	94.8	335.1		0.89	0.36	0.80
		300	0.1	0.2		0.01	0.00	0.00
	10SFQ	0	0.0	550		0.00	0.00	0.00
		28	72.6	289.1		0.12	17.45	0.17
		90	75.3	289.1		0.05	8.33	0.12
		300	15.8	44.3		0.00	1.11	0.11
LiOH	PC	0	0.0	0.0	550.0	0.00	0.00	0.00
		28	115.7	404.2	351.6	2.10	0.37	0.11
		90	122.6	337.7	354.5	1.60	0.27	0.12
		300	113.1	319.8	308.4	0.00	0.20	0.10
	10MK	0	0.0	0.0	550.0	0.00	0.00	0.00
		28	91.3	216.7	275.2	0.26	0.61	2.59
		90	79.6	165.7	285.3	0.95	0.80	1.57
		300	79.2	182.1	260.8	0.00	0.50	0.80
	10SFQ	0	0.0	0.0	550.0	0.00	0.00	0.00
		28	67.4	132.5	172.9	0.04	12.78	0.18
		90	67.0	131.0	129.1	0.05	6.70	0.10
		300	60.1	120.6	101.3	0.02	1.50	0.01

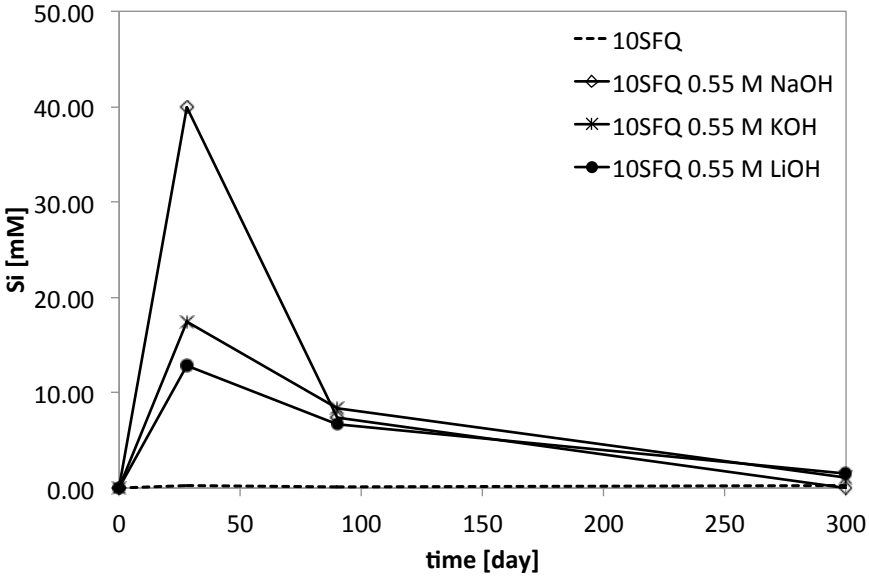

Figure 3. Silicon concentration in 10 % silica fume – quartz blends with 0.55 M alkali addition

(a)

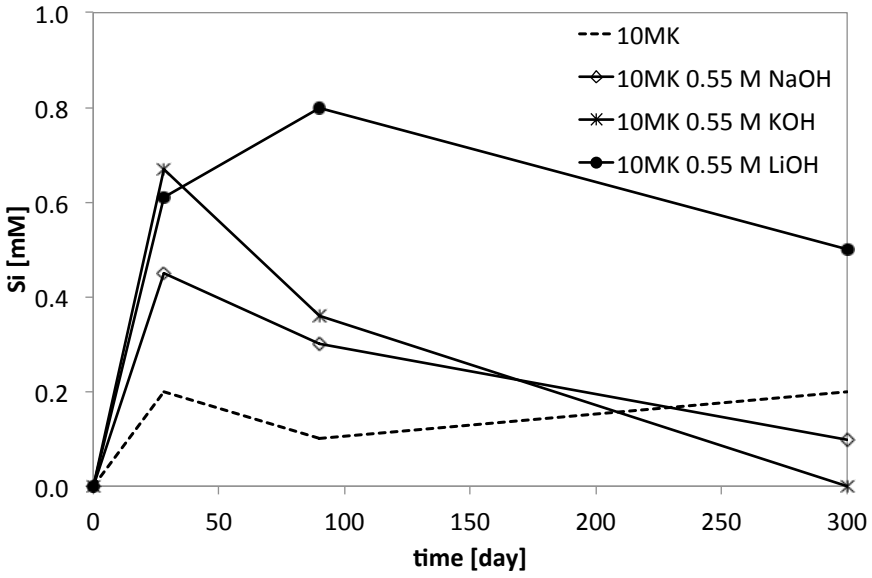

(b)

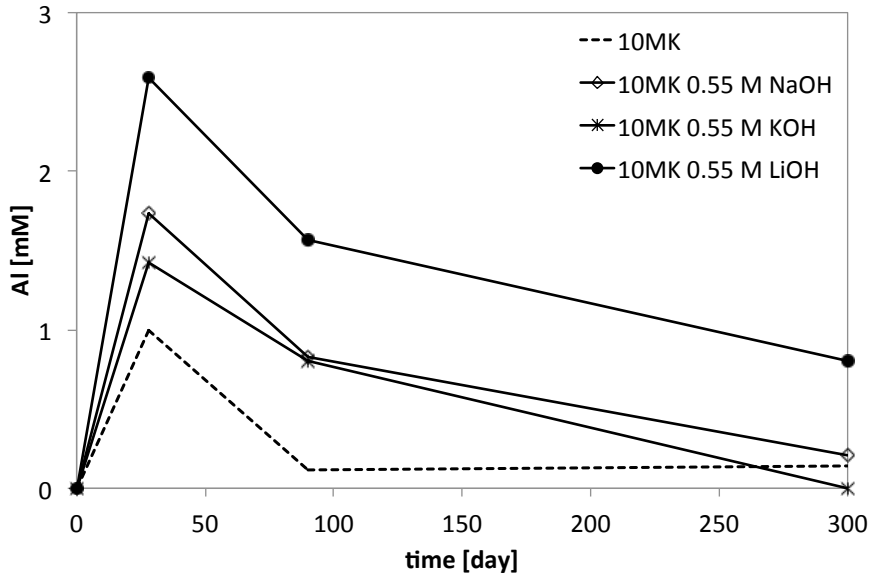

Figure 4. Silicon (a) and aluminium (b) concentration in 10 % metakaolin blends with 0.55 M alkali addition

3.3. C-S-H composition

The EDS analyses of the outer C-S-H of the PC and 10 % blends (MK and SFQ) are shown in Figure 5 for the 3 different alkalis at 0.55 M. The pastes are 90 days old. The lithium addition in the PC pastes tends to slightly increase the silicon and aluminium concentration in the C-S-H (graphic a). But they are not significantly influenced by the other added alkalis.

The graphic (b) shows the C-S-H composition of the 10% SFQ pastes. The sodium hydroxide is the most influent cation on the hydration of the blend. NaOH increases the silicon and slightly the aluminium concentration in the C-S-H. LiOH and KOH have less impact on the phase formation in blended pastes.

The 10 % metakaolin blends pastes (graphic c) present a high dispersion of the C-S-H composition. This is one of the main difficulties with metakaolin blended pastes. The C-S-H phase is intermixed with strättlingite and other phases that lead to an SEM EDS response with a dispersed composition. This tendency seems to be increased by the presence of alkalis. The addition of LiOH have the biggest influence on the phase composition at 70 days. It shows a higher aluminium and silicon content at 70 days, compared to the two other alkalis addition and to the classical 10 % MK blend at 90 days (graphic of Figure 2.8).

(a)

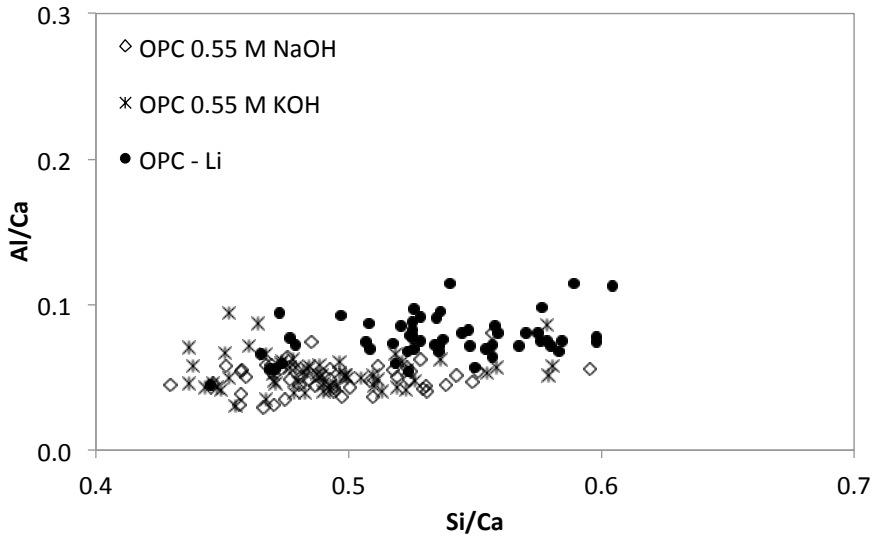

(b)

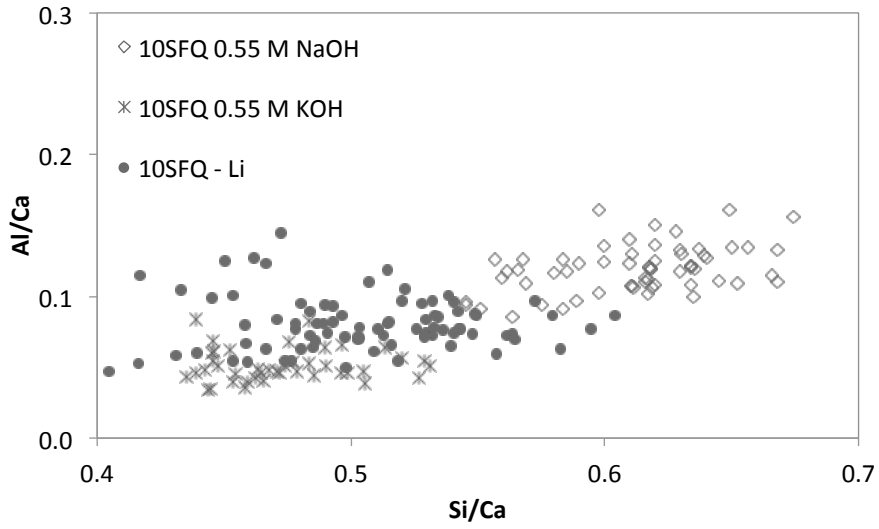

(c)

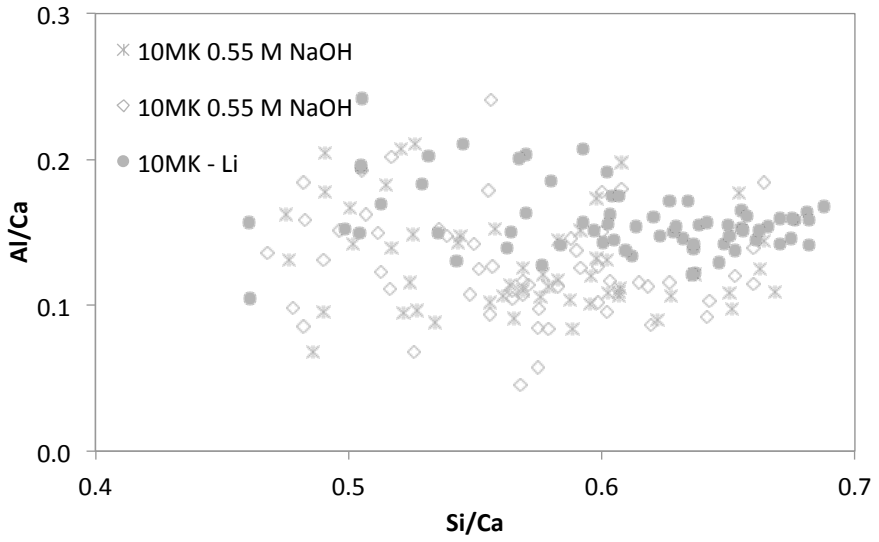

Figure 5. Al/Ca as a function of Si/Ca of outer C-S-H for the PC and 10% blends with NaOH, KOH and LiOH addition. 90 days old.

4. Discussion

This study about the effect of lithium hydroxide gives new insights into the mechanisms controlling ASR. The addition of lithium compounds seems to result in several mechanisms to reduce ASR expansion. The main ones were mentioned in the section 4.1.2.

It was observed in this study that silica fume is mainly dissolved by NaOH then by KOH and LiOH. Wijnen et al. [15] observed that the dissolution rate of silica is lower for LiOH than NaOH and KOH, as observed here for silica fume. It is possibly due to the formation of an insoluble lithium silicate product as mentioned by Goguel [14].

However, PC and metakaolin blended pastes were mostly influenced by LiOH. Lithium hydroxide tends to increase the dissolution of the aluminosilicate in a wider extend than pure silica, providing some additional aluminium and silicon in the pore solution (and C-S-H). The substitution of aluminium by lithium in aluminosilicates [13] may provide this additional aluminium in the pore solution.

It seems also possible that lithium incorporates the surface of silica at kinks and edges reducing its surface dissolution in the same way as aluminium does it (Chapter 3).

Earlier studies mentioned that about half of the added lithium was adsorbed by hydration products. It seems that this is true for PC systems only. The blended systems fix more lithium, until 4/5 for the 10 % SFQ systems. This is probably due to the higher concentration in silicon in the C-S-H phase and maybe to a higher amount of hydration products due to the pozzolanic reation, as already studied in the chapter 2.

In a future work, the C-S-H and pore solution study should be provided with reactive aggregate in presence of lithium to fully understand this mechanism.

5. References

[1] X. Feng, M.D.A. Thomas, T.W. Bremner, B.J. Balcom, K.J. Folliard, Studies on lithium salts to mitigate ASR-induced expansion in new concrete: a critical review, Cement and Concrete Research, 35 (2005) 1789-1796.

[2] B. Taha, G. Nounu, Using lithium nitrate and pozzolanic glass powder in concrete as ASR suppressors, Cement and Concrete Composites, 30 (2008) 497-505.

[3] A.G.Caldwell. W.J. McCoy, New approach to inhibiting alkali silica expansion, Journal of the american concrete institute, 22 (1951) 693-706.

[4] C.L. Collins, J.H. Ideker, G.S. Willis, K.E. Kurtis, Examination of the effects of LiOH, LiCl, and LiNO3 on alkali-silica reaction, Cement and Concrete Research, 34 (2004) 1403-1415.

[5] K.E. Kurtis, P.J.M. Monteiro, Chemical additives to control expansion of alkali-silica reaction gel: proposed mechanisms of control, Journal of materials Science, 38 (2003) 2027-2036.

[6] M. Prezzi, The alkali reaction part 1: Use of the double-layer theory to explain the behaviour of the reaction product gels, ACI Mater, 94 (1997) 10-17.

[7] M. Prezzi, The alkali silica reaction - part 2: the effect of chemical admixtures, ACI Mater, 95 (1998) 391-401.

[8] X. Feng, M.D.A. Thomas, T.W. Bremner, K.J. Folliard, B. Fournier, New observations on the mechanism of lithium nitrate against alkali silica reaction (ASR), Cement and Concrete Research, 40 (2010) 94-101.

[9] D.S. Lane, Laboratory investigation of lithium-bearing compounds for use in concrete, in, Charlottesville, Virginia, 2002.

[10] B. Durand, More results about the use of lithium salts and mineral admixtures to inhibit ASR in concrete, in: 11th ICAAR international conference on alkali aggregate reaction, Québec, 2000.

[11] T. Sakagushi, M. Takakura, A. Kitagawa, T. Hori, F. Tomozawa, M. Abe, The inhibitive effect of lithium compounds on alkali–silica reaction, in: 8th International Conference on Alkali–Aggregate Reaction, Kyoto, 1989, pp. 229.

[12] M. Berra, A.E.P. T. Mangialardi, Use of lithium compounds to prevent expansive alkali–silica reactivity in concrete, Adv Cem Res, 15 (2003) 145.

[13] H.-M. Seitz, A.B. Woodland, The distribution of lithium in peridotitic and pyroxenitic mantle lithologies ‚Äî an indicator of magmatic and metasomatic processes, Chemical Geology, 166 (2000) 47-64.

[14] R. Goguel, Hydrothermal extraction of potassium, sodium, rubidium and cesium from rocks by lithium hydroxide and determination at very low natural levels, Analytica Chimica Acta, 169 (1985) 179-193.

[15] P.W.J.G. Wijnen, T.P.M. Beelen, J.W. de Haan, C.P.J. Rummens, L.J.M. van de Ven, R.A. van Santen, Silica gel dissolution in aqueous alkali metal hydroxides studied by 29SiNMR, Journal of Non-Crystalline Solids, 109 (1989) 85-94.

ANNEX 2 STUDY OF FLY ASH ON ASR

1. Materials and methods

Mortar bars (40*40*160 mm) containing 15, 20, 25 and 30% of fly ash (Table 1) and Swiss reactive gneiss were cast with metallic measurement studs. The aggregate to cement ratio was 3. The mortars were first cured for 28 days at 20°C and 95% RH. The mortar bars were then put in an alkaline solution containing 0.9 molar NaOH at 38°C, in order to accelerate the expansion. The pore solution extraction of the same blended pastes were done following the methodology described in chapter 2.

Table 1. Oxide composition of the fly ash

%w.	LOI	Na_2O	MgO	Al_2O_3	SiO_2	P_2O_5	SO_3	P_2O_5	MnO	K_2O	Fe_2O_3	CaO
Fly ash	1.32	0.03	0.18	23.92	69.96	0.05	0.03	0.05	0.05	0.61	2.21	0.23

2. Mortar expansion

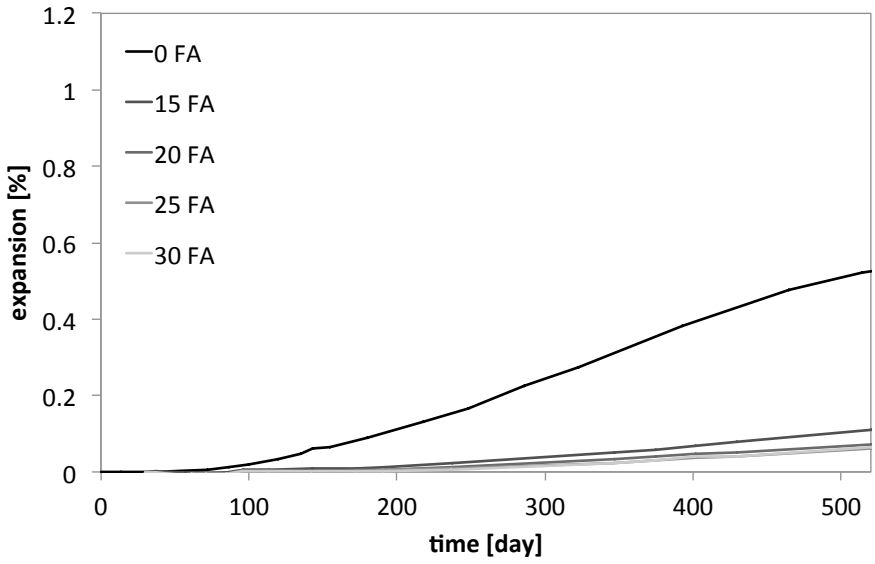

Figure 1. Accelerated expansion test of FA mortars with Swiss reactive gneiss

3. Pore solution extraction

The ICP analysis of the pore solutions over 1 year is shown in the Table 2 and in the Figures 2 and 3. The aluminium concentration is increased in the FA systems and reaches a stable value at 28 days. The alkalis are fixed in the paste and potassium has a decrease of 65% at 90 days compared to OPC.

Table 2. Pore solution composition of the fly ash blended pastes

15%	Na [mM]	K [mM]	Ca [mM]	Si [mM]	Al [mM]
0d	0	0	0	0	0
28d	97.4	268.6	2.2	0.1	0.1
90d	65.2	171.1	1.6	0.1	0.24
300d	68.2	192	1.1	0.1	0.23
30%					
0d	0	0	0	0	0
28d	79.6	184.4	2.1	0.1	0.1
90d	47	116.4	1.2	0.2	0.35
300d	51	125	0.7	0.1	0.42

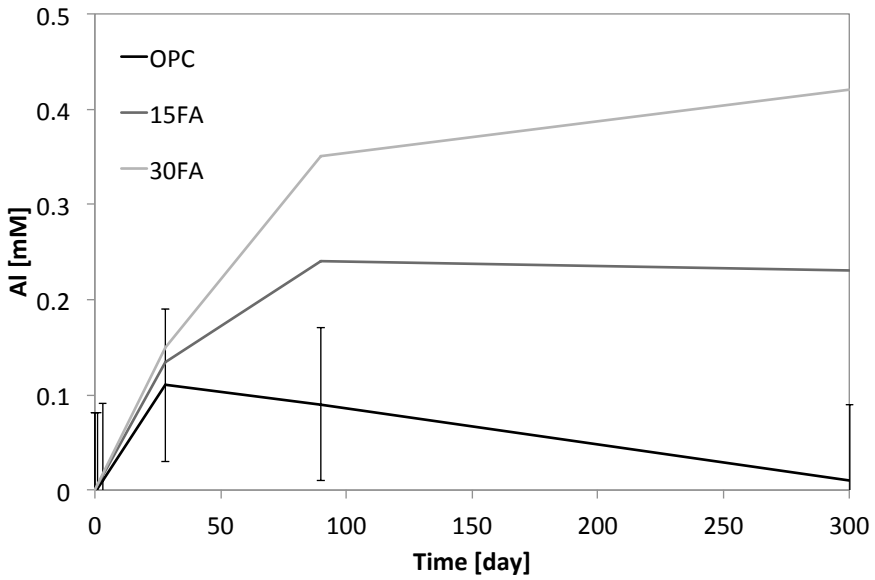

Figure 2. Aluminium concentration in the pore solution of FA blended pastes as a function of time

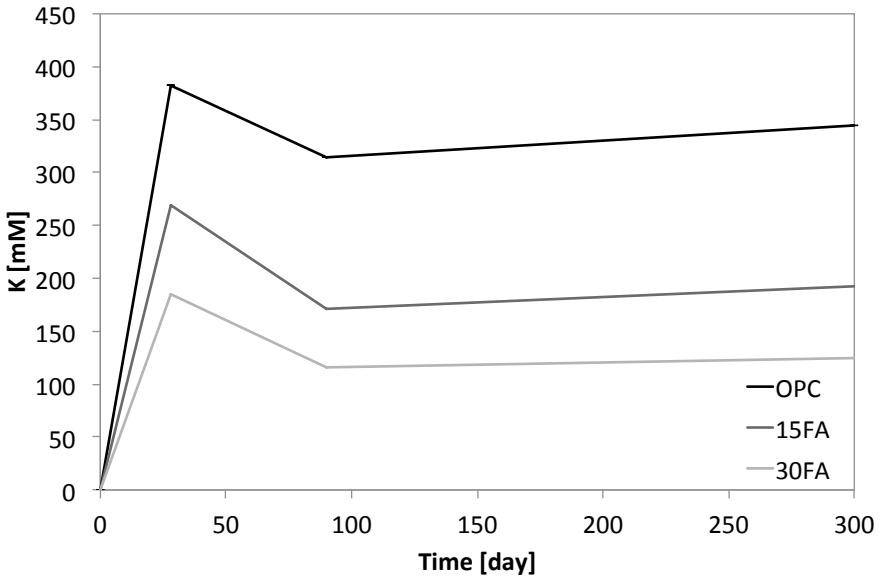

Figure 3. Potassium concentration in the pore solution of FA blended pastes as a function of time

ANNEX 3 THE ALUMINIUM PRE-CURING OF AGGREGATES

Aggregates were cured in an aluminium containing solution to see the effect of aluminium on aggregates deterioration. The aggregates were then mixed in a PC mortar and put in accelerated conditions to measure expansion (chapter 2). The test showed a reduction of expansion due to aluminium curing only on the highly reactive aggregate. This annex presents the test conditions and the limitations of the method.

1. Method

The two aggregates used in this work (chapter 2) were pre-cured during 90 days in simulated solutions (0.2 M NaOH, 0, 5 or 10 mM Al) at 20°C.

Mortar bars (40 x 40 x 160 mm) containing these cured aggregates were cast with metallic measurement studs. The aggregate to cement ratio was 3. The mortars were first cured for 28 days at 20°C and 95% RH. The mortar bars were then put in an alkaline solution containing 0.6 molar NaOH at 38°C, in order to accelerate the expansion (3 bars in 1.5 liters soak solution).

2. Results

The Figure 1 shows the expansion in accelerated conditions of the both systems with pre-cured aggregates. The test procedure is severe: as proposed in the study of chapter 3, to efficiently control ASR over the long term, the aluminium source has to be present over the long term and not only at the start of the expansion, as it is the case for this test. Moreover, the paste doesn't reduce the alkali content of the pore solution over the long term, as it is the case in blended pastes. The highly reactive North American aggregates show a small but visible reduction of expansion over 1 year. This is not the case with the reactive schist. Some assumptions can be made to explain the different behaviour between the two aggregates: The reactive schist is already well cracked at the origin. The mixing in the mortar mixer probably induces deterioration and crushing of the aggregates, inducing new reactive zones, which is not the case of the highly reactive aggregate, being a compact bulk material providing smooth surfaces. The apparition of these new reactive zones that cannot be further stabilized by aluminium are good starting surfaces for dissolution and gel formation.

(a)

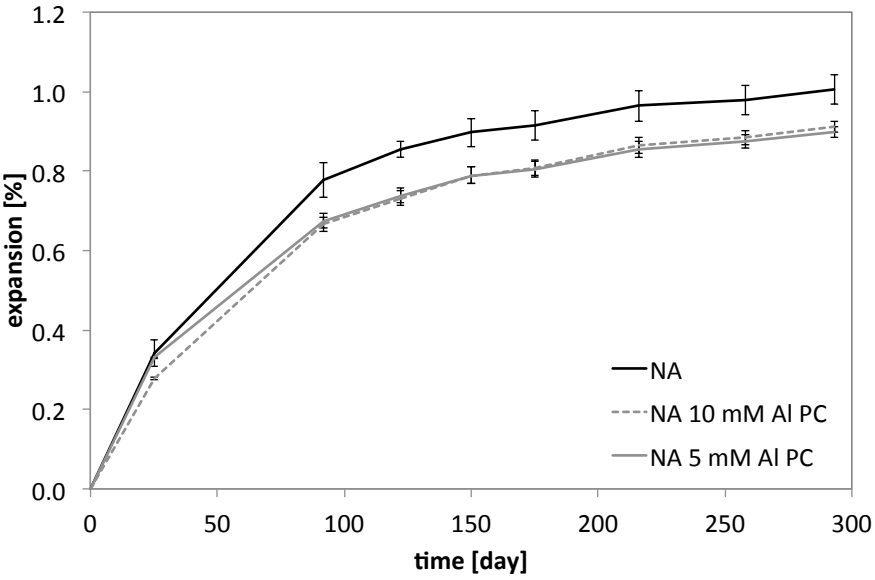

(b)

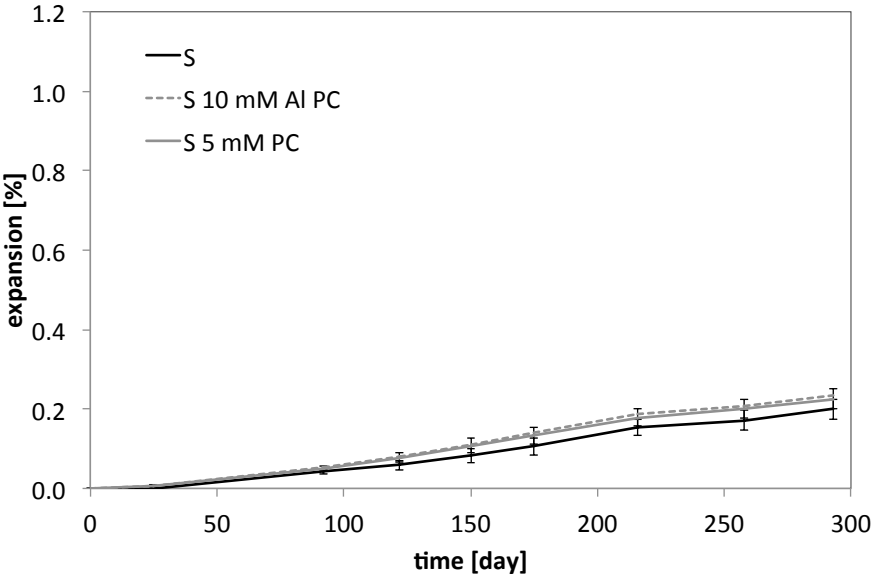

Figure 1. Mortar expansion at 38°C in 0.6 M NaOH soak solution with Al pre-cured aggregates, a) North American highly reactive aggregates, b) Swiss reactive schist

ANNEX 4 THE CHEMICAL SHRINKAGE OF REACTIVE AGGREGATES

A first approach to study the degradation of reactive aggregates in simulated pore solutions was tried by chemical shrinkage. The formation of ASR gel inside the aggregates adsorbs water. The orientation of the water molecules inside the gel surface should reduce the overall volume of the system e.g. [1]. This technique was found to be inappropriate and was not further investigated. The main conditions and the reasons why it doesn't work are presented in this annex.

1. Method

Reactive aggregates (the same as studied in the thesis) were put in simulated pore solutions in a chemical shrinkage device. This device was developed in [2] for cementitious systems. The conditions were adapted for aggregates testing:

10 grams of aggregates sand (0-300 µm or 315-650 µm) were put in 50 ml of pore solution. The solution had 0.6 or 0.9 M NaOH and certain systems were saturated with $Ca(OH)_2$ in excess. The bottles were closed with a rubber stopper crossed by a graduated pipette. The system was put in a 38°C bath to accelerate the test. A drop of orange oil indicates the overall solution level inside the pipette. A camera recorded the shrinkage over 120 days.

2. Results

No valuable results were obtained by this method. Only insignificant shrinkage was recorded. Several problems appeared:

- Even by vacuum pre-saturation of the aggregates, their porosity was difficult to fill before the start of the test. Degasing of the aggregates was observed even after the

experiment started, which distorted the results, changing the overall volume of the system in the pipette.

- It is possible to roughly estimate the shrinkage present in such system:

  The expansion mortars with highly reactive North American aggregate at 38°C at 120 days is approximately 0.7 % vol (chapter 2). The assumption that the volume uptake of the bar corresponds to the volume of water absorbed by the gel is made here. Knowing that the volume uptake is present only in the aggregates, and that the aggregates volume is of 67.5 % of the total volume of the mortar bar, the volume uptake of the aggregates corresponds to approximately 1%. In the chemical shrinkage device, 3.8 ml of aggregates were tested in solution. At 120 days, the volume change in the aggregate can be estimated at 0.038 ml on the expansion curves. It is estimated that the water orientation reduces the original water volume of 10 % (estimation from cement shrinkage study [2]). Following these assumptions, the shrinkage in the testing system corresponds to 0.0038 ml at 120 days. This shrinkage is way bellow the experimental error of the device, and this calculation confirms the non-efficiency of the method.

3. References

[1] S.-P. Ju, C.-Y. Chang, W.-J. Lee, S.-H. Yang, C.-H. Chao, J.-Y. Huang, H.-L. Chen, J.-G. Chang, K.-C. Fnag, Investigation of the adsorption mechanism of water nanocluster on the substrate: The size and interaction strength effect, Applied Surface Science, 254 (2008) 3606-3612.

[2] V. Kocaba, Development and Evaluation of Methods to Follow Microstructural Development of Cementitious Systems Including Slags, in: Laboratoire des Matériaux de Construction, Ecole Polytechnique Fédérale de Lausanne, Lausanne, 2009.

REMERCIEMENTS

Cette thèse a été financée durant les six premiers mois par B&G Ingénieurs Conseils et par la suite par Sika AG.

J'aimerais remercier sincèrement les personnes ayant participé de près ou de loin à cette thèse:

- Tout d'abord la directrice de ce travail, professeur Karen Scrivener, pour m'avoir permis de réaliser cette thèse dans son laboratoire, pour son soutien et ses conseils scientifiques, mais également pour m'avoir permis de présenter mes recherches dans plusieurs conférences.
- Cyrille Dunand et Emmanuel Gallucci pour m'avoir transmis le goût des matériaux de construction et plus particulièrement de la durabilité lors de mon travail de Master.
- Les membres de mon jury de thèse : Dr. Emmanuel Gallucci de Sika A.G., Dr. Paul Bowen du laboratoire de technologie des poudre à l'EPFL, Dr. Maarten Broekmans du Geological Survey of Norway, ainsi que le président du Jury, Prof. Pierre Stadelmann du CIME.
- Les collaborateurs du CIME, en particulier Vincent Laporte et Nicolas Xanthopoulos pour leur accueil et leur aide précieuse en XPS.
- Les étudiants ayant participé à ce travail lors de projets de semestre
- Mes collègues du LMC pour les bons moments partagés ensemble, pour les discussions scientifiques et leur amitié.
- Finalement je tiens à remercier ma famille : mon amie Marie, ma sœur Eve-Eléonore et ma mère Katia pour leur soutien, ainsi que mon père Alain pour avoir su me transmettre cet intérêt pour la science et le métier d'ingénieur.

CURRICULUM VITAE

Name	Chappex
Surname	Théodore
Date of Birth	Mars 10th 1982
Education	2012, ASRETC Level 1, rope access certificate 2003–2008, Material Science and Engineering at Ecole Polytechnique Fédérale de Lausanne (EPFL), Switzerland Master thesis, Laboratory of Construction Materials (LMC) **« Analysis of the alkali-silica reaction in the Serra dam »** Specialisation : Matériaux struturels pour les transports, l'énergie et les infrastructures. 1996–2003, Kollegium Spiritus Sanctus Brig, Switzerland
Professional experience	2008 – 2012, Laboratory of Construction Materials, Department of Material Science, EPFL, Switzerland. PhD thesis – **« The mechanisms controlling alkali-silica reaction with the use of SCMs »** 2006, Internship in the firm KONG SPA, Lecco, Italy, conception of climbing devices, CAD and material optimization, R&D department. 2008–2012, Assistant at EPFL, LMC since 2009, technical advisor for E.B. France
Special interests	Rock climbing and Mountaineering
Languages	French, Mother Tongue German/Swiss german, Bilingual English, Excellent knowledge Italian, Notions (spoken)
Distinction	Best student paper Award in the 14th International Conference on Alkali Aggregate Reaction (ICAAR), Austin, Texas, 2012